Development of passive anti-icing surfaces

by incorporating ice-binding proteins

Laura Hoebus

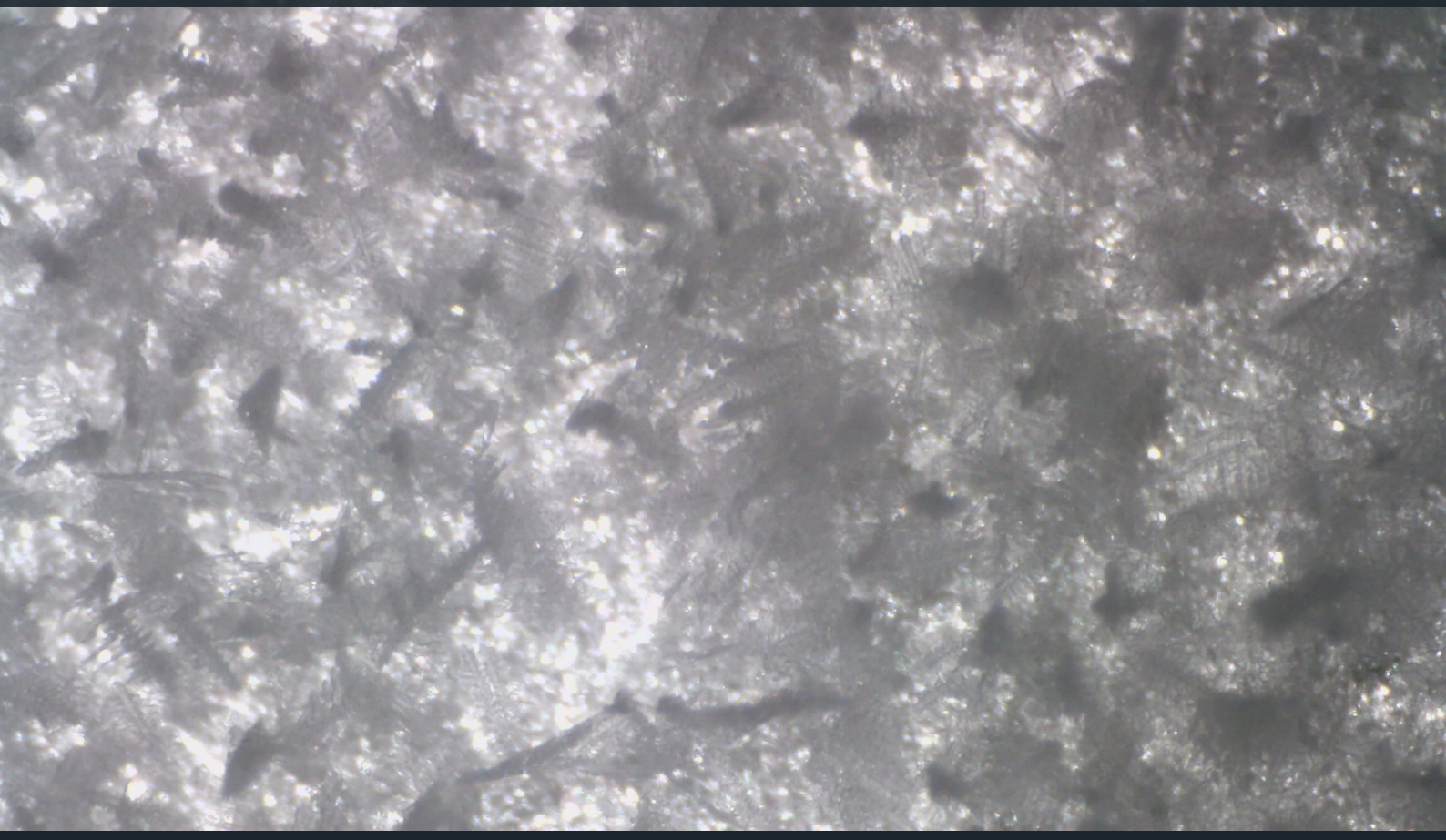

TU Delft

Development of passive anti-icing surfaces by incorporating ice-binding proteins

by

Laura Hoebus

for obtaining the degree of Master of Science in Aerospace engineering at Delft University of Technology

To be defended publicly October 30^{th} at 9.30 a.m..

Supervisors

Miisa J. Tavastsjerna	TU Delft, Aerospace faculty
Dr. Santiago J. García Espallargas	TU Delft, Aerospace faculty

Committee members

Dr. Baris Kumru	TU Delft, Aerospace faculty
Dr. Julie Teuwen	TU Delft, Aerospace faculty

Acknowledgments

First of all, I would like to thank my promotor, Santiago, who gave me the possibility to work on this topic which I found very interesting. Next, I would like to thank my daily supervisor Miisa who helped me a lot throughout the entire research. Thank you for your continued guidance and support. In addition, I would also like to thank the entire NovAM group who were always very open to help me.

Finally I would like to thank my family who was always there for me and supported me during stressful times. A special thanks to my grandfather who was very interested in my topic and proofread my thesis multiple times.

Abstract

In cold regions, the formation and accumulation of ice can cause safety hazards and impede proper operation of equipment. By example, ice accumulation on aircraft wings can increase drag, increase weight, reduce upward force and decrease aircraft speed.

For these reasons, proper anti- or de-icing techniques need to be developed. These techniques can be divided in passive and active systems. Active systems require a supply of external energy. On the other hand, by physical or chemical surface modification, passive systems inherently possess anti-/de-icing characteristics without the requirement of external energy. For this reason, this master thesis focuses on the development of passive anti-icing coatings. One possible new approach to develop passive anti-icing coatings could be to modify surfaces with ice-binding proteins, more specifically anti-freeze proteins (AFPs). These proteins can be found in organisms living in cold climates. They are able to inhibit freezing, thus making life in cold environments possible. Currently, limited research has been performed regarding these AFPs as anti-icing coating material. As a result, this thesis delves deeper into the behaviour of AFPs as an anti-icing coating material.

In a first step, AFPs are directly attached to the surface in various concentrations using a polyethylene glycol (PEG) chain with a specific chain length. From the freezing data, an unexpected phenomenon was observed. It appears that AFP-surfaces freeze faster with increasing AFP concentration. As such, they act as ice promoter instead of the expected ice inhibitor. It was hypothesized that this phenomenon could be largely attributed to the limited protein mobility on the surface. To further test this theory, AFPs with various chain lengths were attached to the surface. Indeed, freezing was detected at later time points with increasing chain length meaning that AFPs with higher mobility are able to inhibit ice growth. In addition, the incorporation of AFPs showed another interesting phenomenon as well. Ice dendrites on the AFP surfaces appeared to grow more straight compared to their silane-treated counterpart. Because of this, dendrites on the AFP-surfaces were also more easy to blow away.

Except for attaching AFPs directly to the surface, their behaviour within a polymeric environment is also studied. For this purpose, various concentrations of AFPs were incorporated within a PEG hydrogel. DSC was used to study the different types of water within the different AFP-hydrogels. Interestingly, the amount of freezable bound water increased with increasing AFP concentration. No clear trend could be found between the amount of non-freezing water and the AFP concentration. In addition, freezing tests showed that hydrogels with increasing AFP concentration inhibited ice growth. This behaviour is opposite to the behaviour that was detected for AFPs attached directly to the surface. Finally, the hydrogels are dehydrated and again subjected to freezing tests. Now, the freezing behaviour follows a similar trend as the AFP-surfaces, meaning that with increasing AFP concentration, ice formation is promoted. From these results

it is clear that the environment of the AFPs plays a crucial role in the AFP behaviour. Depending on the type of environment in which they are introduced, they can either act as ice inhibitor or ice promotor.

Contents

List of Tables

List of Figures

List of abbreviations

AA2024
Aluminium alloy 2024

AA2024-2.5mg/ml AFP-PEG2
Aluminium alloy 2024 functionalized with 2.5 mg/ml AFP using a PEG2 linker

AA2024-2.5mg/ml AFP-PEG12
Aluminium alloy 2024 functionalized with 2.5 mg/ml AFP using a PEG12 linker

AA2024-2.5mg/ml AFP-PEG24
Aluminium alloy 2024 functionalized with 2.5 mg/ml AFP using a PEG24 linker

AA2024-5.0mg/ml AFP-PEG12
Aluminium alloy 2024 functionalized with 5.0 mg/ml AFP using a PEG12 linker

AA2024-2.5mg/ml INP-PEG12
Aluminium alloy 2024 functionalized with 2.5 mg/ml INP using a PEG12 linker

AA2024-5.0mg/ml INP-PEG12
Aluminium alloy 2024 functionalized with 5.0 mg/ml INP using a PEG12 linker

AA2024-OH
Aluminium alloy 2024 activated by 10s immersion in NaOH

AA2024-OH-NaOH-5s
Aluminium alloy 2024 activated by 5s immersion in NaOH

AA2024-OH-NaOH-10s
Aluminium alloy 2024 activated by 10s immersion in NaOH

AA2024-OH-NaOH/HNO_3
Aluminium alloy 2024 activated by 6min immersion in NaOH followed by a desmutting step in HNO_3

AA2024-OH-Pir5
Aluminium alloy 2024 activated by 5min immersion in Piranha solution

AA2024-OH-Pir15
Aluminium alloy 2024 activated by 15min immersion in Piranha solution

AA2024-SH
silane treated aluminium alloy 2024

ABP
Aluminium-binding peptide

AFP
Anti-freeze protein

CRD
Central repeating domain

DSC
Differential scanning calorimetry

DWC
Dropwise condensation

EPL
Expressed protein ligation

FTIR
Fourier transform infrared spectroscopy

FWC
Filmwise condensation

$^{1}H - NMR$
Proton nuclear magnetic resonance

HNO_3
Nitric acid

H_2O_2
Hydrogen peroxide

H_2SO_4
Sulphuric acid

IBS
Ice-binding site

INP
Ice-nucleating protein

IRI
Ice recrystallization inhibition

Mal-PEG2/12/24-AFP/INP
AFP/INP functionalized with a Mal-PEG2/12/24-NHS linker

Mal-PEG-2/12/24-NHS
Maleimide - polyethylene glycol 2/12/24 - N-Hydroxysuccinimide

MPTS
3-mercaptopropyltrimethoxysilane

mRNA
Messenger ribonucleic acid

NaOH
Sodium hydroxide

NIBS
Non-ice-binding site

PBS
Phosphate buffered saline

PDMS
Polydimethylsiloxane

TH
Thermal hysteresis

WCA
Water contact angle

Chapter 1

Introduction

In colder regions, the formation and accumulation of ice can cause safety hazards and lead to damages of building roofs, power transmission, wind turbines, aircraft wings, etc. This way, proper operation of the equipment is impeded leading to decreased efficiency. By example, ice accumulation on aircraft wings can decrease aircraft speed and reduce upward force. Furthermore, ice formation can inhibit movement of moving parts and change the hydrodynamics of aircraft surfaces (such as wings and airfoils), thus instigating dangerous situations [2], [3].

For these reasons, proper anti- or de-icing methods need to be available. All different types of anti- or de-icing techniques can roughly be divided in active and passive systems. In active anti- or de-icing, a supply of external energy is required. A commonly used active de-icing technique in aircraft is hot air de-icing. Simply said, electric energy is converted to heat by resistive heating. Next, the hot air flow is guided to the desired position. The necessity of external energy is a major disadvantage of this technique. In addition, the hot air can cause damage to the material of the aircraft as well. Alternatively, anti-freeze liquids can be sprayed on the aircraft surface to hinder freezing. This chemical liquid reduces the freezing point of water, this way making ice melt easier [2]. However, also this method has significant disadvantages. Excessive use of de-icing fluids can lead to high costs and detrimental effects on the environment [4]. In addition, because the fluids need to be reapplied, costs and labour become significant over time. A more efficient active system was proposed by Kandagal and Venkatraman [5]. Piezoceramic actuators were used to induce vibrations in a flat plate. Successful de-icing was detected at resonance frequencies where the peak values of the shear stresses were higher than the adhesive shear strength of the ice. In extension, these actuators can be placed on critical aircraft locations (e.g. aircraft leading edge) where ice accretion is significant. This method has shown to be less energy demanding and light-weight compared to other active systems [5], [6]. Nonetheless, the need for external energy and the increase of weight remain two undesirable side-effects of the active systems. As such, special attention goes towards passive systems.

By chemical or physical surface modification, the surface can exhibit anti- or de-icing characteristics without the necessity of external energy or liquid anti-freezing fluids [2]. However, the fabrication of anti-icing surfaces is not as easy as one would expect. Ice formation processes in nature are complex and diverse. Due to differences in temperature and environmental conditions, different types of ice crystals can be formed in nature such as frost, snow, rime and glaze. These different icing scenarios lead to difficulties in developing the anti-icing surface [7]. As such, creating a highly efficient, versatile and durable anti-icing material remains a challenge. One possible

new approach to passive anti-icing could be to modify surfaces with ice-binding proteins that can bind themselves to ice crystals. One class of these ice-binding proteins are AFPs. AFPs have been a material of interest in various biological and industrial fields. They have the ability to control ice formation and are often encountered in organisms living in cold environments. Since AFPs are able to regulate ice growth and inhibit ice recrystallization, incorporating AFPs in an anti-icing coating could significantly ameliorate the anti-icing capabilities of the coating. On the other hand, ice-nucleating proteins (INPs) enhance ice formation. With these proteins, ice formation might be controlled toward specific wanted locations on the surface.

In this first chapter, background information is provided regarding the general freezing process, AFPs, INPs and anti-icing surfaces. In the final section of this chapter, the scope of the master thesis and the further outline of the report are defined.

1.1 Passive bio-inspired anti-icing strategies

As was described above, a distinction can be made between active and passive anti-icing mechanisms. Since active methods rely on external energy supply, they are less attractive compared to the passive systems. Passive systems use the intrinsic surface characteristics of the material. A lot of passive systems have been explored in literature. However, only bio-inspired strategies will be discussed in more detail. Overall, bio-inspired passive strategies can be grouped in: strategies that act before freezing, strategies that act after freezing and some alternative strategies [8].

1.1.1 Before freezing

Superhydrophobic surfaces repel water thus making ice nucleation difficult. They are commonly fabricated by decreasing the surface energy of macro/nanostructured surfaces by chemical modification or by creating a micro/nanostructured surface on a hydrophobic material [2], [9]. This micro/nanostructured surface leads to superhydrophobicity due to entrapped air which is present in the grooves of the rough surface. This way, water droplets remain in a nonwetting Cassie-Baxter state (**Figure 1.1 a**) and the liquid/solid contact area is greatly reduced, leading to a delay in onset of heterogenous ice nucleation [8].

However, in high humidity environments, moisture is able to condense in the grooves of this superhydrophobic surface over time, leading to an ice layer. Due to the mechanical interlocking between the ice and the superhydrophobic surface, the ice adhesion strength can signifcantly increase. Furthermore, these surfaces are prone to wear and the micro/nanostructure has shown to gradually degrade during subsequent icing/de-icing cycles. As such, these coatings are not durable [10].

1.1.2 After freezing

Alternatively, when ice is already present on the surface, it would be desirable to easily remove this ice. Lubricating layers have shown to greatly decrease ice adhesion (**Figure 1.1 b**). Dou et al. created a coating with polymers containing many hydrophilic pendant groups. The hydrophilic groups can absorb water in humid environment and the pendant groups ionize in water. Since ions lower the activity of water, they are also able to melt snow or ice. This way, a lubricating layer can be formed naturally, even in freezing conditions. They reported a significant drop in ice adhesion strength after applying the coating. By example, the adhesion strength of copper decreased from around 1000 kPa to 30 kPa after coating the samples [11].

1.1.3 Alternative strategies

Finally, other bio-inspired anti-icing strategies can also be identified. Anti-icing surfaces with ice-binding proteins fall within this category. By example, O'Brien et al. created a hydrophobic surface with hydrophilic regions by selectively depositing INPs along these hydrophilic regions. The hygroscopic ice stripes act as humidity sinks, meaning that ice nucleation will preferentially form along these stripes. This way, regions in between these strips are free of condensation or frost and result in dry zones, as can be seen on **Figure 1.1 c** [12]. Also anti-icing surfaces with AFPs have been developed. Before going into greater detail about the AFP and INP anti-icing surfaces, the different classes and working mechanism of INPs and AFPs will be described.

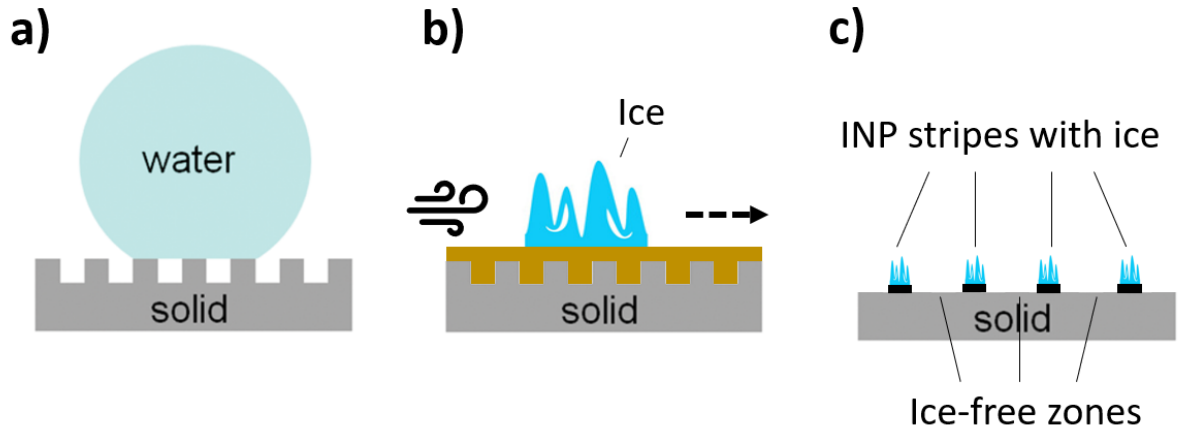

Figure 1.1: a) water droplet in a nonwetting Cassie-Baxter state, b) Lubricating layer to decrease ice adhesion and c) Hydrophobic/hydrophilic surface with INPs as described by [12]

1.2 Classification of ice-binding proteins

1.2.1 Classification of AFPs

AFPs are present in many different organisms living in cold climates. Under these organisms we can understand fish, diatoms, bacteria, fungi, insects, plants, etc. [13]. Since many different types of organisms produce AFPs, the discussion is limited to AFPs from fish and insects.

The most commonly described AFPs from fish can be divided in 3 separate categories; AFP types I, II and III. Different types of fish express different AFP types. The working mechanism of these different types is similar, however, their primary sequence and three dimensional structures are fundamentally different. Type I AFP is the most simple one consisting of a straight α-helix. Depending on the exact built of the protein, its molecular weight ranges between 3.3-4.5 kDa [14], [15]. On the other hand, Type II AFPs have 2 α-helices and nine β-strands. β-strands contain cysteines which form disulfide bonds between the β-sheets. These bonds increase the structural stability of the type II AFPs. Their molecular weight ranges from 11 to 24 kDa [15]. Finally, type III AFPs have an average molecular weight of 6.5 kDa and can be found in different fish like wolf fish (*Anarhichas lupus*) and eelpout (*Zoarcidae*). They have a spherical/triangular prims three-dimensional structure with two relatively flat surfaces [14], [15].

AFPs from fish are categorized as moderately active AFPs. They are only able to bind on one or two ice crystal planes which can include the primary prism plane, secondary prism plane and/or the pyramidal ice crystal plane. This can lead to a hexagonal bipyramidal ice crystal shape [16]. On the other hand, also hyperactive AFPs exist. These AFPs are mostly encountered in insects.

Even though the structure of insect AFPs can vary, all of them are termed hyperactive, because they are 10 to 100 times more effective than AFPs from fish [14]. Compared to the moderately active AFPs, one hyperactive AFP can bind to more crystal planes. They can bind to the primary and secondary prism plane. However, the structure of their IBS makes it also possible to bind to the ice crystal basal plane, leading to disk-like ice structures. The fact that hyperactive AFPs can bind to this additional basal plane might explain their greater inhibitory effect [16]. As such, insects are able to withstand lower temperatures. **Figure 1.2** clearly illustrates the ice binding planes and the difference in affinity for various ice binding planes depending on the AFP type.

	Fish						Insect	Bacterium	Plant
	Type I AFP			Type II AFP	Type III AFP	AFGP	DcAFP	MpAFP	LpAFP
Structure element	α-helix, Alanine rich	α-helix, Alanine rich	α-helix, Threonine-(Alanine rich)	Globular; S–S bonds	Globular; β-sandwich	AAT-repeat; Disaccharide	β-solenoid; S–S bonds	β-solenoid	β-solenoid
Representative structure									
Binding plane			Sub mM mM	or					
Natural source	Winter flounder fish (wfAFP1)	Shorthorn sculpin fish (ssAFP1)	Righteye flounder, barfin plaice (bpAFP)	Longsnout Poacher sea raven, rainbow smelt, Atlantic herring	Eel pouts; ocean pout fish	Cods and Antarctic notothenioids	Beetle Dendroides canadensis	Antarctic bacterium Marinomonas primoryensis	Lolium perenne

Figure 1.2: Different AFPs and their corresponding ice crystal binding planes [17]

1.2.2 Classification of INPs

In comparison to AFPs, INPs are very large (120-150 kDa). In nature, these proteins are often associated to the cell membrane from bacteria where they increase the freeze tolerance by forming ice crystals outside the cell. The heat which is formed because of this can be used as a heat source for the bacteria to avoid freezing. In addition, INPs can damage the epithelium of fruits and vegetables which can free nutrients to bacteria. Currently, the most well known INP is found on the outer membrane of bacterial plant pathogens (*Pseudomonas syringae*) [18].

1.3 General working mechanisms of ice-binding proteins

1.3.1 General working mechanism of AFPs

In the Arctic and Antarctic regions, seawater temperature consistently lies below zero due to the presence of dissolved salts. These low temperatures can be deadly for polar organisms. However, nature has adapted to this by the production of AFPs. Such proteins can protect the polar organisms from freezing. AFPs have two major features; they are able to inhibit ice

recrystallization, meaning that ice crystal size cannot increase in materials which are already frozen, and they can reduce the freezing temperature of a solution, thus separating the melting and freezing point [14]. This concept is called thermal hysteresis (TH). Both features of AFPs can be explained by their adsorption to certain ice faces as described by the adsorption-inhibition model proposed by Raymond and Devries in 1977 [19].

According to this model, AFPs irreversibly adsorb on ice surfaces. This way changing the microscopic ice surface growth pattern. At these IBSs, further ice growth is inhibited while ice continues to grow at other locations [20]. Later on, Celik et al. confirmed the irreversible adsorption of AFPs on the ice surface by using AFPs which were fluorescently tagged [21]. Both ice recrystallization inhibition (IRI) and TH work in a slightly different way. For anti-icing applications, TH is mostly of interest and its working mechanism will be further discussed.

Due to the fact that AFPs irreversibly bind to an ice crystal plane, ice crystal growth is inhibited within a specific region and a temperature gap is created. This temperature gap in which ice growth is inhibited is called the hysteresis gap while the temperature difference between the melting point and the hysteresis freezing point is named the hysteresis activity [22]. Normal collagitive antifreeze materials, such as ethanol, decrease the freezing point linearly with the solution osmolality. AFPs decrease this freezing point in an non-collagitive way, which is much more efficient [23]. They already act at low concentrations and a hyperbolic relationship can be found between the hysteresis activity and the protein concentration [22].

Two related approaches can explain why AFP adsorption and formation of a curved water/ice interface inhibits ice crystal growth and leads to TH [15], [22].

1.3.1.1 Pressure elevation within the ice

Under normal circumstances, two phases are in equilibrium when their free energy is the same. Below the melting point (T_m), the free energy of the solid (ice) becomes lower compared to the liquid. The difference in free energy further increases with decreasing temperature and can be described as:

$$\Delta G_v = \frac{\Delta H \Delta T}{T_m} \tag{1.1}$$

where ΔG_v is the difference in free energy per unit volume, Δ H is the heat fusion of water, ΔT is the degree of supercooling and T_m is the melting point. During TH, the free energy of water should be equal to the free energy of ice since the system stays the same within this gap and no molecules go from one phase to the other. This can be explained by evaluating the bulk pressure of both phases. It is known that a bulk pressure difference exists between two phases depending on the curvature of the interface according to:

$$\Delta P = \frac{2\sigma}{r} \tag{1.2}$$

where ΔP is the difference in pressure between the two phases, σ is the surface tension and r is the radius of the curvature. The pressure below the surface increases for convex surfaces and decreases for concave surfaces. Furthermore, increased pressure leads to an increase in free energy of that phase. In an incompressible solid phase like ice, ΔG_v is equal to ΔP. As such, the free energy difference as was formulated in **Equation 1.1** is compensated in convex surfaces by the increase in pressure (and thus free energy) in the ice phase (**Equation 1.2**). By combining

Equation 1.1 and **1.2**, the critical radius can be found where the pressure difference due to the convex surface completely compensates the original free energy difference at any temperature:

$$r^* = \frac{2\sigma T_m}{\Delta H \Delta T} \tag{1.3}$$

As such the TH can be completely attributed to the bulk pressure changes due to surface curvature [22].

1.3.1.2 Kelvin effect

Another way to explain TH is by means of the Kelvin effect. Normally, water molecules transfer from water to ice below T_m because the equilibrium vapor pressure of ice is lower than water. However, in the presence of AFPs, ice crystals remain unchanged in the hysteresis gap. This would only be possible if the vapor pressure of ice and water are the same in this region. This way, an equal amount of water molecules added to the crystal surface will also detach from it. As such, no net change is detected in the hysteresis gap [24]. Westh et al. demonstrated that AFPs do not decrease water vapor pressure, meaning that AFPs will elevate the vapor pressure of ice [25]. Furthermore, **Figure 1.3** shows that the difference between the vapor pressure of ice and water increases with temperature. This means that AFPs are temperature dependent and will have a larger influence on the ice vapor pressure depending on temperature [24]. The Kelvin effect describes the change in water vapor pressure at convex and concave interfaces. The vapor pressure is lower at a concave surface and higher at a convex surface. According to Poynting, the vapor pressure is proportional to the total pressure of that phase and according to **Equation 1.2**, the total pressure is linked to the curvature [26]. As such, the vapor pressure of ice increases leading to a decrease in vapor pressure difference between water and ice [26].

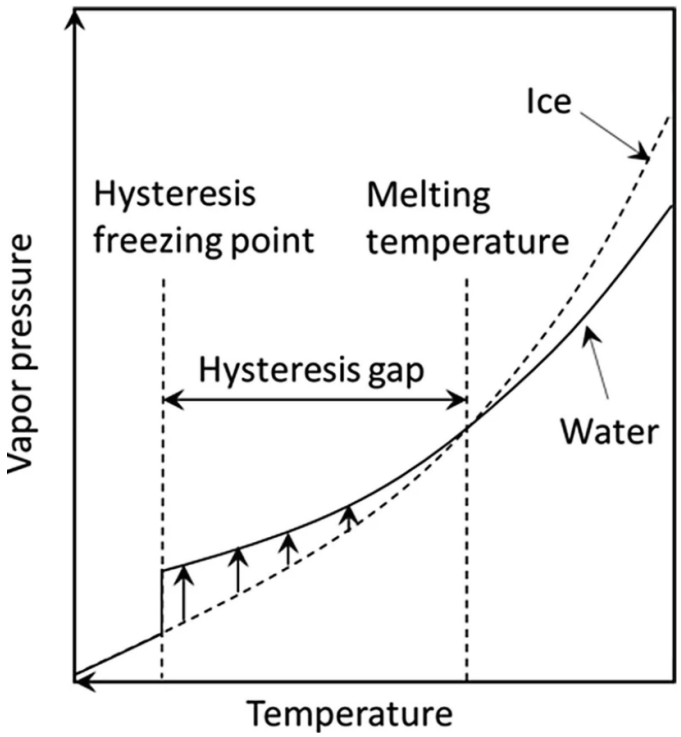

Figure 1.3: Pressure-temperature diagram showing the vapor pressures of water and ice [24]

Furthermore, as was described before, AFPs should act in a temperature dependent way. With decreasing temperature, the convex shape increases, leading to further increase of the ice vapor pressure (and the total bulk pressure of ice) [24]. Thus, at each temperature within the hysteresis gap, the surface is filled with small convex ice caps in between the AFPs. All spheres have equal convexity at a specific temperature. When the temperature becomes sufficiently low, the caps will reach a critical radius which is equal to a half sphere. Further growth after this point decreases convexity and lower the (vapor) pressure thus leading to spontaneous ice nucleation. The point where this phenomenon occurs is called the hysteresis freezing point [22].

1.3.2 General working mechanism of INPs

The general working mechanism of INPs is much more straightforward compared to AFPs. INPs comprise of three distinct domains: the N-terminal domain, C-terminal domain and the central repeating domain (CRD). The CRD most likely contains the ice-nucleating site. This site is able to order water in an ice-like arrangement which facilitates the kinetically hindered phase transition from water to ice [27]. This way, INPs promote ice formation.

1.4 Direct immobilization of ice-binding proteins to the surface

Attaching proteins to a surface without hampering their functionality is very challenging. Even though only a limited amount of papers have attempted to attach AFPs and INPs to surfaces, protein attachment to surfaces has already been widely studied for biomedical applications. Because of this, the following sections will focus on various approaches that are commonly used in the biomedical sector.

Many different bonding strategies can be distinguished to attach a protein to a surface. However, they can be mainly divided into physical adsorption, bioaffinity interactions and covalent bonds, as can be seen on **Figure 1.4** [28].

Physical adsorption is a spontaneous process, where adsorption of the protein to the surface is accomplished by intermolecular forces such as hydrophobic, electrostatic, van der Waals interactions,... By simply incubating the surface in a protein solution, immobilization can be achieved. Even though it is an easy one-step process, proteins can detach from the surface. The formed protein layer is relatively unstable since the intermolecular forces are greatly influenced by environmental conditions such as temperature, pH and surface conditions. In addition, random protein binding sites can participate in this process which this can hamper the protein functionality [28].

Alternatively, proteins can be attached by bioaffinity reactions. Here, a bioaffinity reagent (e.g. avidin-biotin, genetically engineered protein ligands, ...) acts as an intermediate binding molecule between the surface and the protein. Compared to the physical adsorption strategy, this approach leads to more specific and stronger immobilization. However, most of these strategies are time-consuming and costly [28].

One of the most commonly employed immobilization approaches is a covalent linkage between the protein and the surface. Except for direct attachment of the protein to the surface, a spacer can also be used where one end of the spacer is connected to the protein, while the other end is attached to the surface. Most often, click chemistry is employed since it is robust in water and has high yield. In addition, there is no need for an additional catalyst which might hamper

the protein functionality. To be able to immobilize the protein, both the protein and the surface need to have appropriate functional groups. An extensive amount of conjugation strategies exist. However, only the most prevalent ones will be described in greater detail. The first section will delve into modification of the protein to attach specific functional groups, while the second section will go deeper into surface modification techniques to obtain relevant surface chemistry [28].

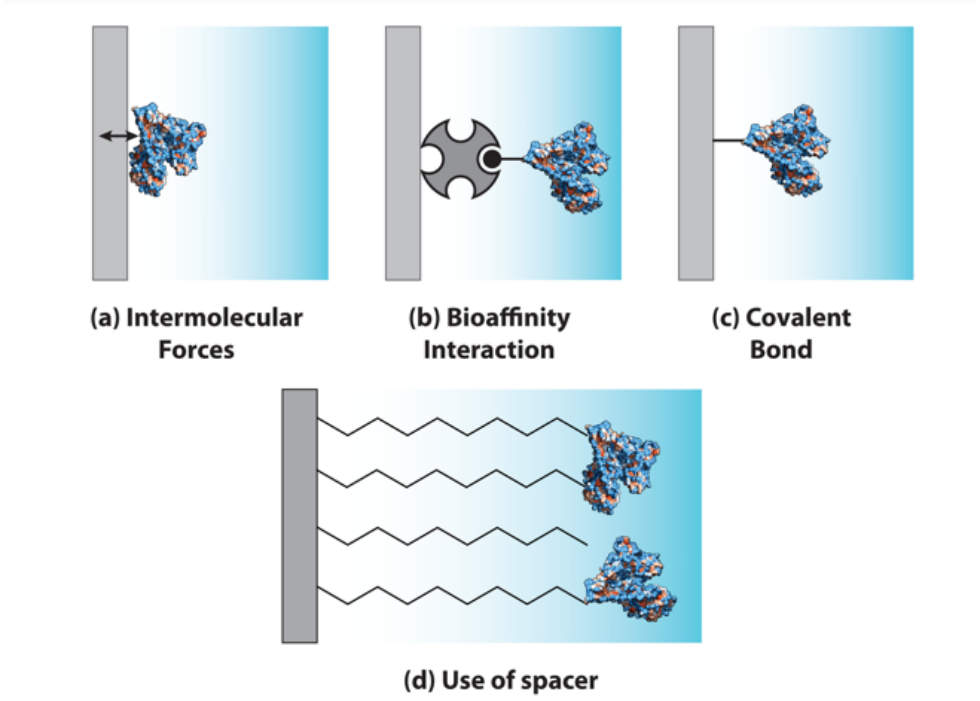

Figure 1.4: Protein immobilization approaches: (a) physical adsorption, (b) bioaffinity interaction, (c) covalent bond and (d) use of spacer [28]

1.4.1 Modification of proteins

To be able to attach a protein to the surface by a covalent bond, native chemical groups of the protein can react with the surface. This way no modification of the protein is required. Alternatively, site-specific protein modification incorporates specific functional groups in the protein which can later react with appropriate functional groups of the surface.

1.4.1.1 No protein modification

Jeong et al. attached AFPs to the surface without altering the protein itself but only modifying the surface. Due to the interactions between the unmodified protein and the functionalized surface, immobilization on the surface was achieved [29]. Also, Liu et al. immobilized AFPs on the surface without any post-modification of the proteins. They modified the surface in such a way that hydroxyl groups and amine groups of the protein were targeted for effective immobilization. Successful immobilization of the AFPs was verified using atomic force microscopy and X-ray photoelectron spectroscopy [30].

Not modifying the protein results in a very easy immobilization route without many steps.

However, there is no control in which functional group will react with the surface. Because of this, functional groups on the protein active sites can be used which decreases the protein activity [30].

1.4.1.2 Site-specific protein modification

Alternatively, it is possible to modify proteins with specific functional groups. Many different modification techniques exist but they can be mostly divided in three groups: In translation protein modification, chemoenzymatic protein modification and chemoselective protein modification [31]. In translation and chemoselective protein modification are of most interest and will be further discussed.

A) In translation protein modification

Translation is the process where messenger ribonucleic acid (mRNA) is decoded in the ribosome, resulting in the synthesis of a specific amino acid chain depending on the mRNA. Different strategies exist that use this translation process which results in more specific labeling during protein synthesis [31]. In translation protein modification was used by Gwak et al. to develop a fusion protein [32]. They immobilized AFP from an Antarctic marine diatom (*Chaetoceros neogracile*) on an aluminium surface by using an Al-binding peptide (ABP). A 5' forward primer that encodes the ABP was used. This way, ABP-AFPs fusion proteins were developed and immobilization could be easily achieved by a dip coating process. An advantage of this technique is the fact that the surface does not need to be functionalized. However, the protein modification is difficult and time consuming [32]. In addition, the metal-binding peptide makes the technique limited to specific surfaces such as silver, gold, gallium arsenide, mild steel and aluminium [29]

B) Chemoselective protein modification

A more straightforward technique is chemoselective protein modification. Small molecules target endogenous thiols, aromatics, amines and protein termini, this way adding specific functional groups to the protein. Lysine residues are often targeted due to their abundance and their ϵ-amine on its side chain. However, the fact that they are abundantly available makes site-specific labeling more difficult. As such, protein reactivity can be decreased. Alternatively, cysteines can be targeted as well. They have a thiol group in their side chain. Maleimide functionalities are commonly used to react with these side groups. However, in natural proteins, most thiol groups from cysteine are tied up in disulfide linkages and thus not freely available. Even if the thiol group can be targeted, this can lead to dimensional changes in the protein which affects the protein reactivity. Because of this, an extra cysteine residue is commonly incorporated in the protein via genetic engineering. Because of this, this strategy is not very straightforward [31].

N- and C-termini of the protein can be targeted as well. They have a few advantages above other targets. All linear polypeptide chains contain C- and N- termini. This way, a more general technique can be developed since it does not depend on the protein primary structure. Furthermore, the protein termini can be easily accessed. This way, extensive protein engineering can be avoided [31].

Different strategies exist to target the protein termini. Esser-khan et al. positioned a ketone on the protein C-terminus by means of expressed protein ligation (EPL). It is based on a naturally occuring process called protein slicing. Protein slicing is a multi-step process in which a protein undergoes intramolecular rearrangements where an internal sequence called an intein is extruded and the two lateral sequences (exteins) are joined together. This process gives rise to a thioester

intermediate. The general protein slicing mechanism is given in **Figure 1.5a**. In a first step, an S-N acyl shift occurs due to nucleophilic attack of the thiol group on the carbon from the carbonyl group. Next, another nucleophilic attack of another thiol group on the carbonyl group leads to transesterification where both exteins and the intein are still connected to eachother. Afterward, the intein is excluded and both exteins are joined together [33].

Based on this concept, the EPL strategy can be seen in **Figure 1.5b**. The first step is exactly the same as in the protein slicing mechanism; an S-N acyl shift occurs due to nucleophilic attack of the thiol on the carbon from the carbonyl group. Next, by addition of an external thiol, transesterfication occurs similarly as was explained for protein slicing. Next, this thioester undergoes native chemical ligation with an N-terminal cysteine from a synthetic peptide. This way, a semi-synthetic protein can be formed [33].

A disadvantage of this technique is the fact that protein engineering is often required [31]. By example, Esser-Khan et al. positioned an alanine-glycine pair to the N-terminus to aid the transamination reaction and a lysine residue was added to the C-terminus to assist cleaving from the intein after expression [34].

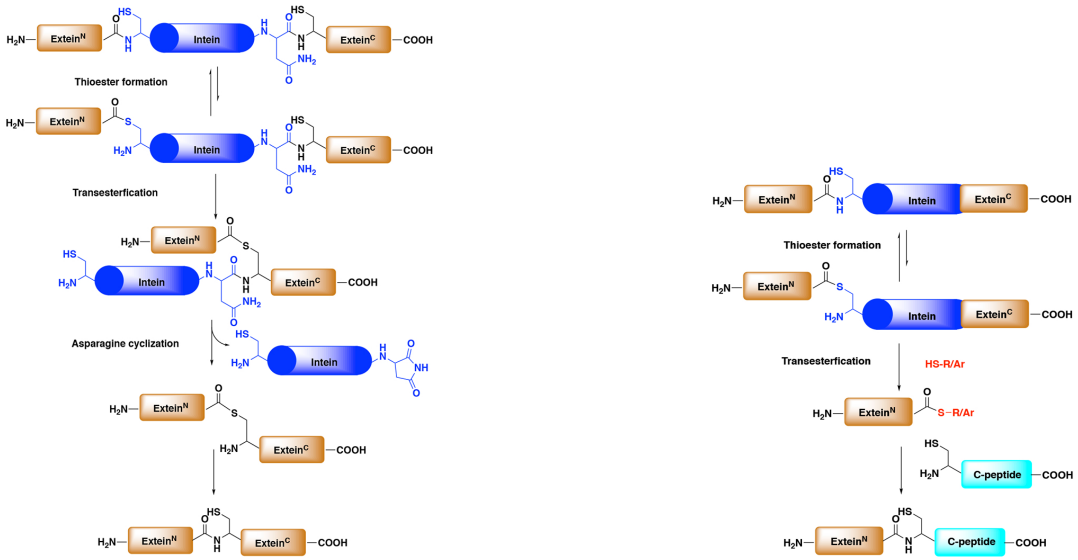

(a) (b)

Figure 1.5: (a)Working mechanism of protein slicing and (b) expressed protein ligation based on protein slicing [33]

Alternatively, it is also possible to alter the protein termini without any protein engineering. Slight differences in redox potential, reactivity and pK_a between the C-termini carboxylic acid and the carboxylic acid on glutamic/aspartamic amino acids and the N-termini and lysine side chains can direct the reaction towards the termini [31]. The basicity of the α-amine on the N-terminus (pK_a = 6-8) is significantly lower compared to the aliphatic amines on lysine residues (pK_a = 10.5). This can be ascribed to inductive effects of the nearby carbonyl group [35]. Because of this, the amines on the lysine residues are protonated and possess a positive charge while the α-amine on the N-terminus are unprotonated at low-to-neutral pH values [36]. This way, acylation or alkylation of the primary amine on the N-terminus is favored at these pH

values. Lower pH values lead to higher selectivity but can significantly decrease the conjugation yields, as such the pH value should be carefully selected [35].

This strategy was followed by Charpentier et al. [37]. They modified the protein N-terminus with a heterobifunctional crosslinker. This crosslinker was a PEG24 chain with a maleimide functionality on one end and a succinimidyl functionality on the other end. The crosslinker and the AFPs were incubated in a phosphate buffered saline (PBS) solution of pH 7.2 for 1 hour at room temperature. The pH of 7.2 allowed the selective reaction of the succinimidyl functionality with the primary amine on the protein N-terminus to form a stable amide bond. This way, an acylated product with a maleimide functionality is obtained, as can be seen on **Figure 1.6**. In a next step, these maleimide-activated AFPs can further react with functional groups on the surface. This strategy shows a relatively easy modification process without the need for any protein engineering. In addition, by carefully choosing the optimal pH, the reaction can be relatively selective toward the protein end-groups [35]. Since AFPs are tolerant toward end-group modification, this shows to be a promising strategy.

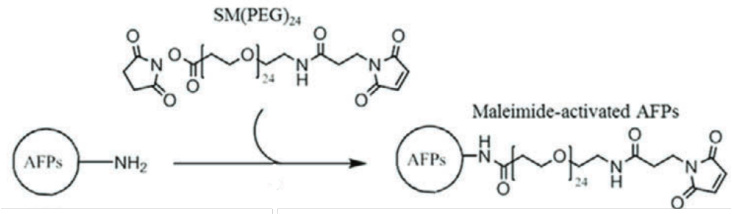

Figure 1.6: Reaction of maleimide-PEG24-succinimidyl with primary amine of protein [37]

1.4.2 Modification of surface

As described above, both the protein and the surface need to have compatible functional groups. In certain cases, the surface does not need to be modified [32], [38]. However, most approaches do require surface modification to incorporate these functional groups on the surface. Many different techniques exist to modify surfaces. However, hydroxylated and metal surfaces are often modified with siloxane chemistries [39], [40]. Silane coupling agents are commonly employed to modify many types of surfaces. In addition, they are commonly employed for biofunctionalization of the surface as well [41]. Silanes comprise a silicon atom to which an organic arm is connected. Typically, this organic arm terminates in a specific functional group which covalently links to another organic molecule. In addition, three silane-reactive groups are directly connected to the silicon atom. Often, these silane-reactive groups need to hydrolyse and form a silanol. This silanol is the highly reactive compound that is able to bind to inorganic or hydroxylated surfaces. The overall reaction mechanism is depicted in **Figure 1.7**. In a first step, the silane-reactive groups hydrolyse and form a silanol. Next, when the reaction occurs in solution, a polymer matrix is formed by condensation of the silanols. This polymer matrix is linked together by the -Si-O-Si- bonds. This growing silane network then reacts with the substrate -OH groups by the formation of hydrogen bonds. Finally, due to the presence of vacuum or heat, water is removed and another condensation reaction occurs. This way depositing the organosilane polymer coating to the surface. When immersing the surface in a silane solution (solution-phase deposition), this type of coating is obtained. The coating is not a monolayer and its thickness depends on the amount of water and concentration of silane coupling agent. Nonetheless, solution-phase deposition is generally the preferred method due to its simplicity. On the other hand, vapor-

phase deposition (chemical vapor deposition or molecular layer deposition) can also be used. With this technique, a repeatable silane monolayer can be deposited onto the surface [42].

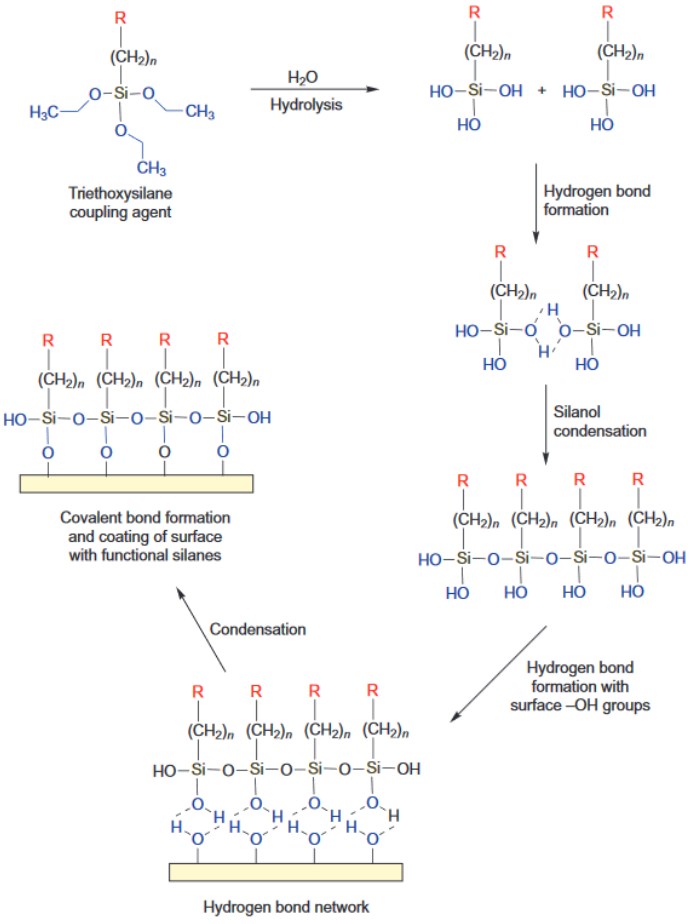

Figure 1.7: Deposition of a silane layer [41]

Charpentier et al. modified an aluminium surface using silane chemistry. In a first step, hydroxyl groups were introduced on the surface by immersion into a Piranha solution. Next, the samples were immersed in a silane solution for 30 minutes. This way, thiol groups were attached to the surface. These thiol groups further reacted with maleimide functionalities that were attached to the AFPs [37].

1.4.3 Effect of ice-binding proteins on freezing at the surface

Incorporation of AFPs onto the surface have a clear effect on freezing. However, the different types of AFP surfaces yield conflicting results. Gwak et al. showed a clear anti-icing effect of the AFP coating. The AFP coated sample clearly inhibits ice formation after three hours in a cold chamber [32]. Also Jeong et al. saw an anti-freezing effect. Ice formation was delayed up to 30 minutes on the AFP-coated samples. Compared to the uncoated samples, a seven fold increase in freezing time was detected [29]. On the other hand, AFP coatings developed by Charpentier et al. showed completely different results. The AFP-grafted samples sped up the nucleation process

as opposed to inhibiting it. By changing the energy barrier for critical ice embryo formation, ice nucleation was accelerated [37]. Kobashigawa et al. had already shown that ice-nucleating proteins can be converted into AFPs by reducing their size [43]. Charpentier et al. hypothesized that the opposite effect was seen. By forming a high density of AFPs on the surface, they could act as a template on which water could assemble leading to easier ice growth compared to bare aluminium [37].

O'brien et al. deposited INPs on a substrate. They found that INPs were able to freeze supercooled condensation two orders of magnitude faster compared to standard hydrophilic surfaces. In addition, by selectively deposition INPs, they were able to keep the hydrophobic regions dry and free of condensation, even below supersaturation conditions. This means that the hydrophilic INPs stripes with ice act as a siphon for all nearby moisture in the environment [12].

1.5 Ice-binding proteins in hydrogel

Except for directly immobilizing the AFPs on the surface, it is also possible to incorporate the AFPs in a coating. This technique is more durable compared to direct immobilization. Based on papers for biomedical applications, it is clear that proteins can be incorporated in gels. In addition, hydrogels with INPs have already been made. Hydrogels exhibit a relatively benign environment for proteins. Their hydrated network prolongs the protein activity and protects against proteolytic degradation. As such, investigating AFP functionalitiy in a hydrogel is a first step toward the development of an actual coating with AFPs.

Recently, gels have drawn a lot of attention due to their potential for inhibiting ice nucleation, propagation and minimizing ice adhesion [7]. When a solid material has at least one strongly crosslinked material and one liquid, it is classified as gel. Both hydrogels and ionogels have the ability to depress the freezing point [44]. However, in this study, the focus lies on protein-hydrogels.

1.5.1 Protein-hydrogel incorporation technique

Proteins have been widely incorporated in hydrogels for drug release purposes. As such, different strategies have been explored. In general, proteins are loaded inside a hydrogel in three different ways: physical loading, adsorption/affinity interactions and chemical linking.

1.5.1.1 Physical loading

Physical loading can be understood as follows. A protein can be kept in the hydrogel by the hydrogel network if the hydrogel mesh size is smaller than the protein size. This way, the protein does not require any modification. As such, this technique is relatively simple compared to other incorporation approaches. The protein can be simply mixed with the hydrogel forming protein solution. This approach was followed by Wang et al. [33]. INPs were mixed together with the monomers, crosslinking agent and visible light initiator. Compared to INPs (110-180 kDa [45]), AFPs are relatively small (6 kDa). Due to their small size, AFPs might leak out of the hydrogel network with this approach. As such, this approach is feasible for INPs but not for AFPs.

1.5.1.2 Adsorption/affinity interactions

Alternatively, electrostatic interactions, hydrogen bonding and van der Waals forces cause adsorption of the protein to the hydrogel [46]. Similar as for the surface approach, these interactions are reversible and relatively unstable. On the other hand, affinity hydrogels have been developed as well. The strategy is based on the mechanisms by which bioactive molecules are stored and presented in the extracellular matrix [46]. Affinity hydrogels are equipped with specific ligands for protein recognition. These ligands physically immobilize the protein in the hydrogel. This way, protein uptake and release can be carefully controlled [47]. During this thesis, protein release is not required. As such, this approach is not employed.

1.5.1.3 Chemical linking

Finally, proteins can also be covalently linked to the hydrogel. Compared to physical entrapment and non-covalent/affinity reactions, covalent attachment generates superior hydrogel mechanical properties. In addition, the protein-hydrogel is more stable and controlled [46].

This strategy has many similarities with direct immobilization of the protein on the surface. The reaction conditions should maintain the protein structure and function. As such, moderate temperature and aqueous reaction conditions are required. Furthermore, the functional groups of the protein that will be targeted should be chosen with great care since random immobilization can alter protein conformation or can sterically block the protein active site. In most cases, the proteins are modified following similar strategies as were discussed in section 1.4.1. A few commonly employed chemistries to develop protein-hydrogels are photo-immobilization and click-chemistries.

A) Photo-immobilization

Protein hydrogels can be made by using a photoreactive heterobifunctional crosslinker. In these cases, one end of the crosslinker reacts with the desired functional group of the protein while the other end is photoreactive. A commonly used photoreactive heterobifunctional crosslinker is N-sulfosuccinimidyl-6-(4 -azido-2 -nitrophenylamino) hexanoate (sulfo-SANPAH) which has a photoreactive phenyl azide group and an amine reactive succinimidyl group. Even though photoimmobilization of proteins appears to be an attractive technique (e.g. control over reaction kinetics), it has several important disadvantages. The irradiation of the proteins with UV and the formation of radicals might have a significant impact on the protein bioactivity. As such, reaction conditions, photoinitiator concentration and type and UV exposure time should all be carefully considered [46].

B) Click-chemistries

Similar to the surface approach, click-chemistry is also commonly employed for the development of protein hydrogels. Generally speaking, click-chemistries occur in benign reaction conditions with high yield and specificity [46].

The copper-ion-catalyzed azide-alkyne cycloaddition reaction is a cycloaddition reaction between azide and alkyne catalyzed by copper ions with the formation of 1,2,3-triazoles. Without the catalyst, the reaction occurs slowly and non-selectively. However, by the introduction of the catalyst, the reactions occurs seven orders faster and is much more selective. As such, it is a straightforward technique to develop hydrogels. One major drawback is the fact that the copper catalyst is biologically toxic. To overcome this, strain-promoted azide–alkyne cycloaddition

reactions were introduced which do not require a copper catalyst [46].

Also thiol-ene click reactions are commonly used in biologocial applications due to several reasons. First off, the reaction occurs rapidly under mild reaction conditions and in an aqueous environment which is compatible with biological specimen. Next, the reaction is well documented with nearly 100% conversion and thorough knowledge about the reaction mechanisms and products. Finally, thiol and alkene groups can be relatively easily incorporated on macromolecules. Because of these reasons, various protein-hydrogels have been made with thiol-ene chemistry. Thiol-ene ractions can occur by two different mechanisms: Thiol-Michael reactions and radically mediated thiol-ene reactions [48].

Radically-mediated thiol-ene reactions require mild aqueous conditions and the presence of an initiator to generate radicals. These radicals attack a thiol group with the formation of a thiyl radical. In a next step, this thiyl radical attacks the alkene double bond (C=C) which leads to a thiol-ene addition and the production of a new thiyl radical (**Figure 1.8 B**). Even though this reaction gives control over the polymerization, the production of a radical might hamper the protein activity. Alternatively, thiol-Michael reactions occur at room temperature, in mild aqueous reaction conditions without the requirement of radicals. A proton is abstracted from a thiol by a base which forms a thiolate anion. This anion acts as a nucleophile and attacks the alkene to form a carbon-centered anion intermediate. This intermediate abstracts a proton from a conjugated base, this way regenerating the original base (**Figure 1.8 A**). The reaction occurs rapidly under mild aqueous conditions, does not require radicals or catalysts and does not form any by-products [48]. For these reasons, it is a very attractive option for the development of protein-hydrogels.

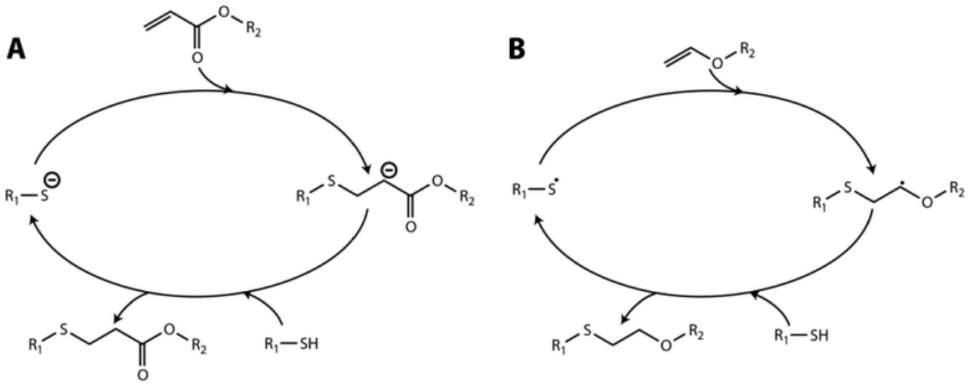

Figure 1.8: (A) Thiol-Michael reaction and (B) radically mediated thiol-ene reaction [48]

1.5.2 Hydrogel freezing point depression

A hydrogel mostly consists of water and under normal circumstances its freezing point lies around 0°C. However, it can be tuned in different ways (by incorporating additives or by modifying the polymer networks) which eventually leads to hydrogels that remain soft below this point. These types of gels are called anti-freezing hydrogels [44].

Solutes are able to decrease the freezing temperature of water since they interfere with the ice crystal formation process. By example, salt is often used to melt ice on roads as it depresses the freezing point of water. As such, additives can be added to hydrogels to obtain similar effects. Different types of additives can be added, such as glycerol, ethylene glycol or salts

[49]. Li et al. fabricated electrolyte hydrogels by infusing sodium chloride into the polymer network. Freezing was delayed up to temperatures as low as -48.4°C. Furthermore, ice adhesion was greatly reduced which makes self-removal of ice possible. Nonetheless, additives have the ability to dissipate from the hydrogel, thus rendering them useless after some time since their anti-freeze abilities will decrease with decreasing additive concentration [50].

Freezing point depression can also be obtained in a different way. Many hydrogel properties are related to the interaction between water molecules and the polymer network. Due to these interactions, water in hydrogels can be roughly divided in freezable water and non-freezable water. Freezable water can be further subdivided in freezable free and freezable bound water. Freezable free water is completely unbound water which has the same properties as deionized water [51]. As such, it freezes around 0°C. Freezable bound water also freezes, albeit at a much slower rate compared to freezable free water. Its ice crystal growth rate is around ten times slower compared to freezable free water [52]. On the other hand, non-freezable water is very tightly bound to the polymer and does not freeze since it is unable to arrange itself into the ice crystal structure. As such, by altering the type of water in a hydrogel, the freezing point can be altered as well.

Wang et al. evaluated the effect of INP concentration and hydrogel crosslinking density on the fraction of non-freezable and freezable water and on the ice nucleation temperature. The INP concentration greatly influenced the ice nucleation temperature. By increasing the INP concentration from 1×10^5 to 15×10^5, the ice nucleation temperature increased from -16.1 to -8.3 °. On the other hand, by decreasing the crosslinking density from 0.6% to 0.01% mol/cm^3, the fraction of freezable water in the hydrogel increased from 50% to 72%. However, they did not see a significant influence on the ice nucleation temperature [33]. On the other hand, Huang et al., did find that the freezing point of a hydrogel decreased with crosslinking density [53]. By increasing the amount of crosslinks, movement of water molecules is restricted. This leads to an increased fraction of non-freezable water [44].

He et al. recognized that also AFPs have the ability to interact with water and are able to tune the properties of interfacial water. This can lead to controlled ice nucleation, growth and adhesion [7]. To illustrate this, **Figure 1.9** shows the structure of interfacial water on the NIBS of an AFP. As can be seen, the protein binds the water molecules in a disordered fashion to its surface, this way hindering ice formation [30].

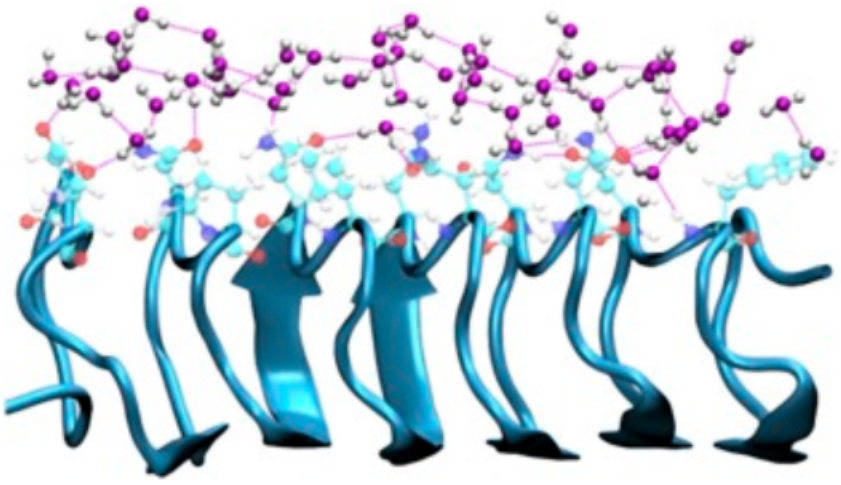

Figure 1.9: Molecular dynamics simulation of disordered interfacial water on NIBS of an AFP [30]

Based on this concept, He et al. grafted hydrophobic polydimethylsiloxane (PDMS) chains on a hydrophilic polyelectrolyte network containing counterions. This way, the interfacial water can be controlled in a similar way as AFPs. It was shown that the hydrogel inhibits ice nucleation since structural water-to-ice transitions are hindered. Moreover, this interfacial water can also act as a lubricating layer, decreasing ice adhesion. Furthermore, both ion specificity and hydrophobicity effectively restricted the ice propagation rate [7].

1.6 Scope of master thesis

Up until now, current papers have not given much attention toward AFPs as anti-icing material. To be able to gain a greater understanding about the AFPs, their behaviour is examined within different environmental condition.

Current papers have only evaluated the behaviour of AFPs directly attached to the surface. However, many interesting aspects remain undiscovered. Based on current research, several interesting aspects can be further investigated:

- **Protein concentration**
  In liquid, it is known that the TH activity is related to the concentration of AFP in solution. However, the effect of different concentration levels of AFP on the surface has not yet been investigated. Up until now, each paper used a different amount of AFP concentration to develop their surface. As an example, Charpentier et al. used 1.4 mg/ml AFP in the solution while Gwak et al. and Jeong et al. used 1 mg/ml [37], [32], [29]. Alternatively, Esser-khan et al. used 25 mg/ml [34]. Nonetheless, the retention level is not determined in most papers, thus the actual amount of AFPs on the surface is unknown. In extension, comparison is further complicated due to the fact that different cooling experiments and different AFPs were used in all papers. Furthermore, the effect of different INP concentrations has also not been studied.
- **Surface chemistry**
  Esser-khan et al. found that ice formation started in the bulk where AFPs cannot reach [34]. As such, it can be interesting to tweak the surface in such a way that AFPs are not

only located on the surface but also more in the bulk liquid by means of dangly chains of various sizes. This way, AFPs might be able to penetrate deeper into the liquid and further hinder ice formation. In addition, depending on the length of the dangly chain, more freedom can be given to the protein. When attached to dangly chains, the protein might be able to move more freely and might be able to mimic its working mechanism as in liquid. In comparison, Inamori et al. determined the optimal surface chemistry for peptide immobilization in on-chip cSrc phosphorylation. They also hypothesized increased phosporylation efficiency due to better accessability of the cSrc and increased peptide mobility. PEGylated peptides indeed showed improved phosporylation [54].

To better understand the working mechanism of ice-binding proteins, it is useful to investigate their behaviour when attached to the surface. However, in a more practical situation, the proteins would not be directly attached to the surface but would be embedded in a coating. To gain insight in the behaviour of ice-binding proteins within polymeric systems, ice-binding proteins can be incorporated in hydrogels. This was already achieved by Wang et al. who incorporated INPs in a hydrogel and studied the hydrogel properties [33]. However, the effect of the proteins on the non-freezable and freezable water was not investigated. In addition, the current knowledge about the behaviour of AFPs in hydrogels is very limited as well.

As such, the scope of the master thesis can be defined as follows:

1. Gain a better understanding of protein functioning on the surface
2. Investigate the protein functioning within a polymeric environment

To gain a better understanding of the protein functioning on the surface first a viable attachment technique needs to be found. Next, the protein concentration, crosslinker chain length and the difference between AFPs and INPs will be investigated.

To investigate the protein behaviour within a polymeric system, proteins will be embedded in a hydrogel. Again, a viable incorporation technique needs to be found. Next, the different types of water, protein concentration and differences between AFPs and INPs will be investigated.

An overall schematic of the master thesis can be found in **Figure 1.10**.

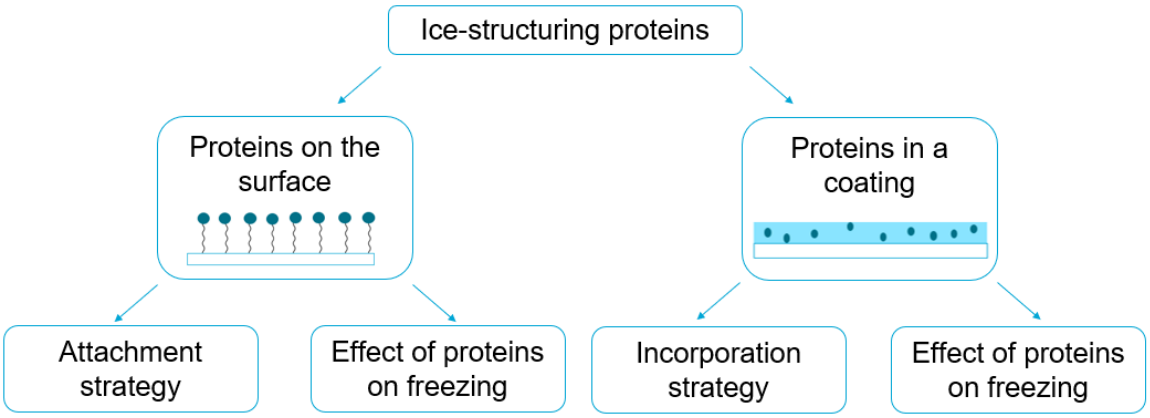

Figure 1.10: Schematic overview of master thesis

Chapter 2

Ice-binding protein behaviour on the surface

In a first step, ice-binding proteins are attached to the surface to gain a better understanding of their behaviour at the surface. The first section describes the materials and methods used to produce, characterize and test the protein surfaces. The second chapter describes and elaborately discusses the found results.

2.1 Materials and methods

2.1.1 Anti-icing surface synthesis

2.1.1.1 Materials

The sodium hydroxide (NaOH) pellets, 3-mercaptopropyltrimethoxysilane (MPTS), methanol, dimethylsulfoxide (DMSO), hydrogen peroxide (H_2O_2), sulphuric acid (H_2SO_4), nitric acid (HNO_3), fumaric acid and the maleimide-$PEG_{2/12/24}$-succinimidyl ester linker (Mal-PEG2/12/24-NHS) were bought from Sigma-Aldrich. The AFPs (type III from *Marcrozoarces americanus*) were obtained from A/F Protein inc.. The INPs (from *Pseudomonas syringae*) were purchased from Snomax inc..

2.1.1.2 Surface functionalization

In a first step, AA2024 samples of 2cm x 2cm x 3mm (length x width x thickness) are grinded with 1000, 2000 and 4000 grit size. They are subsequently polished with diamond paste of 3 μm and 1/4 μm. Next, the samples are washed with aceton. To activate the samples, three different activation routes were evaluated:

1. Acid pretreatment: A Piranha solution is made by adding a 3:1 ratio of H_2SO_4:30 wt% H_2O_2. Next, AA2024 samples are immersed in the Piranha solution for different treatment times (5 minutes and 15 minutes).
2. Alkaline pretreatment 1: AA2024 samples are submerged in a 2M NaOH solution for 6 minutes. Afterward, a desmutting step is perfomerd with HNO_3
3. Alkaline pretreatment 2: AA2024 samples are submerged in a 2M NaOH solution for different immersion times (5 seconds, 10 seconds). No desmutting step is performed.

Finally, all samples from each pretreatment are rinsed with DI water and dried in an oven at 100°C for 30 minutes.

In a next step, a 4 wt% silane solution is prepared by adding 4 ml of MPTS to 6 ml of water in 90 ml methanol which was used as a solvent. The silane solution is stirred for 24 hours to assure sufficient hydrolysis of the MPTS. Afterward, samples are submerged in the silane solution for different immersion times (30 minutes, 1 hour, 1.5 hour and 2 hours). Next, the silane treated AA2024 samples (AA2024-SH) are rinsed in methanol and dried in vacuum for 30 minutes. Finally, the samples are cured for 1 hour at 100°C.

2.1.1.3 Protein modification

In a first step, a 0.1 mM protein solution in PBS (pH of 7.4) is prepared. Next, a linker stock solution (250 mM) is prepared by mixing Mal-PEG2/12/24-NHS with DMSO. Finally, the linker solution is added to the protein solution in tenfold molar excess (4 μl of linker stock solution per ml of protein solution). The mixture is stirred for 1 hour to obtain a good reaction between Mal-PEG2/12/24-NHS and the protein. Finally, the excess linker is removed from the solution by centrifuging thrice for 5 minutes at 4400 rpm. This way, Mal-PEG2/12/24-NHS-modified AFPs and INPs (Mal-PEG2/12/24-AFPs/INPs) are obtained.

2.1.1.4 Protein-surface attachment

Protein-modified surfaces are prepared by immersing AA2024-SH samples for four hours in protein solutions with specific type of protein, type of linker and protein concentration. All different types of protein solutions are listed in **Table 2.1** and **Table 2.2**. After immersion, the samples are rinsed with DI water and dried in a vacuum overnight to remove any excess water.

For each sample that is made with the protein solutions as listed below, another sample is made with the exact same protein solution. To this protein solution a fixed amount of fumaric acid is added (10 fold molar excess of the protein). Aliquots of these protein solutions are taken at the start and the end of immersion and evaluated with H-NMR to get a quantitative idea of the amount of proteins on the surface.

Table 2.1: Different types of AFP protein solutions used for protein-surface attachment

	AFP-solution 1	AFP-solution 2	AFP-solution 3	AFP-solution 4
AFP concentration	**2.5** mg/ml	**5** mg/ml	**2.5** mg/ml	**2.5** mg/ml
linker	Mal-PEG**12**-NHS	Mal-PEG**12**-NHS	Mal-PEG**2**-NHS	Mal-PEG**24**-NHS

Table 2.2: Different types of INP protein solutions used for protein-surface attachment

	INP-solution 1	INP-solution 2
INP concentration	**2.5** mg/ml	**5.0** mg/ml
linker	Mal-PEG12-NHS	Mal-PEG12-NHS

2.1.2 Characterization techniques

2.1.2.1 Water contact angle (WCA) measurements

WCA measurements evaluate the surface wettability by measuring the contact angle between the surface of interest and a liquid. When the liquid is strongly adsorbed to the surface material (high surface energy), the droplet completely spreads out over the surface. Since the WCA is the angle between a tangent to the liquid surface and the solid surface, the WCA will therefore be 0°. Up to a WCA of 90°, materials are called hydrophilic. On the contrary, WCA higher than 90° are considered hydrophobic surfaces. When the WCA reaches over 150°, the droplet is nearly completely round and the material is called superhydrophobic.

Since WCA measurements give an indication of the wettability and subsequently the surface energy of the surface, they can give an indication of chemical changes on the surface.

During this master thesis, a Tensiometer KSV CAM 200 (KSV instruments Ltd., Finland) was used as a qualitative approach to confirm the chemical changes after the surface activation and silane sol-gel step. Three 5μl DI water droplets were placed on the surface. To determine the WCA, the average of these three measurements was taken.

2.1.2.2 Confocal microscopy

To investigate the surface microstructure after activation, confocal microscopy was used. This is a basic non-destructive imaging technique. For this master thesis, a Keyence VK-X1000 with magnification 16x was used.

2.1.2.3 Fourier transform infrared spectroscopy (FT-IR)

FTIR is a non-destructive technique to identify the chemical composition of different types of samples. Simply said, IR radiation is passed through a sample. Some of this radiation will be absorbed by changing the vibrational energy in the chemical bonds in the sample. Depending on the molecules and types of bonds in the sample, different IR wavelengths will be absorbed. This way, a unique spectrum is created which can be used to identify the chemical composition of the sample.

In this master thesis, FTIR is used for multiple purposes. First off, the presence of proteins on the surface is confirmed with FTIR. Next, the reaction between Mal-PEG2/12/24-NHS and AFPs/INPs is quantified with FTIR measurements at different time points during the reaction. For all measurements, a Spectrum 100 FT-IR Spectrometer (Perkin Elmer) is used to produce a spectrum from 4000 to 500 cm^{-1}. The average of 32 scans is taken.

2.1.2.4 Raman spectroscopy

Raman spectroscopy is a non-destructive chemical analysis technique. A Raman spectrum of a sample is generated which gives more information about the surface chemistry of the sample.

When monochromatic laser light is directed to a sample, a part of the light will be scattered. This scattering can be divided in Rayleigh and Raman scattering. Molecules have different vibrational levels with specific energy differences. Photons can excite molecules to a virtual state by the delivery of energy that depends on the laser frequency (μ_L). This molecule can fall back to its original state by releasing a photon with the same frequency (μ_L). This is called Rayleigh

scattering. Alternatively, if the emitted photon has a different frequency than the incident light, it is called Raman scattering. This frequency difference is called the Raman shift and can act as a fingerprint for the molecule.

In this study, Raman microscopy is used to quantitatively investigate chemical changes on the surface after the surface activation and silane sol-gel step. A Renishaw inVia Raman microscope with laser wavelength of 532 nm is operated. For each measurement point, 16 accumulations were made at 10% laser power with an exposure time of 60 seconds.

2.1.2.5 Proton nuclear magnetic resonance (^1H-NMR)

^1H-NMR is a non destructive spectroscopy method to determine the structure of organic compounds. It detects the sample's nuclei. In the case of ^1H-NMR, the ^1H will be detected in the sample. The overall working mechanism goes as follows.

The nucleus contains protons and neutrons, which have an intrinsic property called spin. For nuclei where the spin is non-zero (in the case of hydrogen nuclei, the spin is 1/2), a magnetic moment is induced. This way, the nucleus will act as a small magnetic bar. Under normal conditions, each of these magnets are randomly oriented. However, when an external magnetic field (B_0) is applied to it, the different nuclei will align with (α state, low energy state) or opposite to (β state, high energy state) the magnetic field and start to precess. Understandibly, most of the nuclei will be aligned with the external magnetic field.

To be able to get information from ^1H-NMR, a spin flip from the low energy state to the high energy state needs to be achieved. This requires a certain amount of energy that can be described as:

$$\Delta E = h\nu \tag{2.1}$$

where ΔE is the energy difference between the two states, h is Plank's constant and ν is the frequency given as:

$$\nu = \frac{\gamma B_x}{2\pi} \tag{2.2}$$

where γ is the gyromagnetic constant and B_x is the applied magnetic field for a specific nucleus. This way, the nuclei will be flipped to a higher energy state when a radiofrequency pulse is applied with the corresponding frequency. Due to the electron density distribution, each nucleus will experience a different magnetic field. Nuclei within an electron rich environment, experiences a lower magnetic field compared to nuclei within an electron poor environment. As such, the energy difference between the α and β energy level will be lower for the shielded nuclei. Because of this, a lower frequency for the radiofrequency pulse is required to excite the nucleus. This way, a spectrum can be formed where different hydrogen nuclei give different peaks at various frequencies depending on their chemical environment.

For this master thesis, ^1H-NMR (400 MHz Agilent NMR, Brüker) was used for various purposes. After the reaction between Mal-PEG2/12/24-NHS and the proteins, the samples are centrifuged to remove the byproduct and the excess linker. To confirm that centrifuging indeed removes these compounds, the supernatant after each centrifuging step was evaluated with ^1H-NMR. In addition, to get a quantitative idea of the amount of proteins on the surface after immersion, aliquots of the protein solution with fumaric acid at the start and at the end of immersion were used for analysis with ^1H-NMR. The average of 32 scans was taken with a relaxation delay of 5 seconds and a pulse angle of 45 degrees.

2.1.2.6 Freezing tests

To determine the anti-icing properties of the protein surfaces, freezing experiments are performed. The overall freezing set-up can be found in **Figure 3.3**. A sample is placed on top of a liquid-cooled cold plate (TECA LHP-300CP) (**Figure 3.3 1**). This plate is subsequently powered by a 11.5 DC voltage source (**Figure 3.3 2**). This way, all samples are cooled by 10°C/min. A FLIR A655sc infrared camera with a close-up IR lens (1.5 magnifying factor and 25 m resolution) records the top view of the sample (**Figure 3.3 3**).

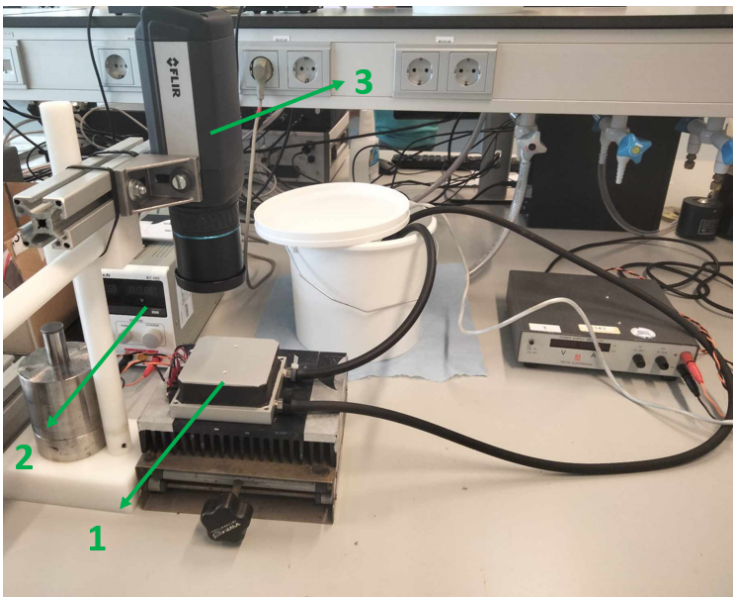

Figure 2.1: Set-up of freezing experiments

From the start of each cooling test, a timer records the time up until the moment of the first freezing event that can be detected by the IR camera. This way the freezing onset time (t_{fo}) is obtained. To get the the freezing onset temperature (T_{fo}), the average temperature on each sample is plotted with the FLIR tools program. To obtain the correct temperature readings form the IR camera, the emissivity of the surfaces is put to 0.4 (emissivity of oxidized aluminium) with the FLIR tools program. This way, a time vs. average temperature is plotted. An example of such a graph can be found in **Figure 3.4**. The temperature on the graph where the freezing event starts (indicated with a rise in temperature) is recorded as the T_{fo} of the sample. All measurements were taken with a relative humidity between 35 and 41%.

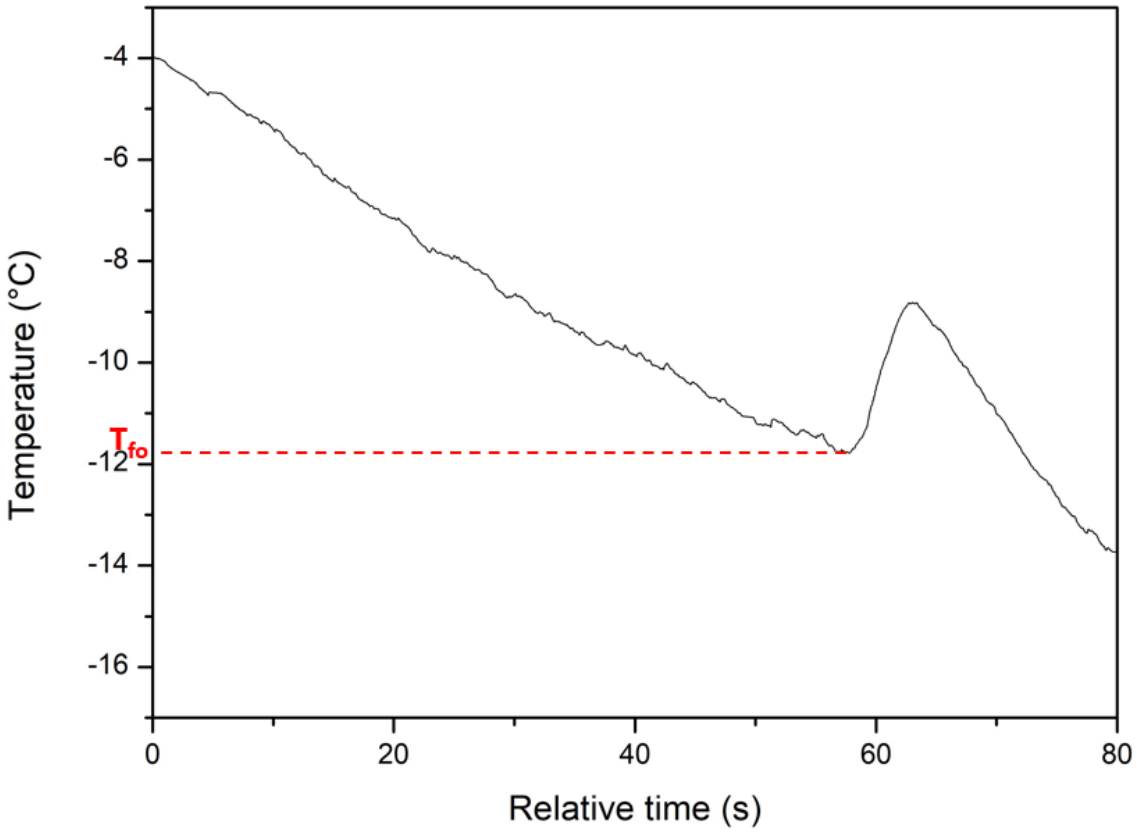

Figure 2.2: Example of relative time vs. average temperature graph obtained for one sample from the IR data

2.1.2.7 Calculation of freezing front propagation

From the IR videos, the freezing front propagation speed (v_{ffp}) is calculated. From each video, 4 different frames are taken and the time of each frame is noted. Since the framesize of the camera is known (16mmx12mm), the pixels in the image can be correlated to a distance in mm. Using this information, the distance between the freezing front at subsequent frames is measured using ImageJ (**Figure 2.3**). This way, the average v_{ffp} can be easily found by dividing the measured distance between the locations of the freezing fronts at subsequent frames with the known time between frames.

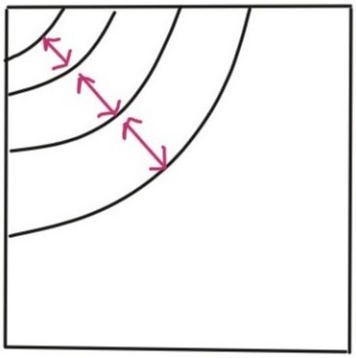

Figure 2.3: Calculation of v_{ffp}

2.1.2.8 Evaluation of condensation and frost growth

To evaluate the condensation and frost growth on the different samples, two digital USB microscopes are mounted around the freezing set-up: a Dino Lite microscope and a Celestron handheld digital microscope Pro. The Dino Lite microscope was used to capture the top view of the sample while the side view was recorded with the Celestron microscope. The set-up can be found in **Figure 3.5**

Figure 2.4: Camera set-up to record condensation and frost growth

2.1.2.9 Ice adhesion set-up

To determine the ice adhesion of the different surfaces, samples are subjected to a cold air stream (10°C) with a wind velocity of 5 m/s. The top view of the surface is recorded with a Dino Lite

microscope. A picture is taken right before subjecting the samples to the air stream and after subjecting the samples to the air stream for 15 seconds.

2.2 Results and discussion

2.2.1 Surface activation

A surface activation treatment is performed to incorporate hydroxyl functionalities to the surface. The effect of both acid and alkaline activation treatments on AA2024 were investigated. Piranha solution, NaOH/HNO_3 and NaOH treatments are known to increase the hydrophilicity of the surface. As such, they were all evaluated to determine the optimal activation treatment.

2.2.1.1 WCA measurements

WCAs vary depending on surface energy. This way, WCA measurements can give a first indication of changes in surface chemistry.

In a first step, samples were activated using a Piranha solution, similar to Charptentier et al. [37]. A Piranha solution is a mixture of H_2SO_4 and H_2O_2. It is a strong oxidiser and is able to hydroxylate different surfaces, making them hydrophilic. Polished AA2024 was immersed in a Piranha solution for 5 minutes (AA2024-OH-Pir5). As can be seen on **Figure 2.6**, the WCA for AA2024-OH-Pir5 did not change significantly compared to untreated polished AA2024. For this reason, the samples were immersed for a significantly longer time (15 minutes) (AA2024-OH-Pir15). However, even after 15 minutes, the WCA only went down by around 10°. Nazarov et al. [55] investigated the effect of acidic Piranha solutions on a titanium surface. Chemical etching by Piranha solution is a complicated phenomenon involving multiple processes such as material removal, oxidation and surface passivation. All these processes are dependent on the etching medium (e.g. difference in ratio between H_2SO_4 and H_2O_2) and reaction conditions (temperature, time,...). As such, very different interactions can occur at the surface at different time scales. If the reaction conditions or the H_2SO_4:H_2O_2 ratio were not optimal during the tests, this might explain the limited effect of the Piranha solution. In addition, Boekerche et al. [56] evaluated the effect of alkaline and acidic solution on aluminium. It was found that alkaline NaOH solutions more rapidly and effectively attacked the aluminium compared to acidic solutions such as H_2SO_4 which might also explain the limited effect of the Piranha solution on the aluminium surface. Up until now, the exact reaction mechanism between sulfates and aluminium (dissolution) is not well understood. It has been reported that doubly charged sulfate ions have a higher adsorptive affinity for adsorbed water and the aluminium surface compared to single-charged ions. Due to the fact that they are adsorbed to the metal surface, they might hinder further reaction between the aluminium surface and the solution. As such, the sulfates may retard the effect of the Piranha solution [56].

As was described in the previous alinea, NaOH solutions have been shown to have a rapid effect on aluminium. In addition, immersion of aluminiun in an NaOH solution is a commonly employed alkaline etching treatment. A similar strategy as Ahmadi et al. was followed [57]. In a first step, the samples were immersed in a 2M NaOH solution for 6 minutes. Afterward a desmutting step with HNO_3 was performed (AA2024-OH-NaOH/HNO3). WCA results for the AA2024-OH-NaOH/HNO3 samples show that the surface became significantly more hydrophilic after NaOH/HNO3 treatment.

Finally, a short dipping process of aluminium in a NaOH solution was also investigated. Samples were immersed for 5 (AA2024-OH-NaOH5s) and 10 seconds (AA2024-OH-NaOH10s) in a 2M NaOH solution without desmutting step. After 5 seconds, the WCA already shows similar values as for the AA2024-OH-NaOH/HNO3 samples. After ten seconds, the sample shows a

WCA around 36°, meaning that the simple NaOH dipping process successfully activates the aluminium samples. Similar results were obtained by Hu et al. [58]. They immersed AA2024 in a 1M NaOH solution and found a WCA of 56°. The increase in wettability was mostly ascribed to the removal of contaminants and the formation of a thin hydroxide layer. Huang et al. [59] describe the formation of the aluminium hydroxide layer as follows. Once aluminium comes into contact with an NaOH solution, an etching reaction occurs that produces hydrogen gas and sodium aluminate as follows:

$$2Al + 2NaOH + 2H_2O \longrightarrow 2NaAlO_2 + 3H_2 \tag{2.3}$$

In addition, native oxides on the aluminium (Al_2O_3) can also react with NaOH and form sodium aluminate as follows:

$$Al_2O_3 + 2NaOH \longrightarrow 2NaAlO_2 + H_2O \tag{2.4}$$

This sodium aluminate is a water soluble salt and further hydrolyzes to form aluminium hydroxide ($Al(OH)_3$):

$$NaAlO_2 + H_2O \longrightarrow NaOH + Al(OH)_3 \tag{2.5}$$

This way, a layer of $Al(OH)_3$ can be deposited on the aluminium surface, making it more hydrophilic [59]. This can be seen in **Figure 2.5**.

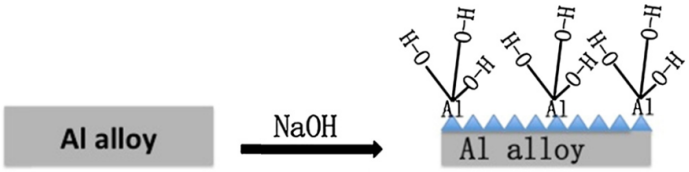

Figure 2.5: Deposition of a $Al(OH)_3$ layer after NaOH treatment [59]

This was further confirmed by Munoz et al. [60] who modified AA2024 by immersion in NaOH. XPS analysis showed that Al-OH was present on the surface of the aluminium. As such, due to the increase in hydrophilic groups on the surface, the decrease in WCA can be explained.

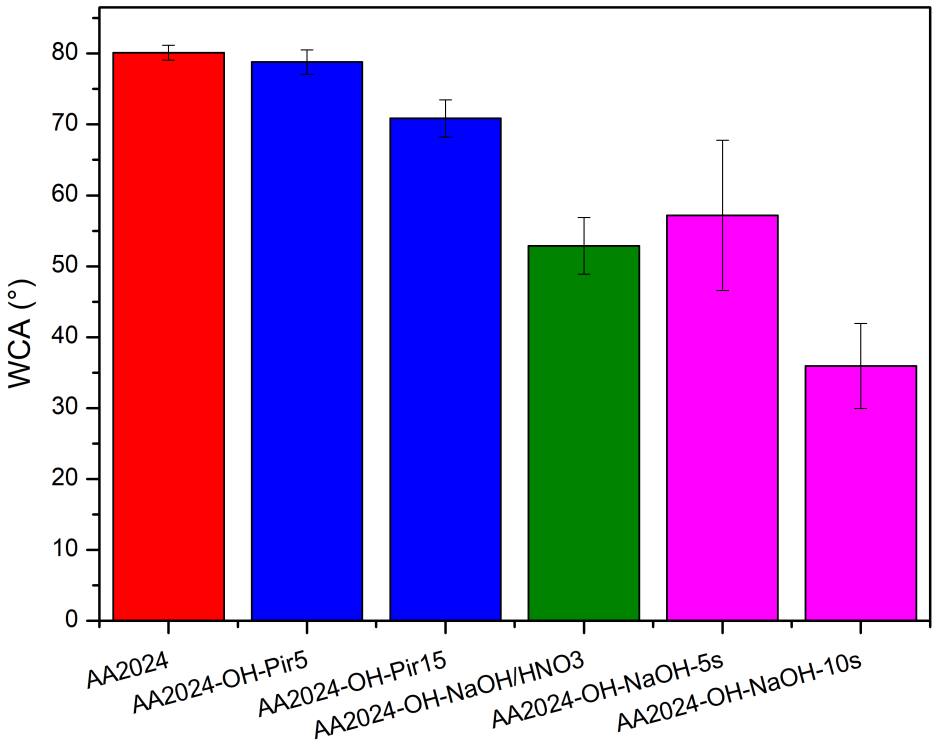

Figure 2.6: WCA of untreated polished AA2024 and various activation treatments

2.2.1.2 Confocal microscopy

Both alkaline and acid etching are aggressive activation treatments. To evaluate the effect of the activation treatment on the sample microstructure, samples were subjected to confocal microscopy

Evaluating **Figure 2.7 A**, untreated polished AA2024 clearly shows the presence of intermetallics (IMs). This follows logically from the fact that AA2024 has different alloying elements such as Cu, Mg, Mn, etc.. Because of this, AA2024 contains a large variety of different IMs. Generally, the IMs can be classified in (a) particles with active elements like magnesium and (b) particles with elements that are more noble than aluminium (e.g. copper) [61]. The most prevalent IM compositions in AA2024 include the S phase (Al_2CuMg), Ω phase, Al-Cu-Fe-Mn-low Si and Al-Fe-Si-Mg [62].

After a 5 minute immersion in Piranha solution (**Figure 2.7 B**), pitting corrosion due to dealloying or particle detachment due to cathodic undermining can be detected [61]. After 15 minutes immersion (**Figure 2.7 C**), corrosion can be clearly detected around the IMs. This might be understood as follows. Copper is one of the most important alloying elements in AA2024 since it increases the alloy strength. However, it also leads to decreased corrosion resistance of the alloy. Since copper is more noble compared to aluminium, IMs with copper lead to a strong galvanic coupling between the IM and the matrix. As such, preferential and accelerated corrosion of aluminium around these IMs can be detected [63].

The AA2024-NaOH/HNO3 samples also shows a significant effect of the activation treatment on the aluminium microstructure (Figure 2.7). Similar to the AA2024-OH-Pir5/15 samples, pitting corrosion after NaOH/HNO3 treatment is prevalent as well. On the other hand, a shorter NaOH treatment was performed without any desmutting step. From **Figure 2.7 E** and **F**, it is clear that shorter NaOH immersion time results in a significantly smaller effect on the aluminium microstructure.

Based on the confocal images, the shortest immersion time (5s) in NaOH led to the most limited effect on the aluminium microstructure. However, also 10s immersion led to a fairly unchanged surface. Furthermore, WCA results showed that AA2024-OH-NaOH-10s led to the smallest WCA. Thus these samples are the most hydrophilic with the most amount of hydroxyl groups. Since the amount of hydroxyl groups is crucial for the further experiments, the 10 second immersion in NaOH was chosen as optimal activation treatment.

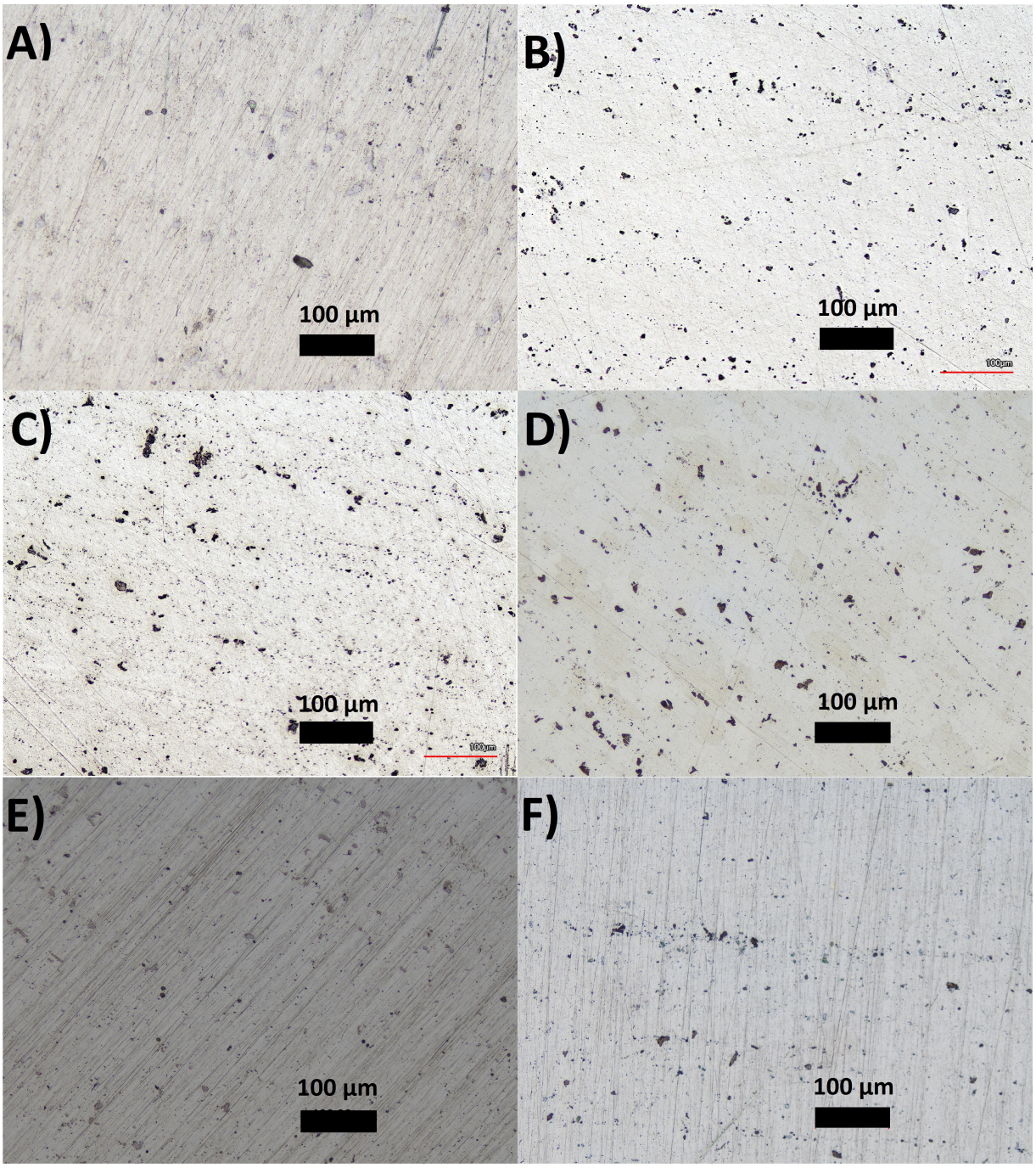

Figure 2.7: A) Untreated polished AA2024, B) AA2024-OH-Pir5, C) AA2024-OH-Pir15 and D) AA2024-OH-NaOH/HNO3, E) AA2024-OH-NaOH5s and F) AA2024-OH-NaOH10s

2.2.2 Silane sol-gel coating

After increasing the hydroxyl content on the surface, the samples are coated by a silane sol-gel coating with hydrolyzed MPTS. Samples were immersed in the hydrolyzed MPTS solution for 30 minutes and 2 hours to find the optimal immersion time.

2.2.2.1 WCA measurements

WCA measurements (**Figure 2.8**) clearly show that the WCA increases after the silane sol-gel step (AA2024-SH). This can be understood as follows. During the coating process, a sol is developed by hydrolysis and condensation reactions. During hydrolysis, alkoxide groups from MPTS are replaced by hydroxyl groups. Next, condensation reactions occur once the hydrolysis reaction has initiated. Condensation reactions lead to the development of Si-O-Si networks. When dipping the aluminium into the sol-gel solution, the hydroxyl groups on the aluminium surface react with the silanol groups (Si-OH) to form Van der Waals bonds. After heat treatment, the coating is fixed by a condensation reaction which produces covalent bonds [64]. This way, thiol functionalities are incorporated on the surface while the amount of hydroxyl groups decrease. Since thiol groups are less hydrophilic compared to hydroxyl groups, the WCA goes up after silanization. In addition, the WCA goes up with increasing immersion time while the standard deviation greatly decreases. With increasing immersion time, the coating becomes thicker and more uniform and more hydroxyl groups on the surface will have reacted, thus the WCA will increase further. The WCA of 64.66° after two hours immersion is comparable to literature. By example, Mihelcic et al. [65] found a WCA of 65.4° after dip coating AA2024 in an MPTS sol-gel solution.

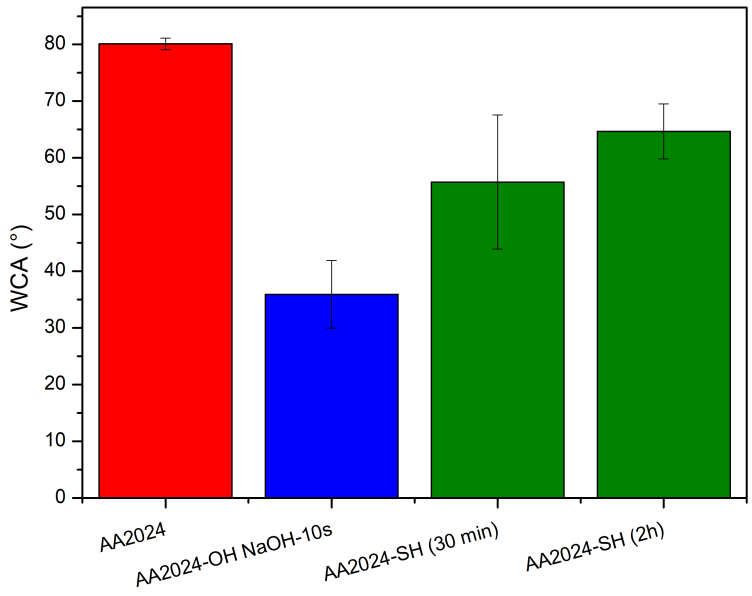

Figure 2.8: WCA measurements of AA2024, chosen activation route (10s NaOH) and silanized samples after 30 min and 2 h immersion in MPTS sol-gel solution

2.2.3 Chosen surface functionalization route

For the surface activation, confocal microscopy clearly shows that samples AA2024-OH-NaOH10s and AA2024-OH-NaOH5s had the least changes to their microstructure. From WCA results, AA2024-OH-NaOH5s showed a slightly higher WCA compared to AA2024-OH-NaOH10s. For this reason, a 10 second immersion in a 2M NaOH solution was chosen as activation step. Furthermore, a longer immersion in a silane solution leads to a more uniform silane layer. As such, samples are immersed in a silane solution for 2 hours.

To further verify the surface chemistry of the samples with preferred activation and silanization steps, Raman spectroscopy is used to investigate AA2024, AA2024-OH-NaOH10s and AA2024-SH (2h). During further discussions, AA2024-OH-NaOH10s will be renamed as AA2024-OH and AA2024-SH (2h) as AA2024-SH.

2.2.3.1 Raman spectroscopy

To further confirm that the surface activation and the silane sol-gel coating were effective, the surface chemistry is evaluated using Raman spectroscopy.

AA2024 does not exhibit any significant peaks, as can be seen on **Figure 2.9 a**. After activation (**Figure 2.9 b**), different peaks can be found. The peaks in the higher wavelength region (3000 cm^{-1}-3600 cm^{-1}) and around 1650 $cm^{-}1$ can be attributed to -OH stretching and deformation vibrations of weakly bound water [66]. This data clearly indicates the presence of hydroxyl groups on the surface after NaOH treatment. In addition, the peak around 1050 cm^{-1} is related to Al-O bending vibrations [67].

After applying the silane sol-gel coating, AA2024-SH samples (**Figure 2.9 c**) exhibit a similar peak as AA2024-OH around 3500 cm^{-1}, albeit smaller. Similar to AA2024-OH, this peak can also be ascribed to the presence of hydroxyl groups (Si-OH). This data further confirms the phenomenon which was also seen with WCA measurements. After silane treatment, the samples become more hydrophobic (less intense peak around 3500 cm^{-1}) but still remain within the hydrophilic region (peak around 3500 cm^{-1} confirms presence of hydroxyl groups). In addition, the peaks around 970 cm^{-1} and 1050 cm^{-1} are characteristic for Si-O-Si stretching vibrations, confirming that the condensation reaction took place [68]. Finally, the strong peak around 2950 cm^{-1} is due to C-H stretching while the peak around 1450 cm^{-1} can be linked to bending vibration of the $-CH_2$ group [69] [70]. As such, the AA2024-SH spectrum clearly confirms the deposition of a silane layer on top of the aluminium surface.

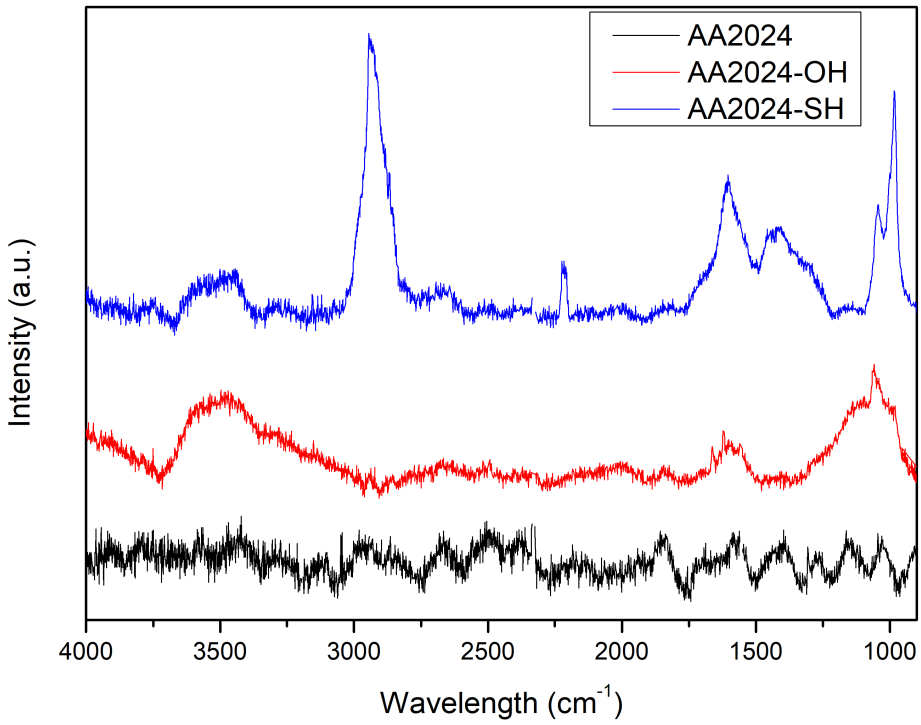

Figure 2.9: Raman spectra from (a) AA2024, (b) AA2024-OH and (c) AA2024-SH

2.2.4 Protein modification

To be able to attach the protein to AA2024-SH, complementary functional groups need to be incorporated in the protein. Maleimide-functionalities react rapidly with thiol by means of thiol-Michael click chemistry. For this reason, the proteins are modified with a heterobifunctional linker (Mal-PEG2/12/24-NHS) where the succinimidyl ester selectively reacts with the protein amine group at its N-terminus, forming an amide bond. This way, maleimide-functionalities are introduced into the protein (Mal-PEG2/12/24-AFP/INP). This PEGylation reaction can be found in **Figure 2.10**.

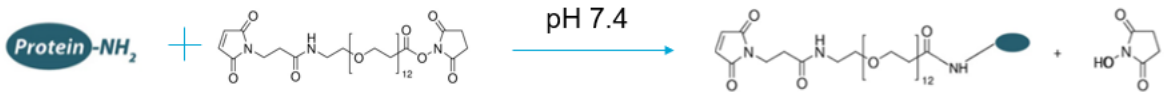

Figure 2.10: PEGylation of protein with Mal-PEG12-NHS

2.2.4.1 FTIR

For the protein modification, Mal-PEG2/12/24-NHS was dissolved in DMSO. A small amount of this linker solution was added to the protein which was dissolved in PBS. To verify whether the reaction between the protein and Mal-PEG2/12/24-NHS indeed took place, FTIR measurements

were taken at the start and the end of the reaction and from dry protein (AFP), DMSO and Mal-PEG12-NHS in DMSO.

The spectrum of the dry AFP powder (**Figure 2.11**) shows a typical spectrum for proteins with two large peaks at 1642 cm^{-1} and 1532 cm^{-1} corresponding to the Amide I and Amide II band respectively. The Amide I peak mostly arises due to C=O stretching vibration while the Amide II peak can mostly be attributed to N-H bending vibrations of the protein [71].

When comparing the spectra of DMSO and Mal-PEG12-NHS in DMSO (**Figure 2.11**), most of the peaks in the Mal-PEG12-NHS in DMSO spectrum can be attributed to the DMSO solvent. However, the sharp peak at 1741 cm^{-1} is associated with the C=O stretching vibration of the succinimidyl ester from Mal-PEG12-NHS. Initially, in the Mal-PEG12-NHS in DMSO solution, the ester peak is slightly higher compared to its neighbouring peaks. However, at the start of the reaction, the intensity of the ester peak is lower compared to its neighbouring peaks, indicating that some of the succinimidyl ester reacts rapidly with the protein. Toward the end of the reaction, the ester peak further decreases, indicating that the reaction indeed took place. Even though the ester peak decreases, no new amide peak is detected. This can be explained by the fact that the solution initially already has a lot of amide groups (both from the protein and Mal-PEG12-NHS). As such, a small addition of amides will not be detected in the spectrum.

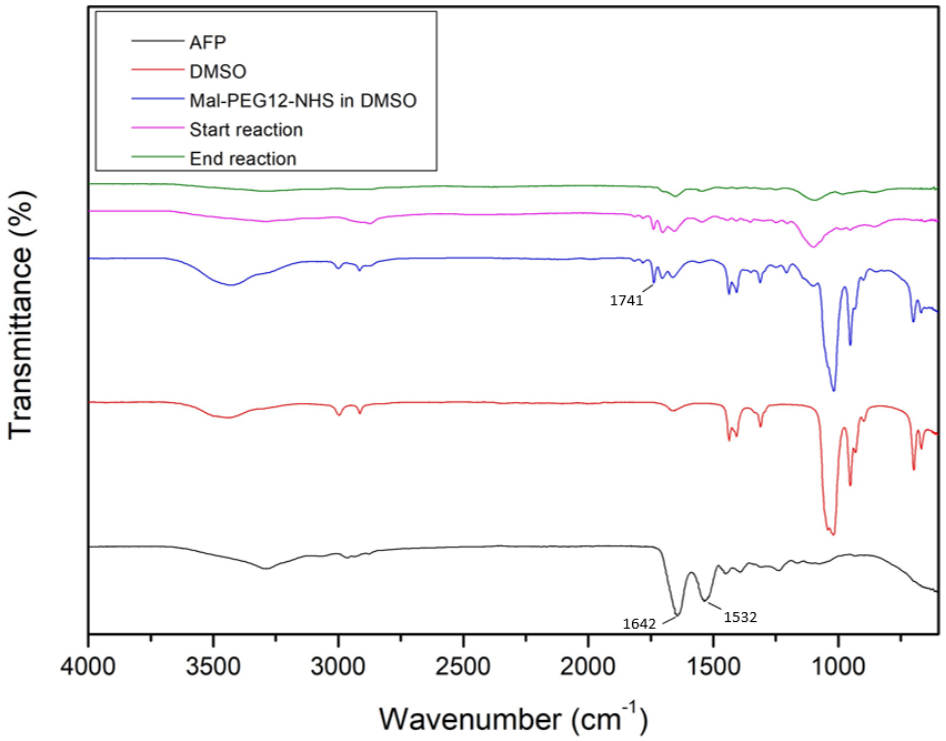

Figure 2.11: FTIR spectra of (a) AFP powder, (b) DMSO, (c) Mal-PEG12-NHS in DMSO, (d) start of the reaction and (e) end of the reaction

After the reaction, the excess linker and the NHS byproduct needs to be removed from the Mal-PEG2/12/24-AFP/INPs. For this reason, the solution was centrifuged thrice. The supernatant was evaluated with ^{1}H-NMR to make sure that there was no excess linker or byproduct present after centrifuging. The results can be found in Appendix C.

2.2.5 Characterization of protein-modified surfaces

After modifying the proteins with the appropriate functional groups, they are attached to the thiol-modified surfaces to optain protein-modified surfaces. These protein-modified surfaces are characterized with FTIR.

2.2.5.1 FTIR

To assure that proteins were indeed immobilized on the AA2024 surface, FTIR measurements were performed.

Figure 2.12 shows the spectra of the AFP and INP protein powders. As can be seen, both spectra are very similar with the characteristic amide I and amide II peaks around 1642 cm^{-1} and 1532 cm^{-1}, respectively. These peaks are present in all protein spectra since they are related to the amide bonds linking the different amino acids in the protein. In addition, both spectra exhibit another large peak around 3284 cm^{-1}. Other studies have shown that this peak is typically related to N-H stretching vibrations of the protein amino acids [72].

Figure 2.13 and **2.14** show the spectra of the protein-surfaces. By comparing these graphs with the protein powder spectra, it is clear that the amide I and II peaks can be distinguished on all spectra, confirming the presence of proteins on the surface. In addition, AA2024-5mg/ml AFP-PEG12 and AA2024-5mg/ml INP-PEG12 samples, who were immersed in solutions with higher protein concentrations, show higher intensities of the amide I and II peaks compared to the other samples, indicating that the amount of proteins on the surface will most likely be higher as well. Furthermore, a broad peak around 3280 cm^{-1} can also be detected in almost all protein-surface spectra (except for AA2024-2.5mg/ml AFP-PEG24). This peak might be ascribed to the N-H stretching vibration, as was explained earlier. However, its shape does not exactly match the N-H stretching vibration peak in the protein spectra. Since the FTIR spectra were recorded after the freezing experiments, it is possible that the samples might not have completely dried during the FTIR measurements. This way, the peak might also be related to hydroxyl (O-H) vibrations from water. As such, it is possible that AA2024-2.5mg/ml AFP-PEG24 was drier compared to the other samples during measurement, explaining the absence of a peak around 3380 cm^{-1}.

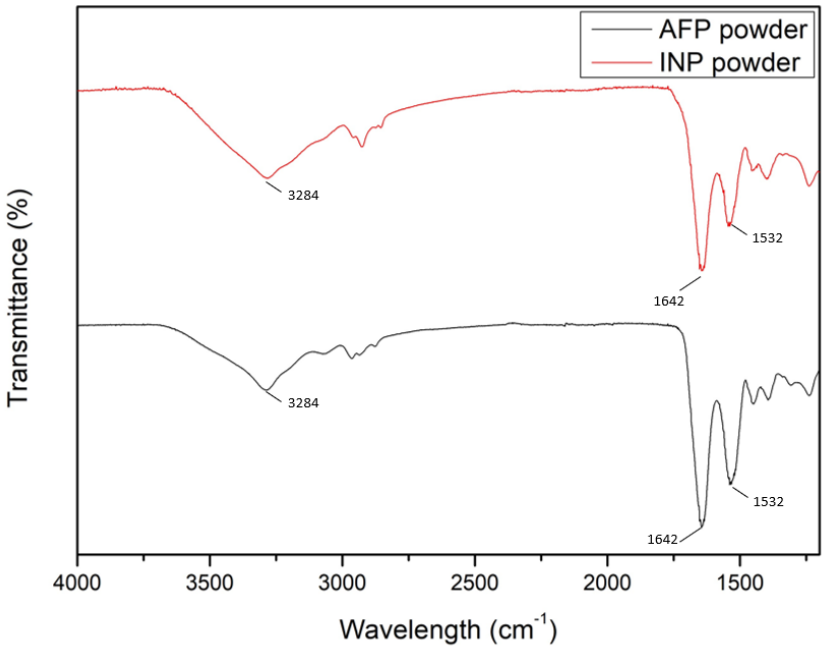

Figure 2.12: Spectra of protein powder: (a) AFP and (b) INP

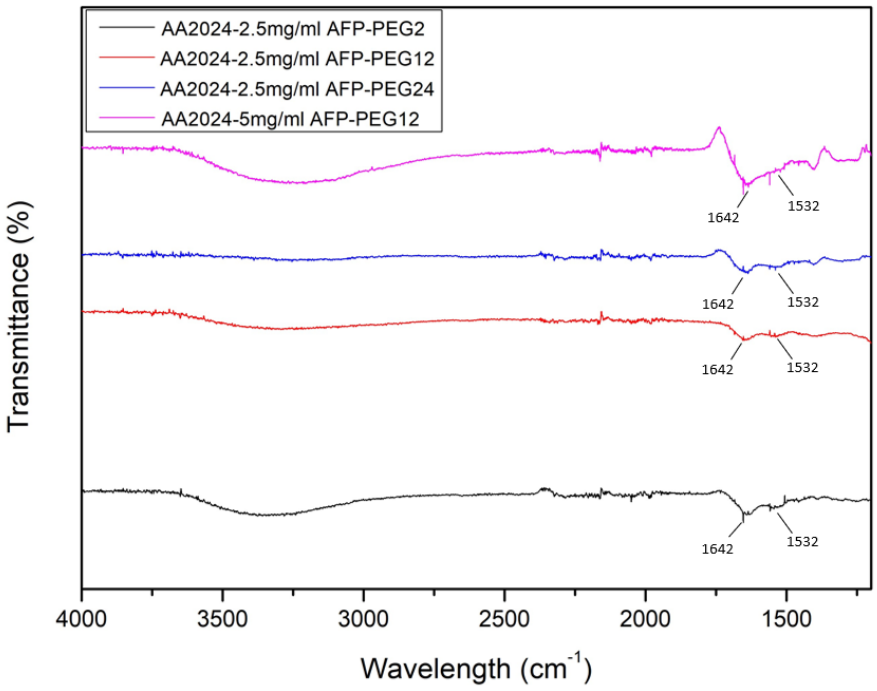

Figure 2.13: Spectra of AFP-surfaces from different protein solutions

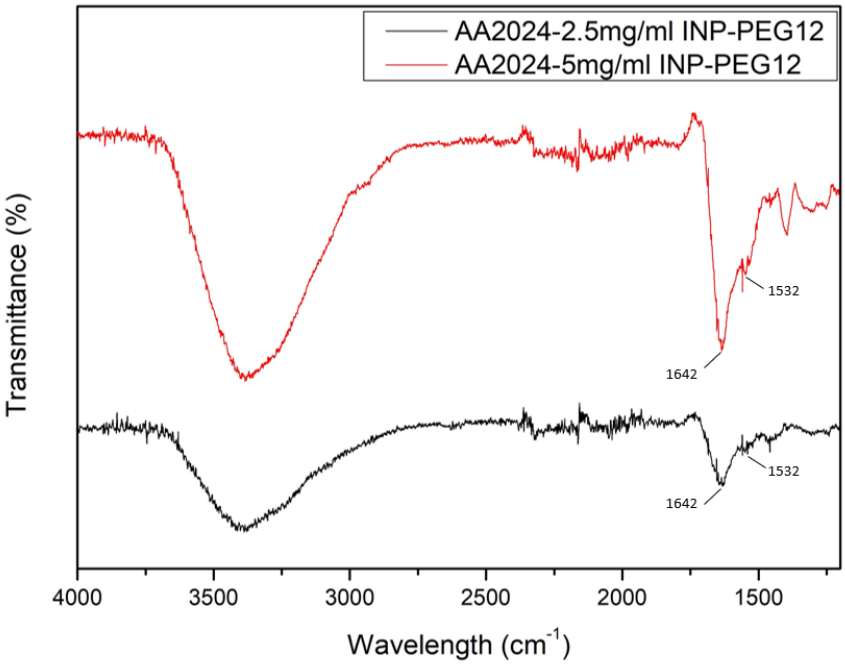

Figure 2.14: Spectra of INP-surfaces from different protein solutions

The FTIR measurements confirm the presence of proteins on the surface. However, the amount of proteins cannot be determined with FTIR. To get a more quantitative idea of the amount of proteins on the surface after immersion, aliquots at the start and end of the immersion are taken and investigated with ^{1}H-NMR. The results of these measurements can be found in Appendix D.

2.2.6 Factors affecting freezing behaviour of protein-modified surfaces

To gain a better understanding about the effect of ice-binding proteins on the surface, different freezing experiments were conducted. In a first step, the effect of different AFP concentrations (with a constant linker chain length) is investigated. Next, AFPs (with the same concentrations) are grafted on the surface with different linker chain lengths. Finally, the behaviour of AFPs on the surface is compared with INPs on the surface.

2.2.6.1 Effect of protein concentration

In nature, AFPs are found within a liquid environment. Previous studies have shown that the thermal hysteresis behaviour of AFP varies according to the AFP concentration in liquid. As can be seen in **Figure 2.15 a**, a hyperbolic relationship can be found between the AFP concentration in liquids versus the thermal hysteresis behaviour [73]. This means that even at low concentrations, AFPs already induce thermal hysteresis. Compared to normal antifreeze materials such as NaCl or ethanol (**Figure 2.15 b**), which lower the freezing point of water in a linear way, this hyperbolic relationship is much more efficient.

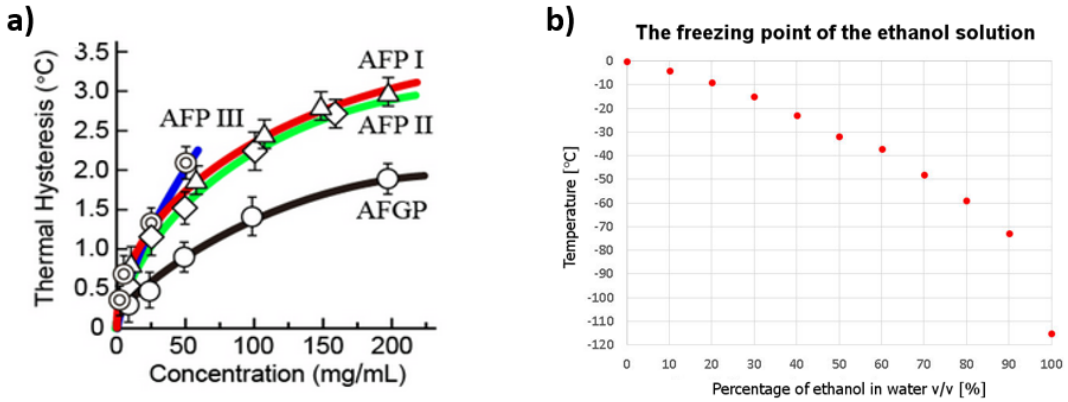

Figure 2.15: a) Hyperbolic relationship between AFP concentration and thermal hysteresis from [73] and b) linear relationship between ethanol content and freezing point depression

Up until now, the effect of the AFP concentration on the surface remains unknown. To investigate this, AA2024-SH samples were immersed in two different protein solutions with the same linker length and different protein concentrations (AA2024-2.5mg/ml AFP-PEG12 and AA2024-5mg/ml AFP-PEG12). The freezing onset time (t_{fo}) and temperature (T_{fo}) for the different samples can be found in **Figure 2.17**. As can be seen, t_{fo} decreases with increasing protein concentration while T_{fo} increases. This means that the surfaces actually freeze faster and at higher temperatures when the protein concentration on the surface is increased. This is an opposite trend in comparison with their behaviour in liquid.

To be able to explain this phenomenon, the behaviour of the protein in a liquid environment needs to be well understood. As was already explained in the introduction, AFPs are thought to work according to the adsorption-inhibition model. Once an ice crystal is formed, AFPs will attach themselves to it. No ice will grow at the location where the protein is attached, leading to a curved ice front. This way, further ice growth is inhibited [24]. The reason how AFPs are able to attach to ice and how no ice will grow over the protein itself can be explained by the protein structure.

The structure of AFPs can be divided in two major regions: the ice-binding site (IBS) and non-ice-binding site (NIBS). In most AFPs, the IBS can be distinguished by being relatively flat and hydrophobic [24]. It is this side that will lead to the attachment of the protein to the ice crystal. However, the exact ice-binding mechanism is still heavily debated. Currently, a lot of attention goes toward the clathrate hypothesis as was described by Garnham et al.. Simply said, 'cages' of water molecules are formed around the hydrophobic regions of the IBS. These regions are able to order the water molecules into an ice-like lattice according to the hydrophobic effect. Next, these water molecules are anchored to the protein by hydrogen bonds. The hydrophobic and hydrophilic regions have a regular arrangement at the IBS which is closely related to the ice crystal lattice [74]. By example, Liu et al. showed that the IBS of MpAFP has hydrophobic methyl groups and hydrophilic hydroxyl groups. The average distance between the oxygen of these hydroxyl groups lies around 4.6 Å which is closely related to the lattice constant of the ice crystal [30]. This way, water molecules can be more easily structured at the IBS which aids in the attachment to the ice crystal [74]. This is illustrated in **Figure 2.16** where the red dots

indicate the hydrophobic regions that structure the water molecules, and blue dots indicate the regions where hydrogen bonds anchor the water molecules to the protein. As such, both the hydrophobic effect and hydrogen bonding play an important role at the IBS.

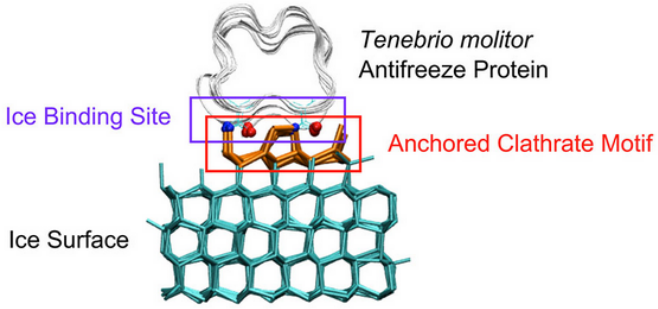

Figure 2.16: Clathrate hypothesis to explain AFP ice-binding [74]

In contrast to the IBS, the NIBS has an irregular arrangement of hydrophilic and hydrophobic sites. In addition, also bulky hydrophobic and charged groups are present on the surface [30]. Because of this, the water is very disorganised at the NIBS. As such, the NIBS assures that the AFP will not be adsorbed in the ice crystal which enables it to steer the ice formation and retard ice growth.

With this information, the ice-promoting effect of the proteins on the surface might be explained. Under normal conditions, the AFPs work together to inhibit ice growth since they attach to the ice crystal at specific locations. In addition, the proteins are free and able to direct their IBS toward the ice crystal. This way, the IBS and NIBS are in the correct position to, on one hand attach the AFPs to the ice crystal and on the other hand to avoid ice growth around the AFP. However, by attaching the proteins to the surface, their mobility is restricted. This way, AFPs are not able to work together in a similar way as in a liquid. As such, the ice front will most likely not be curved and no TH will be induced. In addition, the IBS which normally helps in the AFP attachment to the ice might actually promote ice formation on the surface. Since the hydrophobic moieties order the water molecules, this can decrease the energy barrier for ice formation and act as a template on which further ice can grow. Furthermore, with increasing protein concentration, the effect becomes more pronounced. With higher protein content, the amount of IBSs on the surface will be increased and the ice-promoting effect will be enhanced as well.

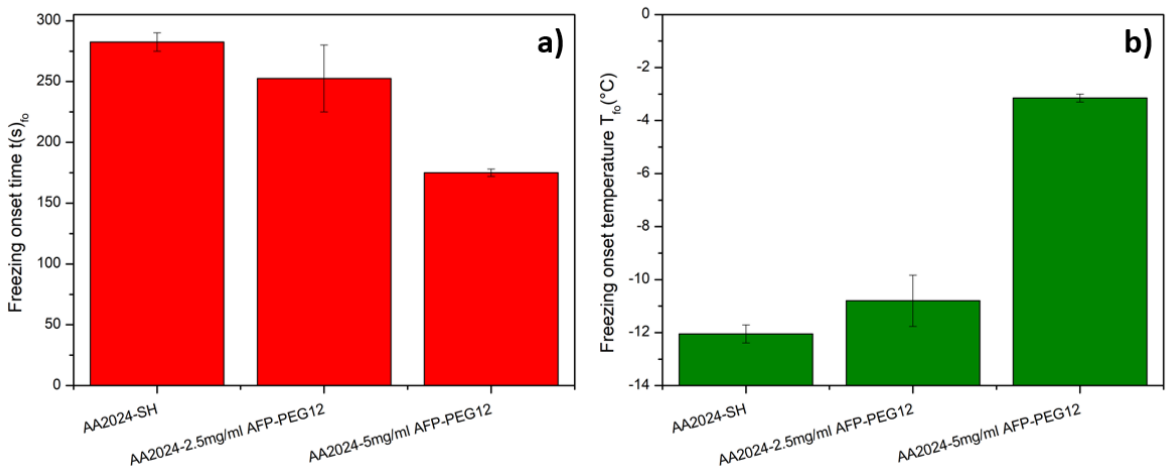

Figure 2.17: Effect of AFP concentration on a) t_{fo} and b) T_fo

Except for the effect of the AFPs on the t_{fo} and T_{fo}, they also influence v_{ffp}, as can be seen in **Table 2.3**. The v_{ffp} for AA2024-SH samples is significantly slower compared to v_{ffp} for AA2024-2.5mg/ml AFP-PEG12 and AA2024-5mg/ml AFP-PEG12. However, there is also a significant difference in speed between the two AFP concentrations. With increasing AFP concentration on the surface, v_{ffp} increases as well.

Table 2.3: v_{ffp} for different samples

	Mean v_{ffp} (mm/s)	**St. dev. of v_{ffp} (mm/s)**
AA2024-SH	0.28	0.04
AA2024-2.5mg/ml AFP-PEG12	36.2	4.33
AA2024-5.0mg/ml AFP-PEG12	58.7	11.0

The difference between AA2024-SH and AA2024-2.5mg/ml AFP-PEG12/AA2024-5mg/ml AFP-PEG12 can be understood when evaluating **Figure 2.18**. During freezing, the freezing front of the AA2024-SH samples show a very fractal pattern (**Figure 2.18 a**). The slow v_{ffp} and fractal ice growth is typical for desublimation freezing. Here, ice is directly formed from moisture in the vapor phase without going through the liquid phase. Slow ice growth is a characteristic element for this type of ice formation. On the other hand, a lot of condensation can be found on the AFP surfaces right before freezing. This condensation subsequently freezes very quickly. The freezing front in this case has a more round shape ((**Figure 2.18 b**) and this type of freezing is called condensation freezing. As such, AFP surfaces do not only freeze earlier but also change the type of freezing from desublimation freezing to condensation freezing. This can be mostly explained by the fact that the AFP surfaces are more hydrophilic compared to the silane surfaces. The reason for this is twofold. First of all, it has been shown that AFPs have the ability to increase the surface hydrophilicity [29]. In addition, the Mal-PEG-NHS linker is also a hydrophilic polymer, further enhancing the surface wettability. Because of this, more condensation will be present on the surface which changes the freezing mode.

In addition, with increasing AFPs on the surface, v_{ffp} increases as well. Again, this might be explained due to the fact that more AFPs and Mal-PEG-NHS linkers lead to a more hydrophilic

surface and thus more condensation.

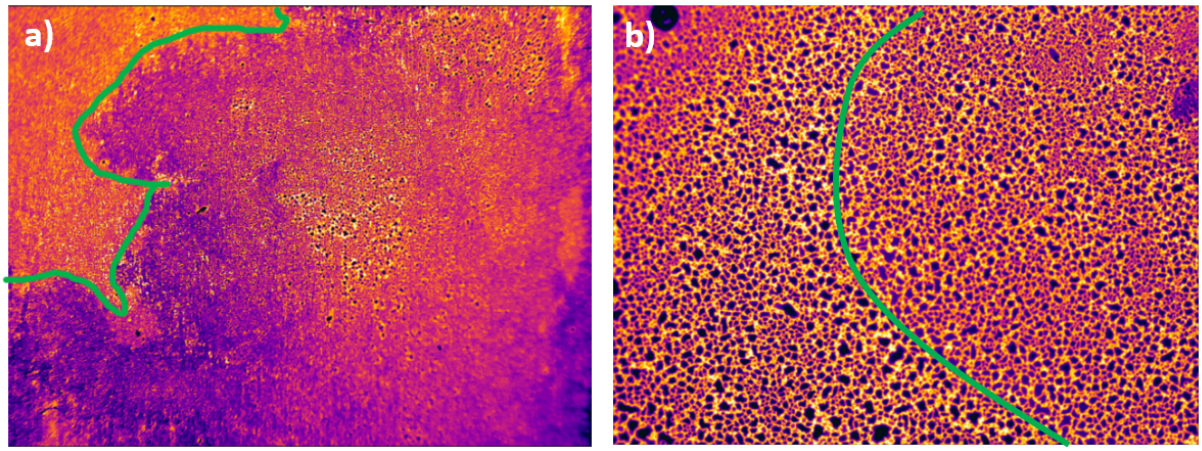

Figure 2.18: a) Surface of AA2024-SH with fractal freezing front and b) surface of AA2024-2.5mg/ml-PEG12 with round freezing front, indicated in green

2.2.6.2 Effect of linker chain length

When immobilizing proteins to the surface, it was seen that protein mobility is an important aspect to consider since it can greatly influence the characteristics of the protein surface. By example, Andresen et al. produced peptide microarrays by coupling biotinylated peptides to NeutrAvidin. Biotion reacted with NeutrAvidin and NeutrAvidin was subsequently physically adsorbed onto an amine-modified surface. They reported that the usage of a PEG spacer between biotin and the peptide increased antibody-binding to the peptide. In addition, also Inamori et al. evaluated different spacer lengths to find the the optimal surface chemistry for peptide immobilization in on-chip cSrc phosphorylation [54]. Even though the working mechanism of AFPs is significantly different compared to the the proteins described in these papers, the idea is very similar. AFPs are attached tot the surface using different linkers of various chain lengths. The different effects of a Mal-PEG2-NHS, Mal-PEG12-NHS and Mal-PEG24-NHS linker on freezing are recorded and the linkers are compared.

As was hypothesized in the previous section, the limited mobility of the AFPs on the surface might explain their ice-promoting behaviour. Increasing the AFP mobility might have an effect on two aspects: with increased mobility, (1) the AFPs might be able to work together more efficiently, which is required for TH and (2) both the NIBS and IBS will have more accessibility toward the bulk water.

Figure 2.19 a and **b** shows that AA2024-2.5mg/ml AFP-PEG2 samples, with the shortest chain length, have the highest T_{fo} and lowest t_{fo}. However, the difference with AA2024-2.5mg/ml AFP-PEG12 samples is not very significant. Both samples freeze at the high temperatures and within short timeframes. The reason for this was already explained in the previous section. The AFP mobility might be heavily restricted for both linker chain lengths. As such, for both conditions, AFPs are not able to work together and induce any TH. In addition, the AFPs are most likely fixed to the surface with their IBS directed toward the bulk water. This way, an ice-promoting behaviour can be observed.

In contrast, AA2024-2.5mg/ml AFP-PEG24 samples show a higher t_{fo} and lower T_{fo} compared

to AA2024-2.5mg/ml AFP-PEG2/12. In addition, when comparing AA2024-2.5mg/ml AFP-PEG24 with AA2024-SH samples, AA2024-2.5mg/ml AFP-PEG24 samples appear to show ice-suppressing behaviour since the T_{fo} of AA2024-2.5mg/ml AFP-PEG24 is lower than the T_{fo} of AA2024-SH. This further supports the theory that AFP mobility is crucial for proper functioning of the protein. With the PEG24 linker chain length, AFPs have obtained sufficient mobility to be able to work together to inhibit ice propagation and show TH behaviour at the surface.

As such, from these experiments, it can be concluded that the protein mobility is crucial for optimal functioning of AFPs. This should be carefully considered when trying to attach AFPs to the surface since it greatly influences the surface behaviour.

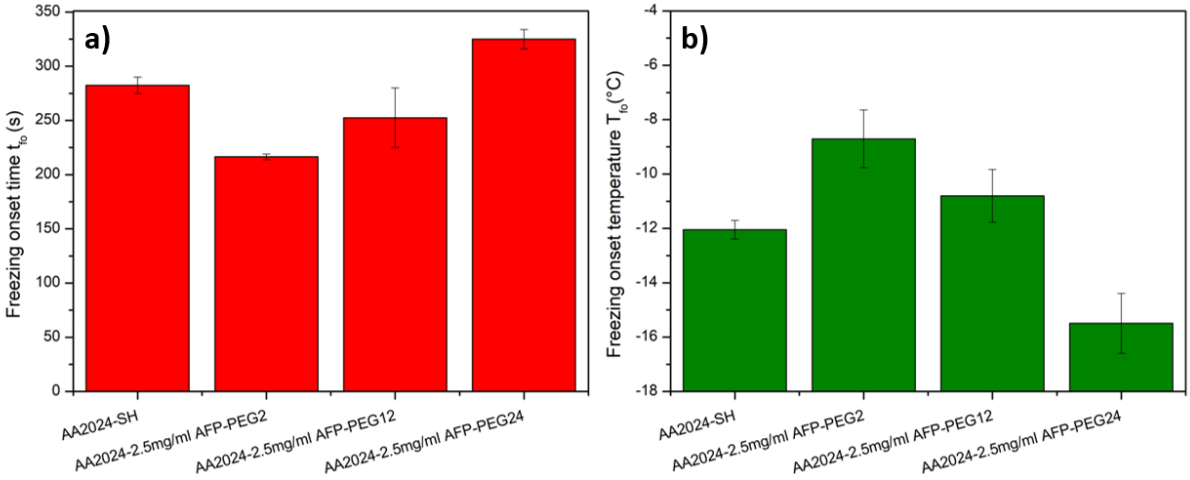

Figure 2.19: Effect of linker chain length on a) t_{fo} and b) T_{fo}

2.2.6.3 Effect of different ice-binding proteins

As was already explained, two types of ice-binding proteins exist: AFPs and INPs. In nature they work in opposite ways. While AFPs retard ice growth, INPs promote ice growth. Since it was shown that AFPs can also act as ice promoters when attached to the surface, it might be interesting to compare them to INPs to better understand how effective their ice-promoting behaviour is.

Figure 2.20 shows the effect of AFP and INP concentration on t_{fo} and T_{fo}. Between the INP samples, there is no visible effect of INP concentration on t_{fo} or T_{fo}. Both concentrations push the ice formation forward and result in similar t_{fo} and T_{fo}. Since INPs are very potent and ice-suppresing behaviour can already be observed at very small concentrations, this might be explained. By example, Wang et al. investigated the effect of INP concentrations in hydrogels and already detected ice-promoting behaviour when using 0.2 mg INPs [33].

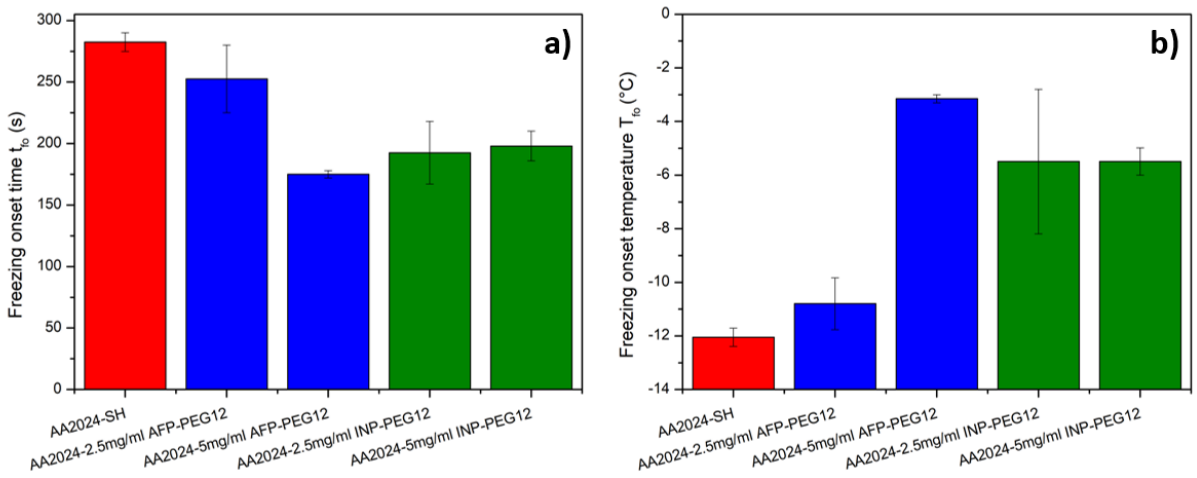

Figure 2.20: Different effect of AFP concentration and INP concentration on a) t_{fo} and b) T_{fo}

Furthermore, when comparing the AFPs with INPs it is interesting to notice that AA2024-5mg/ml AFP-PEG12, with the highest AFP concentration, has a similar t_{fo} and T_{fo} as the AA2024-2.5mg/ml INP-PEG12 and AA2024-5mg/ml INP-PEG12 samples. As such, by attaching the AFPs to the surface, they are actually transformed in to INPs. INPs consist of CRD which structures water into an ice-like structure which speeds up ice formation [27]. According to molecular simulations, this CRD has shown to consist of both hydrophobic and hydrophilic amino acid motifs [75]. **Figure 2.21** illustrates the hydrophobic (red) and hydrophilic (blue) moieties on the IBS of various AFPs and on the CRD of a model INP. From this figure, it is clear that the IBS of AFPs and CRD of INPs are very closely related to each other. Since the previous experiments have shown that AFPs use their IBS to structure water on the surface and INPs structure water on their CRD. Since both the IBS and CRD have a closely related structure, the very similar freezing results between AA2024-5mg/ml AFP-PEG12 and the INP surfaces might be explained.

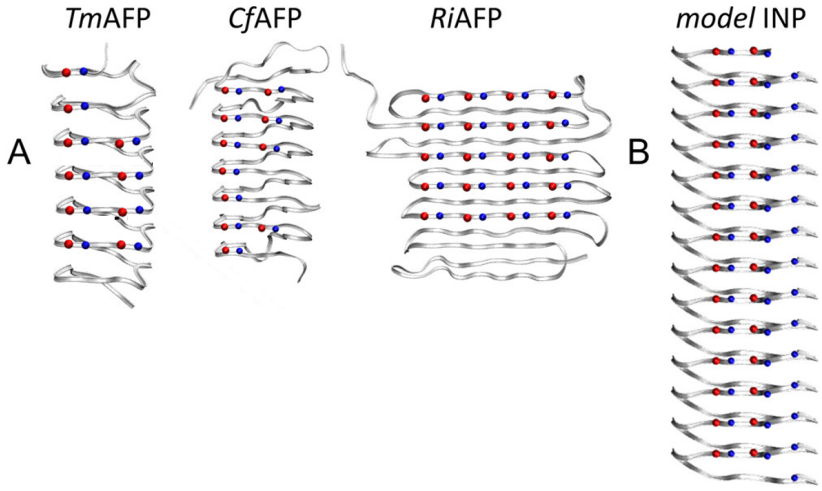

Figure 2.21: A) IBS of various AFPs and B) CRD of a model INP [75]

2.2.7 Condensation and type of frost formation on ice-binding protein-modified surfaces

After the freezing experiments, it became clear that the type of condensation and frost on the surface varies with or without ice-binding proteins. To further investigate this, condensation and frost growth are recorded with a digital microscope. First, the condensation right after freezing is evaluated. Next, the frost formation process will be discussed.

2.2.7.1 Type of condensation

To obtain condensation and subsequent freezing, there are certain requirements for the temperature. When the surface temperature reaches below the dew-point temperature but above 0°C, condensation will start to accumulate on the surface. When the surface temperature eventually decreases below 0°C, the condensation freezes. Under normal circumstances, condensation can be divided in dropwise (DWC) or filmwise (FWC) condensation depending on the surface energy. According to **Figure 2.22 a**, AA2024-SH clearly exhibits DWC with droplets of more or less uniform size. Huan et al. have shown that the type of condensation heavily depends on the surface wettability. At a WCA range between 40° and 100°, a transition region exists where both DWC and FWC can exist [76], [77]. In our case, AA2024-SH clearly show DWC. Molecules with a lower total energy first start forming small clusters which grow and coalesce into larger droplets.

Furthermore, the ice-binding protein surfaces (**Figure 2.22 b-g**) also exhibit DWC. However, the droplets are larger and more irregular compared to AA2024-SH. This means that the ice-binding protein surfaces are more hydrophilic compared to the AA2024-SH surface. These results are comparable to the type of condensation that was found by Esser-Khan et al. who investigated AFP surfaces [34]. There are also some differences that can be detected between the different ice-binding protein surfaces. Firstly, the condensation droplet size on AA2024-2.5 mg/ml AFP-PEG12 is considerably smaller compared to the droplet size on AA2024-5 mg/ml AFP-PEG12 (**Figure 2.22 b and c**) meaning that the surface becomes more hydrophilic with increasing AFP concentration on the surface. This can be explained by two different phenomena. Firstly, AFPs make the surface more hydrophilic. This was confirmed by Jeong et al. who detected a drop in WCA from 53.2° to 43.9° by incorporating AFPs on the surface [29]. In addition, the AFPs are connected to a heterobifunctional linker made from PEG. Since PEG is a hydrophilic polymer, the surfaces become more hydrophilic with an increasing amount of PEG chains on the surface. By example, Rahmini et al. attached PEG chains to an aluminium surface. The water contact angle significantly decreased from 78° to 30° by incorporating the PEG chains [78]. Next, the largest water droplets are found on the AA2024-2.5mg/ml AFP-PEG24 surface and INP surfaces. Since PEG is a hydrophilic polymer meaning, longer PEG chains will lead to a more hydrophilic surface, resulting in larger droplets on the surface. Since the longest PEG chains are used to develop the AA2024-2.5mg/ml AFP-PEG24 samples, this can explain why this surface shows the larger droplets. Lu et al. investigated the effect of PEG chain length in PEG brushes on the surface hydrophilicity. They also found that increasing PEG chain length significantly increased the hydrophilicity of the surface [79]. Furthermore, large droplets are also found on the AA2024-2.5/5 mg/ml INP-PEG12 samples. Comparing AA2024-2.5/5 mg/ml INP-PEG12 samples with AA2024-2.5/5 mg/ml AFP-PEG12 samples, the condensation on the INP samples is clearly more pronounced. O'Brien et al. studied the condensation of INP surfaces and found a film of condensation on the surface before freezing, indicating that the INPs indeed make

the surface very hydrophilic [12]. As such, the presence of INPs are more effective in creating a hydrophilic surface than the AFPs, leading to larger droplets.

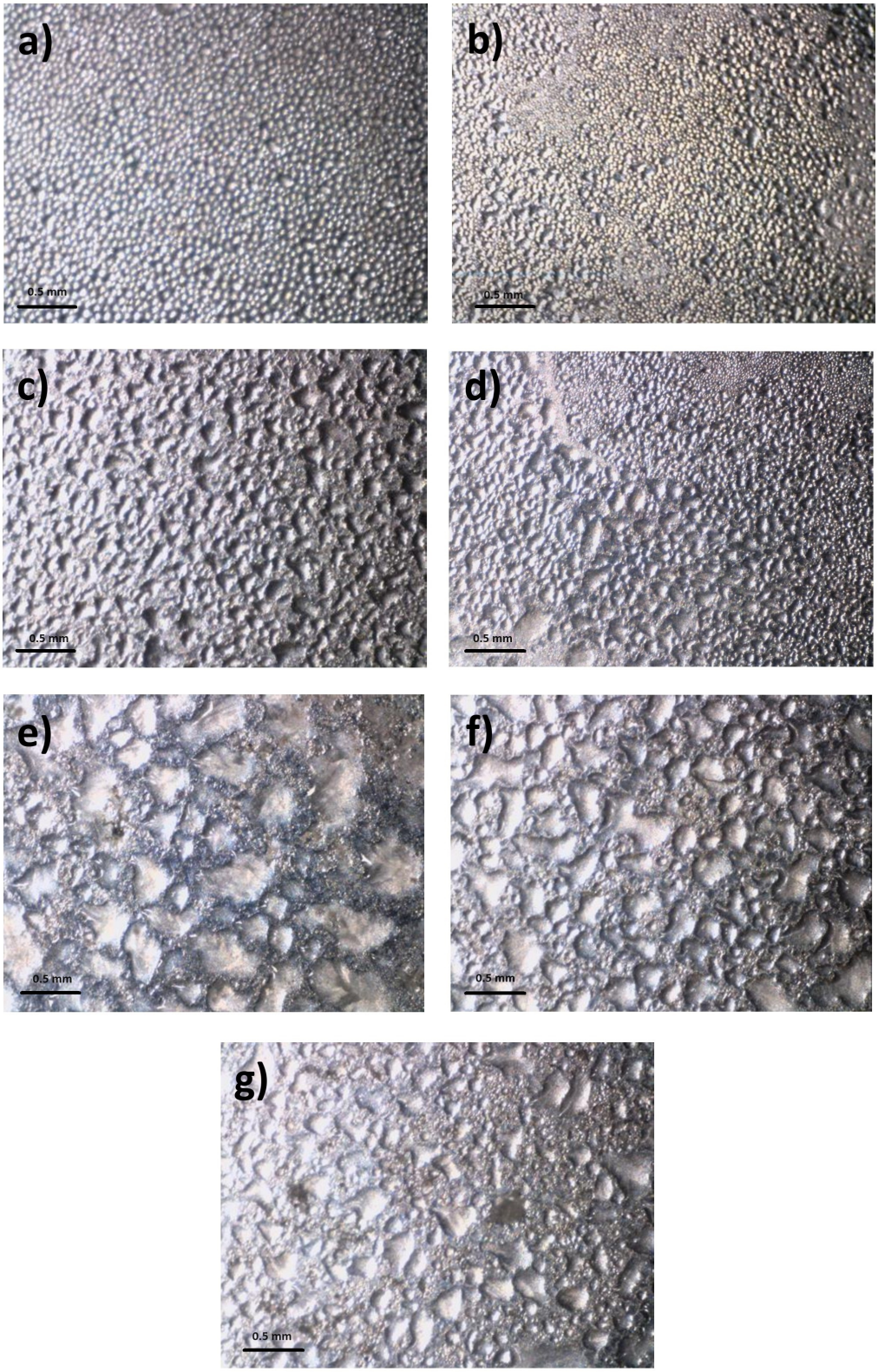

Figure 2.22: Condensation right after freezing event on a) AA2024, b) AA2024-2.5mg/ml AFP-PEG12, c) AA2024-5.0 mg/ml AFP-PEG12, d) AA2024-2.5mg/ml AFP-PEG2, e) AA2024-2.5mg/ml AFP-PEG24, f) AA2024-2.5mg/ml INP-PEG12 and g) AA2024-5.0mg/ml INP-PEG12

2.2.7.2 Type of frost formation

After condensation, coalescence of condensed water droplets and freezing of the water droplets, the deposition of ice on the surface continues up until the surface energy of the ice droplet no longer supports the addition of new molecules. At this moment, new nucleations start to form on top of the already formed ice layer. This way, rodlike ice crystals are formed which results in dendrites on top of the initial ice layer [80], [81].

Huang et al. have investigated ice dendrite growth on top of frozen water droplets. Depending on the position of the droplet (horizontal, vertical or inverted) the dendrite growth can be controlled. For horizontal water droplets, dendrites form on the entire upper part of the droplet. As such, certain dendrites grow upward while other grow more sideway (**Figure 2.23 a**)[81].

To understand why dendrites grow in a specific direction, the process can be simplified to the diffusion-controlled deposition of water vapor on top of the ice-air interface. This way, the concentration gradient (density of constant vapor pressure lines) can give an indication of the dendrite growth rate. As can be seen on **Figure 2.23 b**, the concentration gradient is high on the entire top of the horizontal water droplet, explaining why dendrites grow on top of the entire droplet in various directions [81].

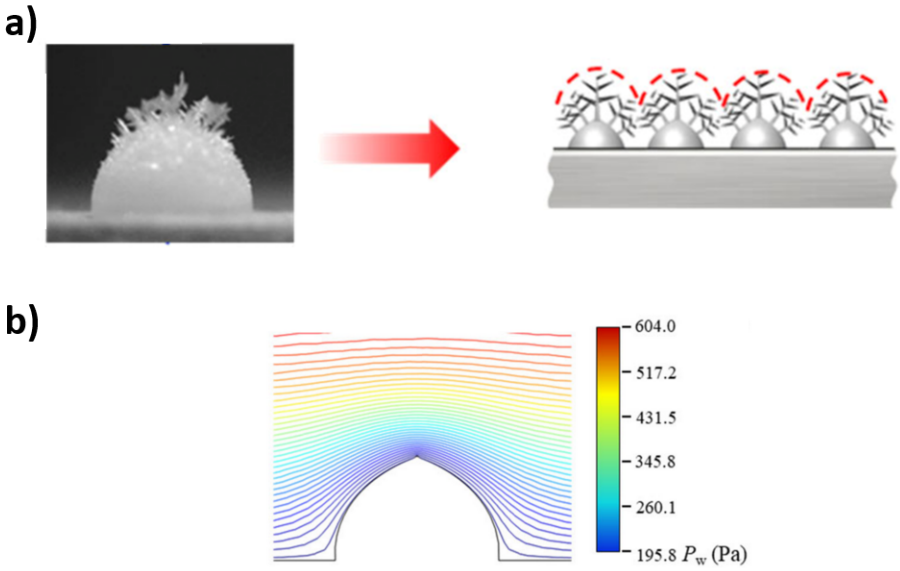

Figure 2.23: a) Dendrite growth on top of a horizontal ice droplet and b) Distribution of water vapour pressure on top of a horizontal ice droplet [81]

Similar dendrite growth can be detected for the AA2024-SH samples. As can be seen on **Figure 2.24 a**, dark cloudlike regions can be found on the surface that correspond to dendrites. These regions are spread out over the surface, indicating that dendrites grow in different directions on the AA2024-SH surface. On the other hand, the AFP surfaces, especially AA2024-2.5 mg/ml AFP-PEG12, AA2024-5.0 mg/ml AFP-PEG12 and AA2024-2.5 mg/ml AFP-PEG2, show a much more directed dendrite growth. The dark regions are much smaller and more confined indicating that the dendrites grow mostly in an upward direction. As such, these results indicate that AFPs also influence the way how ice crystals grow on top of the surface.

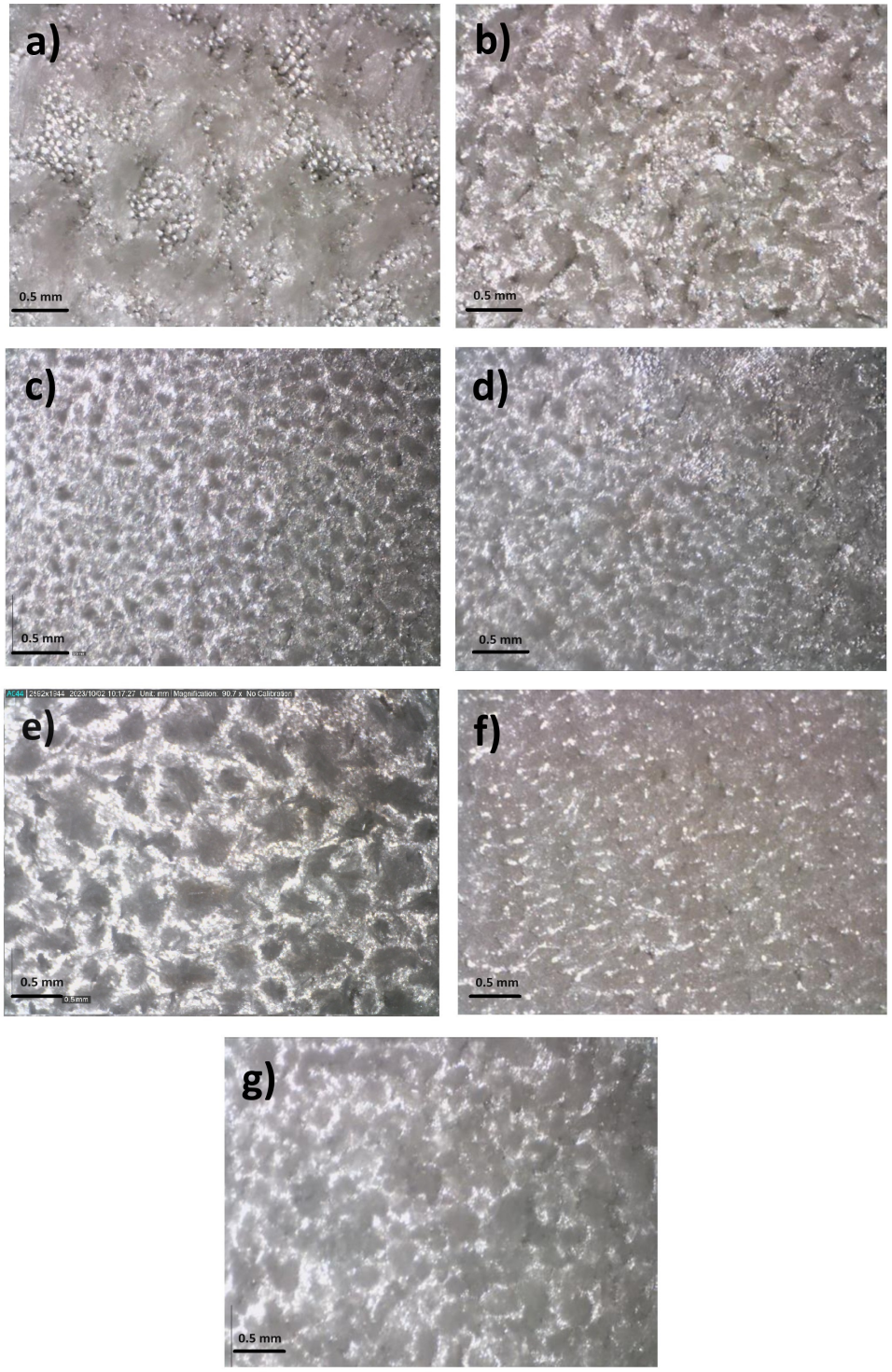

Figure 2.24: Dendrite growth on top of a) AA2024, b) AA2024-2.5mg/ml AFP-PEG12, c) AA2024-5.0 mg/ml AFP-PEG12, d) AA2024-2.5mg/ml AFP-PEG2, e) AA2024-2.5mg/ml AFP-PEG24, f) AA2024-2.5mg/ml INP-PEG12 and g) AA2024-5.0mg/ml INP-PEG12 surfaces

Within a liquid environment, AFPs are also known to drastically change the shape of the ice

crystal. Depending on the type of AFP, they will selectively bind to specific ice crystal planes and inhibit ice growth at these specific planes. This way, the ice growth is governed by the AFPs. By example, under normal conditions, ice forms a flat circular disc or a hexagonal dendrite. However, with the presence of AFP type I, a hexagonal bipyramidal ice crystal is formed due to the fact that AFP type I binds to the 2021-pyramidal planes of ice [82]. Since the IBS of AFPs are speculated to act as a template for ice growth, they might also steer the dendrite growth. This can be seen in **Figure 2.25**. The IBS lowers energy the barrier for ice nucleation, thus promoting ice formation at specific regions. Because of this, ice might continue to grow on the ice that is formed at the IBS, resulting in dendrites pointing relatively upward. Furthermore, the straight dendrite growth is less pronounced for AA2024-2.5mg/ml AFP-PEG24 and AA2024-2.5/5mg/ml INP-PEG12 samples. From the condensation results, it was clear that these samples were also the most hydrophilic. Ice and subsequent dendrite is governed by different parameters. The surface wettability plays an important role in this. By example, Liu et al. developed both hydrophilic and hydrophobic surfaces and evaluated dendrite growth on both. The dendrites on the hydrophobic surface grew more upward compared to the hydrophilic surfaces where the dendrites grew in different directions very close along the surface [83]. As such, dendrite growth on top of the ice-binding surfaces might be governed by a competition between the surface hydrophilicity and the AFP working mechanism.

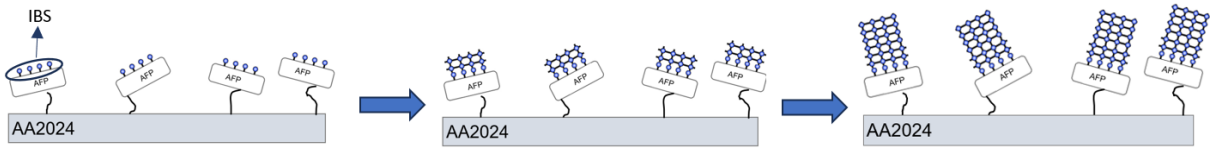

Figure 2.25: Possible mechanism of ice growth on AFP surfaces

Another hypothesis as to why AFP surfaces alter dendrite growth might be that AFPs alter the type of ice structure that is formed inside the condensation. This might subsequently have an effect on the dendrite growth. By example, Gandee et al. investigated dendrite morphology on top of different types of oil-impregnated surfaces [84]. Their results clearly showed that different surfaces showed different types of dendrites. As such, the surface can heavily influence the type of dendrites. However, the effect of AFPs on dendrite growth should certainly be further investigated.

2.2.8 Ice adhesion on ice-binding protein-modified surfaces

From the previous paragraph it is clear that dendrite growth on top of AA2024-2.5mg/ml AFP-PEG12, AA2024-5.0 mg/ml AFP-PEG12 and AA2024-2.5mg/ml AFP-PEG2 is more directed compared to the other samples. Because of this, these samples are further investigated to determine whether this directionality has an effect on ice adhesion on these samples. **Figure 2.26** shows AA2024-SH, AA2024-2.5mg/ml AFP-PEG12, AA2024-5.0 mg/ml AFP-PEG12 and AA2024-2.5mg/ml AFP-PEG2 before and after being subjected to a cold airstream. As can be seen on the images, more frost is removed from the AFP-samples compared to AA2024-SH. Considering that the dendrites on these AFP-samples grow more straight, it makes sense that the dendrites are more easily removed. Nonetheless, after subjecting the samples to a cold airstream, an ice-like layer remains present on the surface which is not able to be blown away.

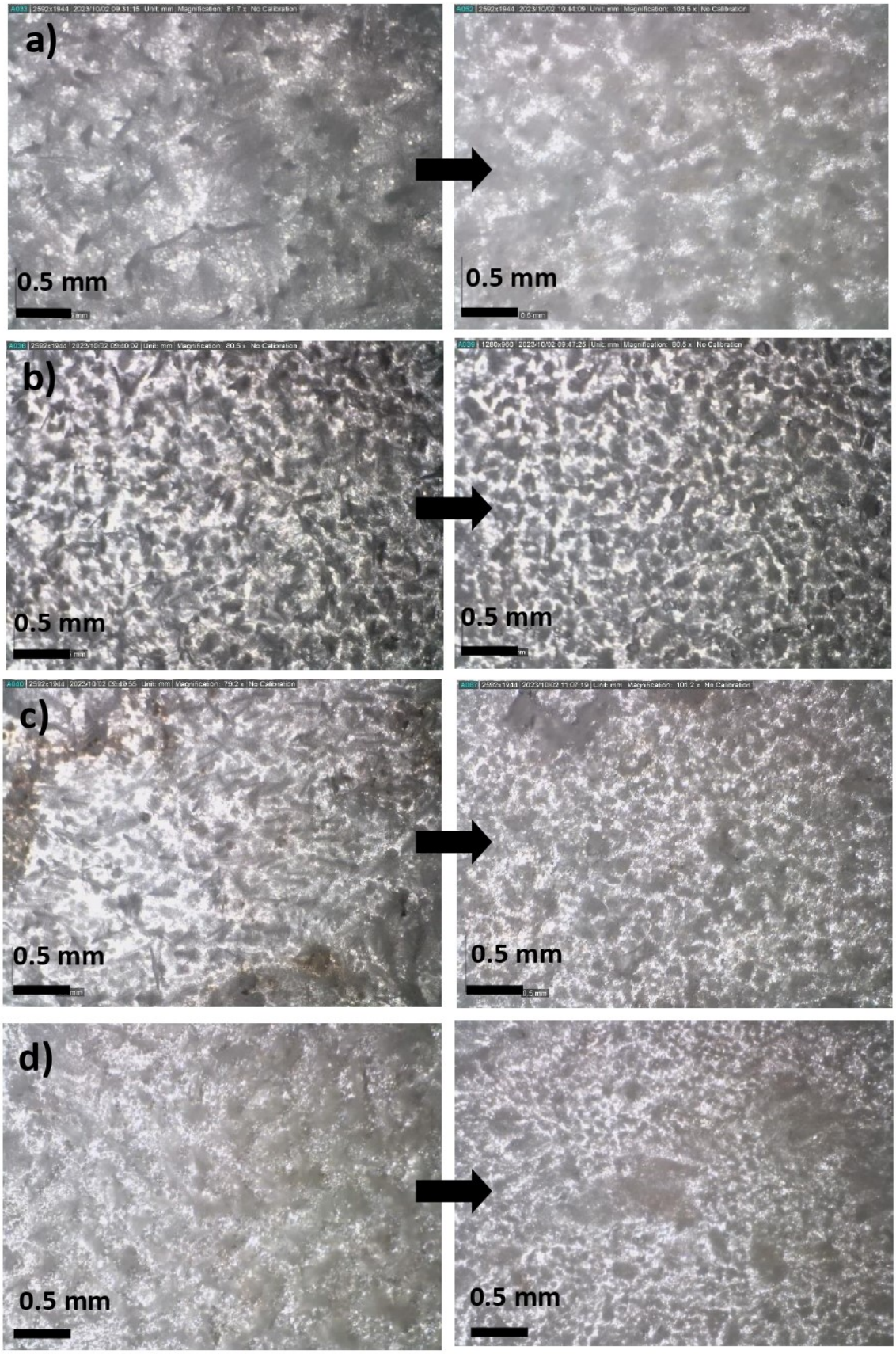

Figure 2.26: Top image of surface before and after blowing for a) AA2024-SH, b) AA2024-2.5mg/ml AFP-PEG12, c) AA2024-5.0 mg/ml AFP-PEG12, d) AA2024-2.5mg/ml AFP-PEG2

Chapter 3

Ice-binding protein behaviour in a polymeric system

The durability of directly attaching the proteins to the surface is very low. It would be desirable to produce a surface that exhibits the same properties even after scratching the surface. For this reason, a coating would be a more viable system. To investigate how ice-binding proteins would act within a polymeric environment, they are incorporated in hydrogels. The first section describes the materials and methods used to produce, characterize and test the protein hydrogels. The second chapter describes and elaborately discusses the found results.

3.1 Materials and methods

3.1.1 Protein-hydrogel synthesis

3.1.1.1 Materials

The NaOH pellets, MPTS, methanol, DMSO, PEG dithiol (average M_n = 1000), 4arm-PEG-maleimide (average M_n = 10 000) and the Mal-PEG2/12/24-NHS linker were bought from Sigma-Aldrich. The AFP (type III from *Marcrozoarces americanus*) was obtained from A/F Protein inc.. The INPs (from *Pseudomonas syringae*) were purchased from Snomax inc..

3.1.2 Surface functionalization

In a first step, AA2024 samples of 2cm x 2cm are grinded with 1000, 2000 and 4000 grit size. They are subsequently polished with diamond paste of 3 μm and 1/4 μm. Next, the samples are washed with aceton. For the activation step, AA2024 samples are submerged in a 2M NaOH solution for 10 seconds. Finally, the samples are rinsed with DI water and dried in an oven.

In a next step, a 4 wt% silane solution is prepared by adding a 2:3 ratio (v/v) of MPTS to water in methanol as solvent. The silane solution is stirred for 24 hours to assure sufficient hydrolysis of the MPTS. Afterward, samples are submerged in the silane solution for 2 hours. Next, the AA2024-SH samples are rinsed in methanol and dried in vacuum for 30 minutes. Finally, the samples are cured for 1 hour at 100°C.

3.1.2.1 Protein modification

In a first step, a 0.1 mM protein solution in PBS (pH of 7.4) is prepared. Next, a linker stock solution (250 mM) is prepared by mixing Mal-PEG12-NHS with DMSO. Finally, the linker solution is added to the AFP solution in tenfold molar excess (4 μl of linker stock solution per ml of AFP solution). The mixture is stirred for 1 hour to obtain a good reaction between Mal-PEG12-NHS and the protein. Finally, the excess linker is removed from the solution by centrifuging thrice for 5 minutes at 4400 rpm. This way, Mal-PEG12-NHS-modified AFPs are obtained.

3.1.2.2 Hydrogel synthesis

For the production of 10 wt% hydrogels, 4arm-PEG-maleimide is mixed with PEG dithiol, with or without the presence of a specific concentration of Mal-PEG12-AFPs or a specific concentration of INPs in PBS (pH of 7.4). The different concentrations of proteins in the hydrogel are depicted in **Table 3.1** and **Table 3.2**.

Table 3.1: Different types of AFP protein concentrations in hydrogel

	AFP-solution 1	AFP-solution 2	AFP-solution 3	AFP-solution 4
AFP concentration	2.5 mg/ml	5.0 mg/ml	10 mg/ml	25 mg/ml
linker	Mal-PEG12-NHS	Mal-PEG12-NHS	Mal-PEG12-NHS	Mal-PEG12-NHS

Table 3.2: Different types of INP protein concentrations in hydrogel

	INP-solution 1	INP-solution 2	INP-solution 3	INP-solution 4
INP concentration	2.5 mg/ml	5.0 mg/ml	10 mg/ml	25 mg/ml
linker	n.a.	n.a.	n.a.	n.a

By Thiol-Michael reactions, a crosslinked network can be formed that covalently binds the proteins to the polymeric system which can be seen in **Figure 3.1**.

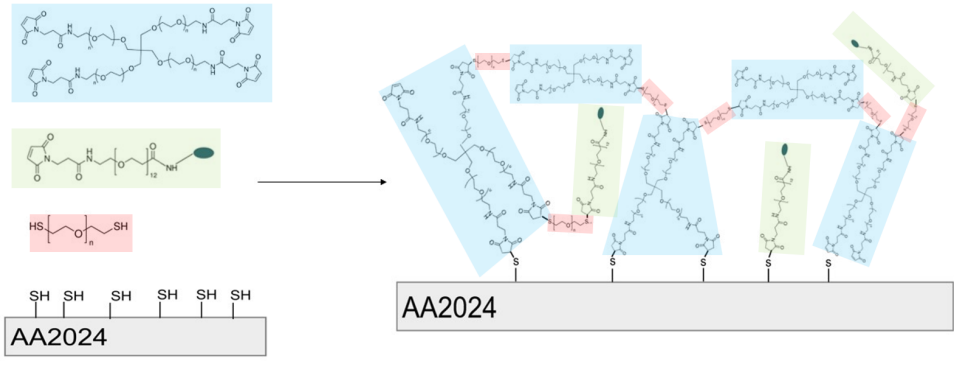

Figure 3.1: Schematic visualisation of hydrogel

The reaction between the thiol and maleimide functionalities occurs very rapidly. To be able to obtain a relatively uniform hydrogel, the samples are spray coated. For this reason, a spray head

was developed as can be seen in **Figure 3.2**. On one end, 4arm-PEG-maleimide in PBS with or without Mal-PEG12-AFPs or INPs is added. The other inlet contains PEG-dithiol. Both inlets are connected to a high pressure and the solution is sprayed on AA2024-SH.

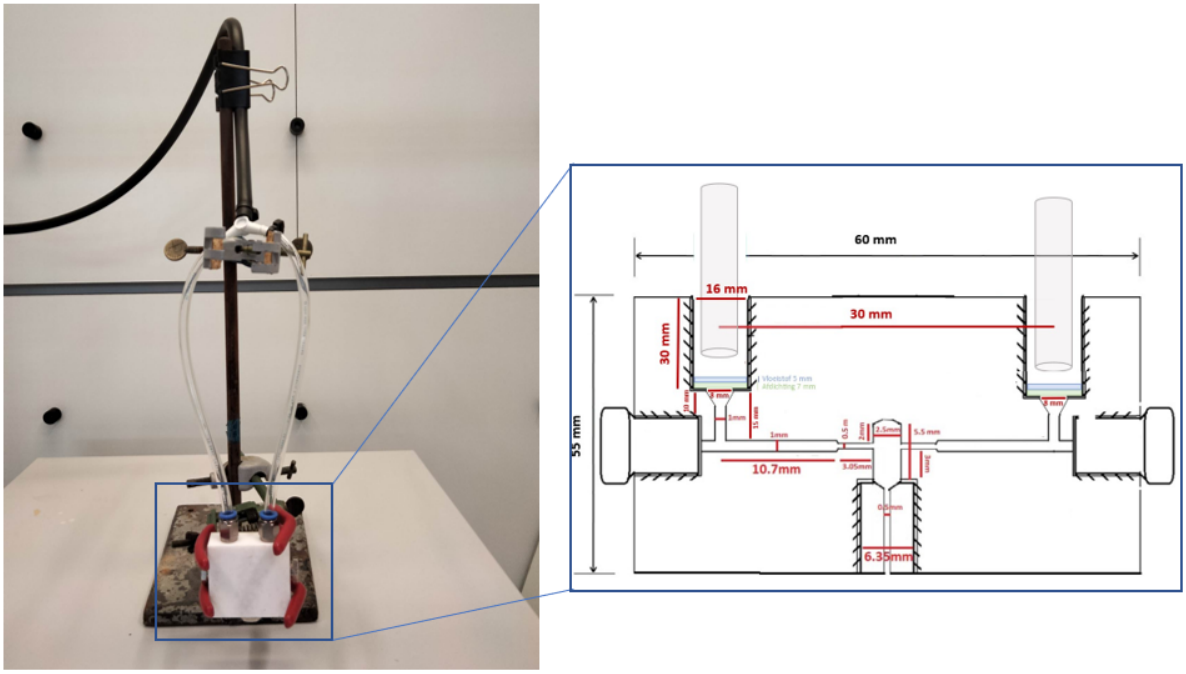

Figure 3.2: Spraying set-up

3.1.3 Characterization techniques

3.1.3.1 FT-IR

FTIR is a non-destructive technique to identify the chemical composition of different types of samples. Simply said, IR radiation is passed through a sample. Some of this radiation will be absorbed by changing the vibrational energy in the chemical bonds in the sample. Depending on the molecules and types of bonds in the sample, different IR wavelengths will be absorbed. This way, a unique spectrum is created which can be used to identify the chemical composition of the sample.

In this study, FTIR is used to confirm the presence of the hydrogel on the surface. For all measurements, a Spectrum 100 FT-IR Spectrometer (Perkin Elmer) is used to produce a spectrum from 4000 to 500 cm^{-1}. The average of 32 scans is taken.

3.1.3.2 Differential scanning calorimetry (DSC)

DSC is a thermoanalytical characterization technique that measures the difference in heat input that is required to change the temperature of a sample vs. a reference. The technique can be used to measure physical properties and thermal transitions of polymers. However, in this thesis it is used to evaluate the different types of water inside a hydrogel.

For this master thesis a DSC 250 (TA instruments) was used. Samples of 5 mg are placed inside a hermetically sealed pan and subjected to a cooling-heating cycle. In a first step, the sample is equilibrated at 20°C for 5 minutes. Next, the sample is cooled from 20°C to -50°C by a rate of -10°C/min. The sample remains for 5 minutes at -50°C. Afterward the sample is heated again to 20°C at 10°C/min. For each hydrogel composition, three samples are made which are all subjected to two subsequent cooling-heating cycles.

3.1.3.3 Calculation of different types of water

To be able to determine the amount of bound freezable, free freezable and non-freezable water, the following strategy was employed.

DSC detects all type of freezable water (bound and free). During heating, the DSC graphs show two different overlapping peaks corresponding to the freezable bound water and freezable free water. These peaks are deconvoluted and the area under each peak is calculated to obtain the melting enthalpy of the bound freezable water and free freezable water, respectively. Next, the fraction of bound freezable water (W_{fb}) and free freezable water (W_{ff}) can be found as:

$$W_{fb} = \frac{\Delta H_{fb}}{\Delta H_{PBS}} \tag{3.1}$$

$$W_{ff} = \frac{\Delta H_{ff}}{\Delta H_{PBS}} \tag{3.2}$$

where ΔH_{fb} is the melting enthalpy of bound freezable water, ΔH_{ff} is the melting enthalpy of free freezable water and ΔH_{PBS} is the melting enthalpy of PBS (293.3 J/g) which was also found by DSC.

Logically, the total amount of freezable water then equals to $W_f = W_{fb} + W_{ff}$. Finally, all hydrogels had a total water content of 90%. As such, the total amount of water fraction (W_{tot}) is equal to 0.9. From this, the fraction of non-freezable water can be found as $W_n = W_{tot} - W_f$

3.1.3.4 Freezing tests

To determine the anti-icing properties of the protein hydrogels, freezing experiments are performed. The overall freezing set-up can be found in **Figure 3.3**. A sample is placed on top of Peltier plates which are attached to a liquid cooled heat sink. These are subsequently powered by a 11.5 DC voltage source. This way, all samples are cooled by 10°C/min. A FLIR A315 IR camera records the top view of the sample.

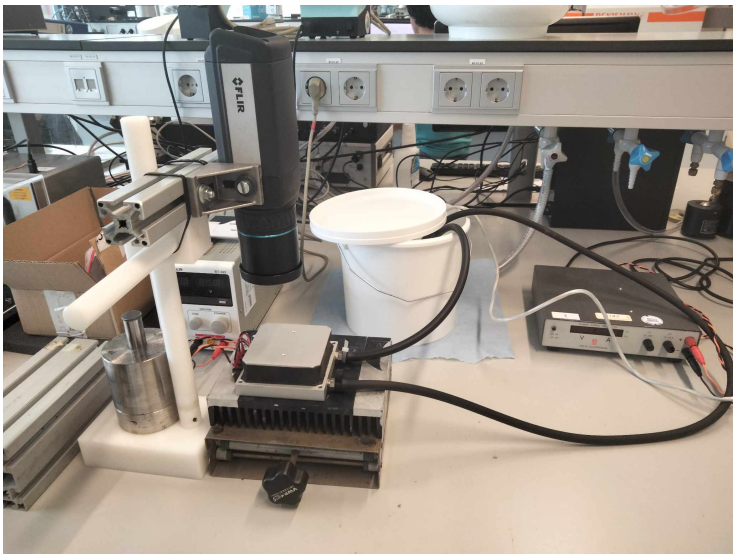

Figure 3.3: Set-up of freezing experiments

From the start of each cooling test, a timer records the time up until the moment of the first freezing event that can be detected by the IR camera. This way the freezing onset time (t_{fo}) is obtained. To get the the freezing onset temperature (T_{fo}), the average temperature on each sample is plotted with the FLIR tools program. An example of such a graph can be found in **Figure 3.4**. The temperature on the graph where the freezing event starts (indicated with a rise in temperature) is recorded as the T_{fo} of the sample. All measurements were taken with a relative humidity of 59%.

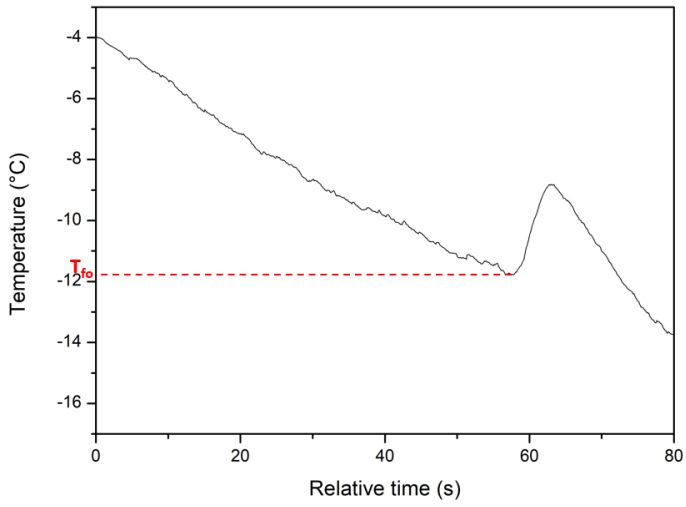

Figure 3.4: Example of relative time vs. temperature graph obtained for one sample from the IR data

3.1.3.5 Evaluation of condensation and frost growth

To evaluate the condensation and frost growth on the different samples, two digital USB cameras are mounted around the freezing set-up: a Dino Lite camera and a Celestron handheld digital

microscope Pro. The Dino Lite camera was used to capture the top view of the sample while the side view was recorded with the Celestron camera. The set-up can be found in **Figure 3.5**

Figure 3.5: Camera set-up to record condensation and frost growth

3.2 Results and discussion

After producing the hydrogels, they are characterized with FTIR to confirm the presence of ice-binding proteins in the hydrogels. In a next step, the different types of water within the hydrogels are investigated with DSC to gain a better understanding of the protein influence on the type water in the hydrogel and subsequently the freezing behaviour of the hydrogel. Finally, the hydrogel samples are subjected to freezing tests and their freezing performance is evaluated.

3.2.1 Characterization of protein-hydrogels

After spraying the hydrogel on the aluminium plates, they are characterized with FTIR. **Figure 3.6** shows the spectra of the different components out of which the hydrogel is constructed. PEG dithiol and 4-arm PEG maleimide show many similar peaks which can be ascribed to PEG. By example, the peak at 2882 cm^{-1} can be ascribed to C-H stretching. Peaks around 1467 cm^{-1} and 1340 cm^{-1} are related to C-H bending. Finally, the peaks at 1280 cm^{-1} and 1097 cm^{-1} are linked to O-H and C-O-H stretching [85]. The 4-arm PEG maleimide spectrum shows an additional peak around 1708 cm^{-1} which is not visible in the PEG dithiol spectrum. This peak is related to C=O stretching of maleimide.

Figure 3.7 shows the FTIR peaks for the hydrogels with and without AFPs. The similar PEG peaks as for 4-arm PEG and PEG dithiol can be easily distinguished. On the other hand, the peak at 1708 cm^{-1} relating to the maleimide functionality is not detectable in any of the hydrogel spectra, indicating that nearly all maleimide functionalities have reacted to form the hydrogel. In addition, two overlapping peaks can be found at 1642 cm^{-1} and 1532 cm^{-1} for the AFP-hydrogels. Comparing these peaks with the AFP spectrum in **Figure 3.6**, they are most likely the amide I and amide II peaks from the protein. As such, the presence of the protein in the hydrogel can be confirmed.

The INP hydrogels show very similar spectra as the AFP hydrogels. Their spectra can be found in Appendix E.

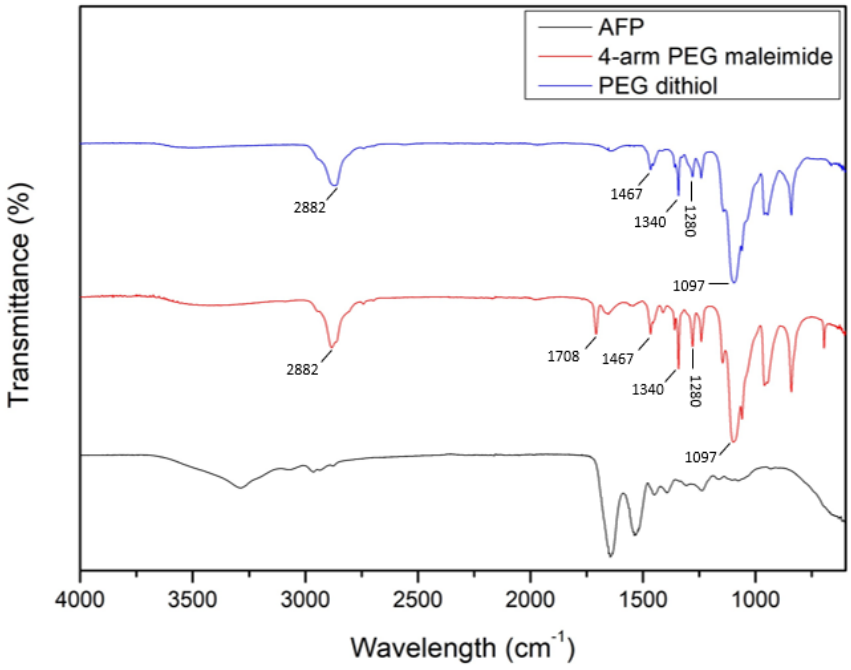

Figure 3.6: Spectra of AFP, 4-arm PEG maleimide and PEG dithiol

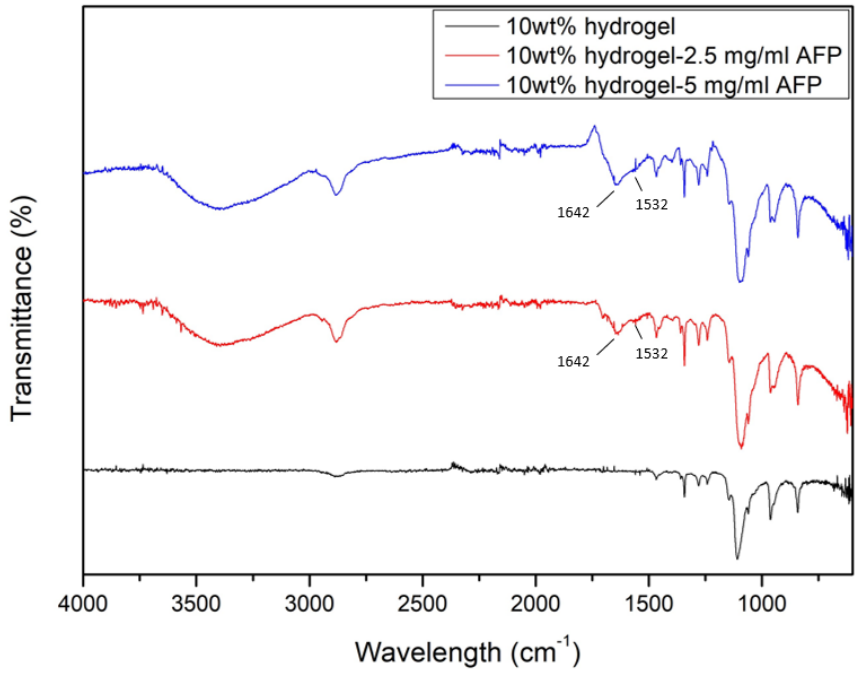

Figure 3.7: FTIR spectra of 10 wt% hydrogel, 10wt% hydrogel-2.5mg/mlAFP and 10wt% hydrogel-2.5mg/mlAFP

3.2.2 Characterization of type of water in hydrogel

It is well known that the freezing behaviour of hydrogels is partly dictated by the different types of water that are present within the hydrogel. Generally, water in hydrogels either have no interactions with the polymer network, which results in freezable free water or interactions between the polymer network and the water do occur which can lead to freezable bound water of non-freezing water depending on the strength of the interactions. When there is nearly no interaction between the polymer network and the water, it is termed freezable free water. This type of water has approximately the same properties as bulk water. On the other hand, when polymer chains are able to capture nearby water, interactions between the polymer network and water occur. Water within hydrogels can strongly interact with the hydrogel polymer structure by means of multiple hydrogen bonds with polar groups within the amphiphilic polymer structure. As a result of this, the water is unable to move and orient itself into an ice crystal structure. Indeed, as can be seen on **Figure 3.8**, the non-freezable water is bound to the polymer network with two hydrogen bonds, hindering any type of movement of the water molecule. Because of this, the water is not able to freeze and is subsequently called non-freezing water. On the other hand, when water has weaker interactions with the polymer network (e.g. one hydrogen bond or van der Waals interactions) it is termed freezable bound water. This freezable bound water is most often found around hydrophobic segments of the polymer and is able to freeze albeit at lower temperatures [86]. Compared to free water, the crystal growth rate of freezable bound water is about ten times slower due to the fact that their movement is slowed down due to the interactions with the polymer. In addition, the ice formed by freezable bound water is metastable when cooled slowly and amorphous when quenched. In contrast, free water in hydrogels forms stable hexagonal ice [86]. This might be explained due to the fact that the freezable bound water molecules are tied to the polymer network and are unable to orient themselves properly to obtain this hexagonal structure.

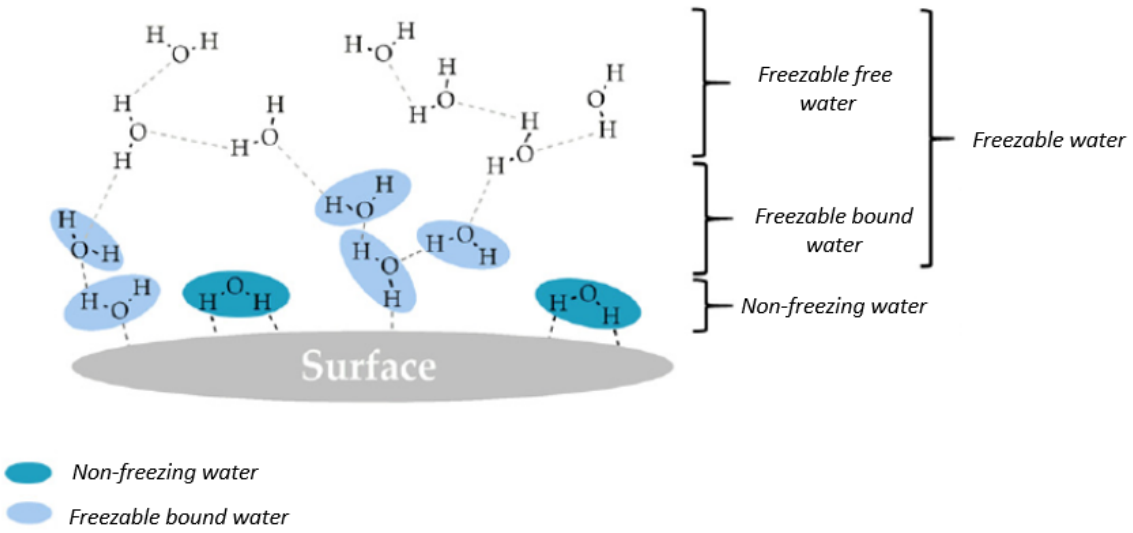

Figure 3.8: Different types of water in a hydrogel [1]

Since the type of water in a hydrogel clearly influences the hydrogel freezing behaviour, it is

interesting to understand if and how ice-binding proteins might impact the distribution of these different types of water within a hydrogel.

Figure 3.9 shows a DSC heating curve from a 10wt% hydrogel-2.5mg/ml AFP. The graph shows two distinct overlapping peaks around -2.9°C and 5°C which are commonly seen in hydrogel DSC heating curves [87]. The peak matching the highest temperature corresponds to melting of free water within the hydrogel. The peak at -2.9 °C can be linked to melting of freezable bound water [87]. In contrast to results in literature, also a smaller broad peak occurs around -20°C. Most likely, this can be explained by the fact that the hydrogels in this study were made with PBS instead of DI water. When evaluating the PBS spectrum (**Figure 3.10**), it clearly shows two distinct peaks. Thorat and Suryanarayanan characterized PBS in frozen state. From their DSC data, they identified two peaks around 0°C and -20°C [88]. The largest peak around 0°C is linked to melting of ice while the smaller peak around -20°C corresponds to the melting of sodium chloride dihydrate-ice [88]. Since the hydrogel is made with PBS, the small peak around -20°C in the hydrogel DSC spectrum is most likely related to the melting of sodium chloride dihydrate-ice from PBS.

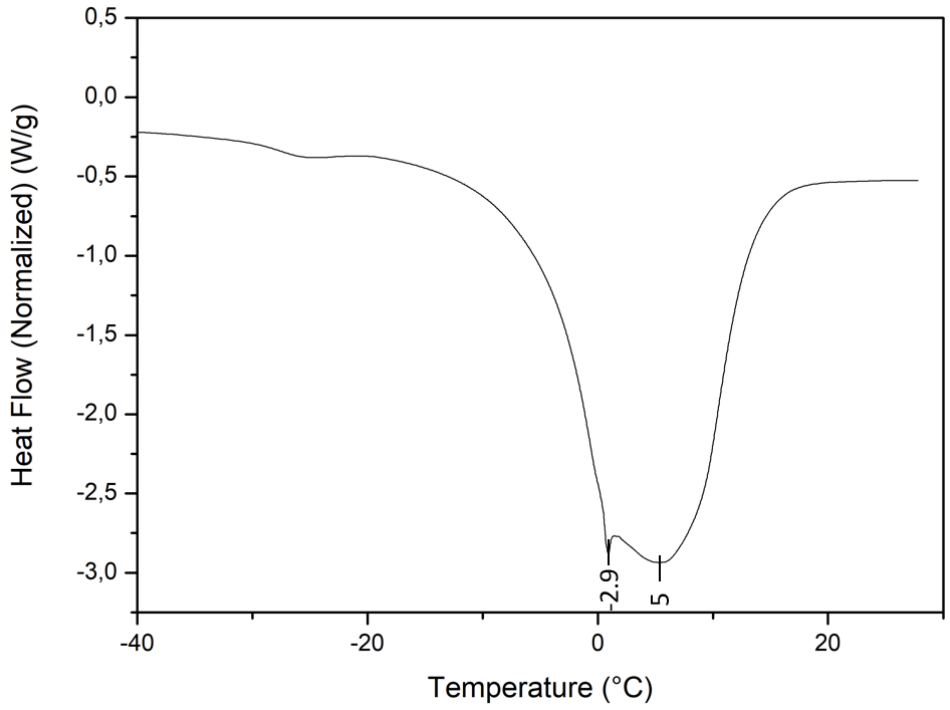

Figure 3.9: DSC heating curve from a 10 wt% hydrogel-10mg/ml AFP

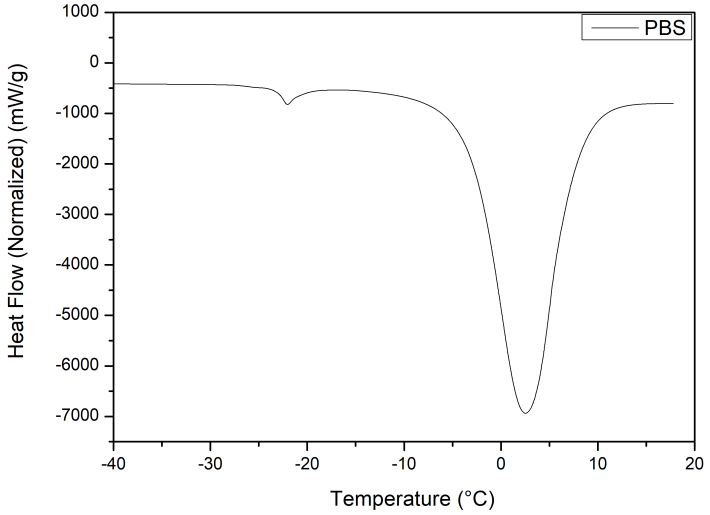

Figure 3.10: DSC heating curve of PBS

From the DSC data (Appendix G), the amount of freezable and non-freezing water in function of the AFP concentration in the hydrogel can be determined. This is represented in **Figure 3.13 a**. For each AFP concentration, the sum of freezable and non-freezing water results in 90% following from the fact that all hydrogels were made to contain 90% water and 10 % polymer. The graph does not show any clear distinguishable trend between non-freezable/freezable water and the AFP concentration. The amount of non-freezing water lies around 13.3% while the amount of freezable water averages around 75.7%. These results are comparable to Cursaru et al. who fabricated PEG hydrogels with diepoxy terminated PEGs. For a hydrogel water content of 91%, 74.2% was classified as freezable water, while 16.9% was classified as non-freezing water [87]. The large amount of freezable water can be easily explained by the fact that the 10 wt% hydrogels have a relatively small polymer network. To be able to strongly interact with the polymer network and create non-freezable water, the water molecule needs to be in close contact with the polymer. Since the polymer network is limited (10 wt%), only a limited amount of water molecules can be tightly bound to the network. As such, only a limited amount of non-freezing water is present in the hydrogel structure. To confirm this hypothesis, Cursaru et al. also developed hydrogels with higher polymer content levels. Indeed, when the polymer content increases from 10 wt% to 20 wt%, the freezable water decreases from 74.2% to 54.1% while the non-freezing water increases from 16.9% to 26.5% [87]. As was depicted in **Figure 3.8**, non-freezing water is mostly formed when the water molecule is fixed to the polymer with two hydrogen bonds, making movement virtually impossible. Considering this, the structure of water on top of hydrated PEG was investigated by Kitano et al. [1]. Their proposed water structure around the PEG chains can be found in **Figure 3.12**. Non-freezing water can be formed by the interaction of water molecules with the ether groups of two neighbouring PEG chains or water molecules can interact with two ether groups on the same PEG chain. To achieve the latter, the PEG chain needs to be slightly bended, which is also represented in **Figure 3.12**. This way, the non-freezing water within the PEG hydrogels can be explained.

From **Figure 3.13 a**, there is no clear trend visible between the AFP concentration and the

amount of non-freezable and freezable water within a hydrogel. Nonetheless, various studies have found that proteins do have interactions with water molecules. Within an aqueous environment, a protein will be surrounded by a hydration layer which plays an important role in protein structural stability, function and dynamics [89]. All water within the hydration shell will have some interaction with the protein. **Figure 3.11** shows the hydration shell around AFP type III. Water within this hydration shell can be divided in nonfreezable hydration water and freezable hydration water. Nonfreezable hydration water will directly interact with the protein surface by electrostatic interactions and hydrogen bonds. On the other hand, freezable hydration water mostly interacts with the nonfreezable hydration water instead of the protein structure itself [90].

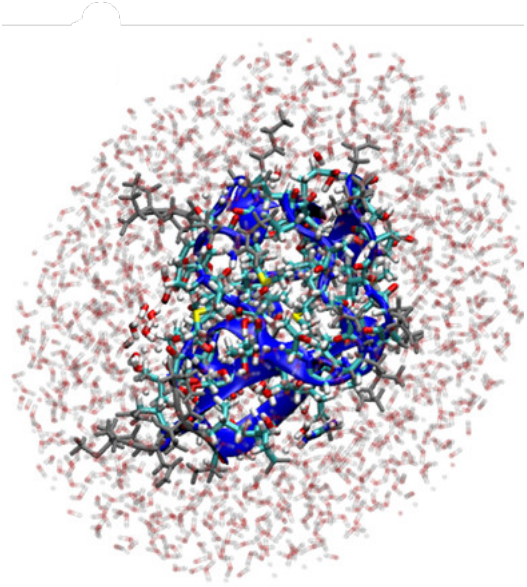

Figure 3.11: 1 nm thick hydration shell at 300K from a type III AFP

From this information it would be expected to find an increase in nonfreezable water and a decrease in freezable water with increasing AFP concentration. However, this is not detected. Berlin et al. determined that a protein has around 0.5 g nonfreezable water for each gram of protein. Taking this into account, the theoretical increase in nonfreezable water would go from 0.125% (2.5 mg AFP/ml of water) to 1 % (20 mg AFP/ml of water). This increase is very small and relatively neglectable compared to nonfreezable bound water introduced by PEG. This might explain why we were not able to record a significant trend with increasing AFP concentration. Nonetheless, even though **Figure 3.13** does not show any clear trends, the freezable and nonfreezable water does vary quite significantly for different AFP concentrations. The reason for these fluctuations are most likely attributed to measurement errors.

To further investigate the interactions between AFPs and water within a hydrogel, the amount of freezable free and freezable bound water is plotted in **Figure 3.13 b**. Initially, the amount of freezable bound water is low but still present. This is comparable to Abasi et al. who also found a relatively low amount of freezable bound water in their Poly((Hydroxyethyl)methacrylate-co-N-(2-Hydroxypropyl) methacrylamide)-based hydrogels [91]. Freezable bound water is either connected to the polymer structure or to another water molecule which is in their turn connected

to the polymer backbone. **Figure 3.12** shows how water can interact with PEG chains to form freezable bound water. It can be formed by an interaction between a water molecule and an ether group from PEG or due to interactions between a water molecule and another water molecule which is bound to an ether group from PEG. Finally, weaker interactions around hydrophobic segments of the PEG chain can also lead to freezable bound water.

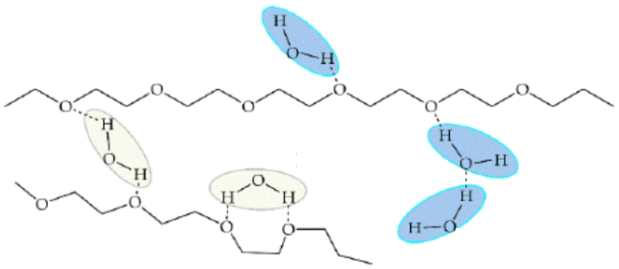

Figure 3.12: Proposed structure of water in hydrated PEG structure (blue = freezable bound water, yellow = non-freezing water) [1]

With increasing AFP concentration, the amount of freezable bound water increases from 0.89 % to 5.33%. This indicates that AFPs clearly have weaker interactions with the water molecules in the hydrogel. The interaction between AFP type III and water molecules is very complex and still not entirely understood. As can be seen on **Figure 3.14 a**, the entire AFP surface is covered in both hydrophilic and hydrophobic regions. The hydrophilic regions bind to water molecules by means of hydrogen bonds while the hydrophobic moieties group the water molecules and position themselves in the ice structure, e.g. in holes in the middle of six-membered water rings [92]. These hydrophobic and hydrophilic regions are important for ice recognition. However, before AFPs attach to ice, they interact with water molecules from the liquid and form a so-called hydration layer (**Figure 3.11**) which consists of both nonfreezing and freezable hydration water, as was described above.

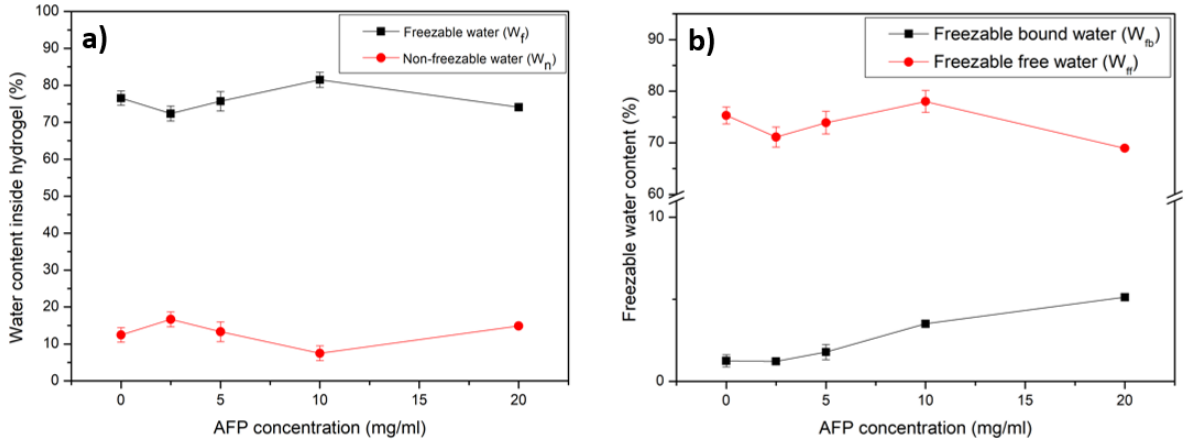

Figure 3.13: A) Amount of freezable and non-freezing water in function of AFP concentration and B) Amount of freezable free and freezable bound water in function of AFP concentration [1]

Brotzakis et al. investigated the water structure and dynamics in the hydration layer of AFP type III. It should be noted that they only investigated the freezable hydration water. They found that water in the hydration layer is able to reorients itself, albeit at a slower rate than bulk water (**Figure 3.15**). Furthermore, AFP type III was split into 5 different regions to investigate the water dynamics in different AFP regions. Slowest reorientation was found around the threonine-18 (THR-18) residue which is found at the AFP IBS [93], this is also seen in **Figure 3.15**. In addition, the water around the IBS was more structured while water around the NIBS was not structured. From this information, it is clear that water indeed interacts with the protein but is still able to move and rotate albeit at lower speeds. Water at the IBS is structured and mimics the ice crystal structure while the hydration water at the NIBS is less structured and retards ice growth since the water molecules in the hydration layer do not match the ice crystal lattice. As such, the water surrounding the large NIBS might act as freezable bound water where the water eventually rotates to accommodate the ice lattice but at slower rates as bulk water due to its interactions with the protein. This might explain why the freezable bound water increases in the hydrogel with increasing protein concentration.

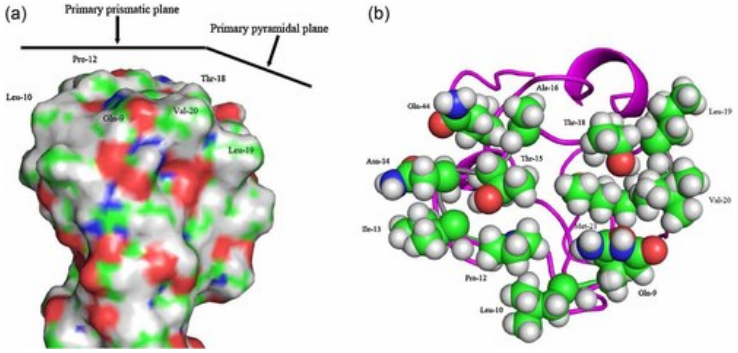

Figure 3.14: a) Side view of AFP type III with IBS on top and b) top view of AFP type III IBS with relevant amino acids, color scheme: blue= nitrogen, red= oxygen, green= carbon and grey= deuterium[92]

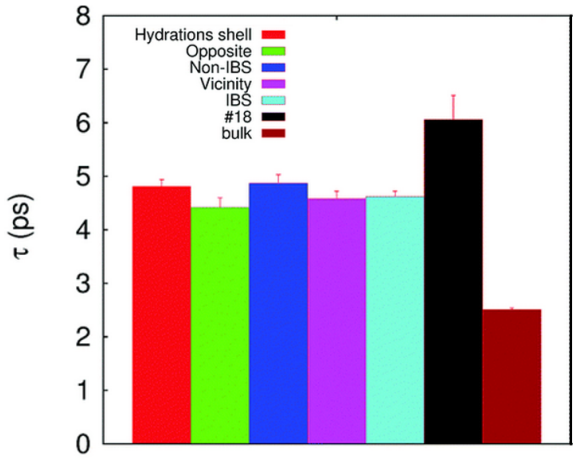

Figure 3.15: Water reorientation of water in the hydration shell of AFP type III [93]

3.2.3 Freezing of as-built hydrogel

After characterizing the hydrogel and the type of water that is present within it, freezing tests are performed to evaluate the hydrogel freezing behaviour. The DSC results indicated that there is an influence of the AFP concentration on the type of water within a hydrogel. Freezing tests are performed using hydrogels with different concentrations of AFP. With the freezing tests, it will become clear whether this change in the type of water can be linked to the freezing behaviour of the hydrogel. In addition, hydrogels with INPs will also be tested and compared to the hydrogels with AFPs.

3.2.3.1 AFP concentration

Hydrogels with two different AFP concentrations are developed (2.5 mg/ml and 5 mg/ml). From the freezing results, it is clear that the t_{fo} increases while the T_{fo} decreases with increasing AFP concentration (**Figure 3.16 a and b**). As such, the AFPs are able to succesfully delay ice growth within the hydrogel environment.

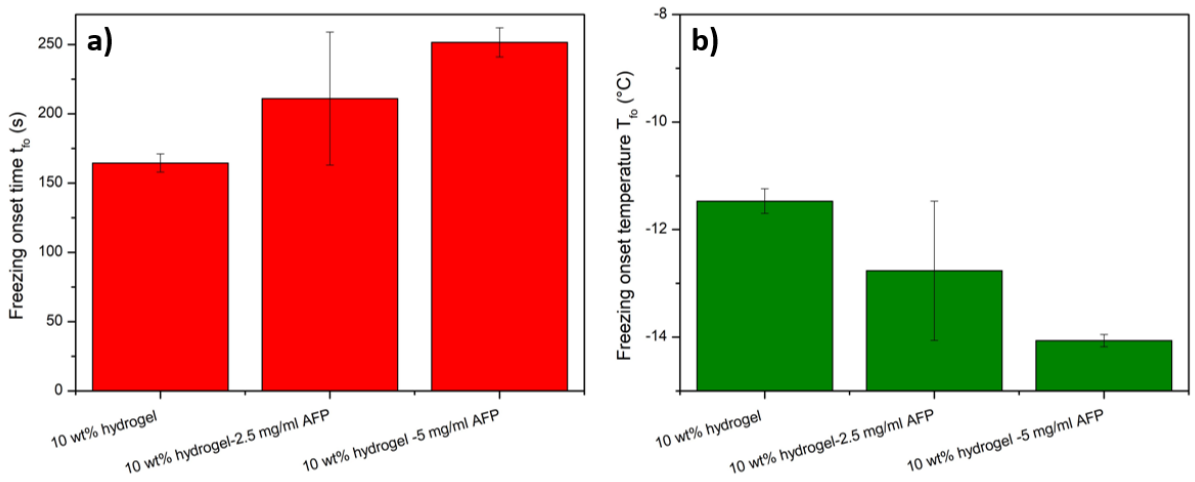

Figure 3.16: Effect of AFP concentration in a hydrogel on a) t_{fo} and b) T_{fo}

The hydrogel environment is able to closely mimic the natural environment of AFPs, meaning that the AFPs are surrounded by water in the hydrogel. This liquid can act as a solubilizing environment which encapsulated and sebsequently protects the proteins from any form of degradation [94]. In addition, the hydrogels are made from PEG which is widely known for its resistance against non-specific protein adsorption. This resistance can be explained a hydration layer around the PEG polymer. By means of hydrogen bonds, a water layer is formed around the PEG molecular chain, avoiding any form of non-specific protein adsorption [95]. This water layer around the PEG chains was characterized by DSC in the previous section.

Furthermore, when evaluating the AFP-hydrogel structure, it is clear that most AFP in the hydrogel will be attached to an arm of the 4-arm PEG maleimide by means of a PEG dithiol molecule. This is indicated with a red circle in **Figure 3.17**. This 4-arm PEG maleimide has an average molecular weight of 10000 g/mol. As such, each arm of the 4-arm star has an average molecular weight of 2500, which corresponds to a very long chain. As reference, the molecular

weight of the longest chain used for the surface approach (Mal-PEG24-NHS) was only 1394.55 g/mol. As such, it is clear that the AFPs have a lot of mobility in the hydrogel allowing them to move freely around.

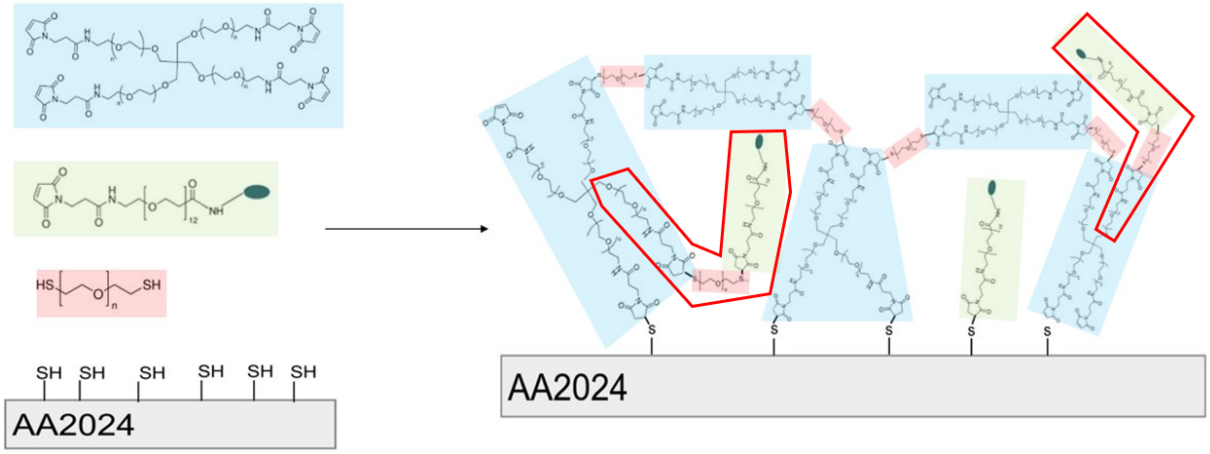

Figure 3.17: Development of an AFP-hydrogel where blue represents 4-arm PEG maleimide, red respresents PEG dithiol and green represents the AFP connected to the NHS-PEG-Maleimide linker

From this information, it is clear that the PEG hydrogel mimics the AFP environment. Firstly, the hydrogel is mostly made up of water (90%) which protects the AFP. Furthermore, due to the choice of PEG as synthetic polymer for the hydrogel, the AFPs have limited interactions with the polymer chains meaning that the hydrogel network itself will have limited interference with the protein working mechanism. Finally, the AFPs are attached to a very long PEG arm, allowing them to very move inside the hydrogel. This way, AFPs are able to work together and inhibit ice growth within the hydrogel in a similar way as they do in their natural environment. A schematic representation of this mechanism can be found in **Figure 3.18 a**.

In addition, the freezing behaviour of hydrogels might also be linked to the DSC results. As was described in the previous section, the amount of freezable bound water increases with increasing protein concentration in the hydrogel. This freezable bound water can most likely be linked to the water connected to the NIBS of the protein. The water at the NIBS has a disorganized structure to avoid ice formation (**Figure 3.18 b**). As such, increasing the AFP concentration leads to an increase of water molecules at the NIBS. These disorganized water molecules at the NIBS will orient themselves to the ice crystal lattice at a slower pace as bulk water, leading to a delay in ice formation. However, the increase in freezable bound water from 0 mg/ml AFP to 2.5 mg/ml AFP in the hydrogel only corresponds to 0.53%. Since this increase is relatively small, the delay in freezing in the hydrogel will likely be mostly governed by the previously described hydrogel environment and protein mobility while the freezable bound water will likely play a smaller role.

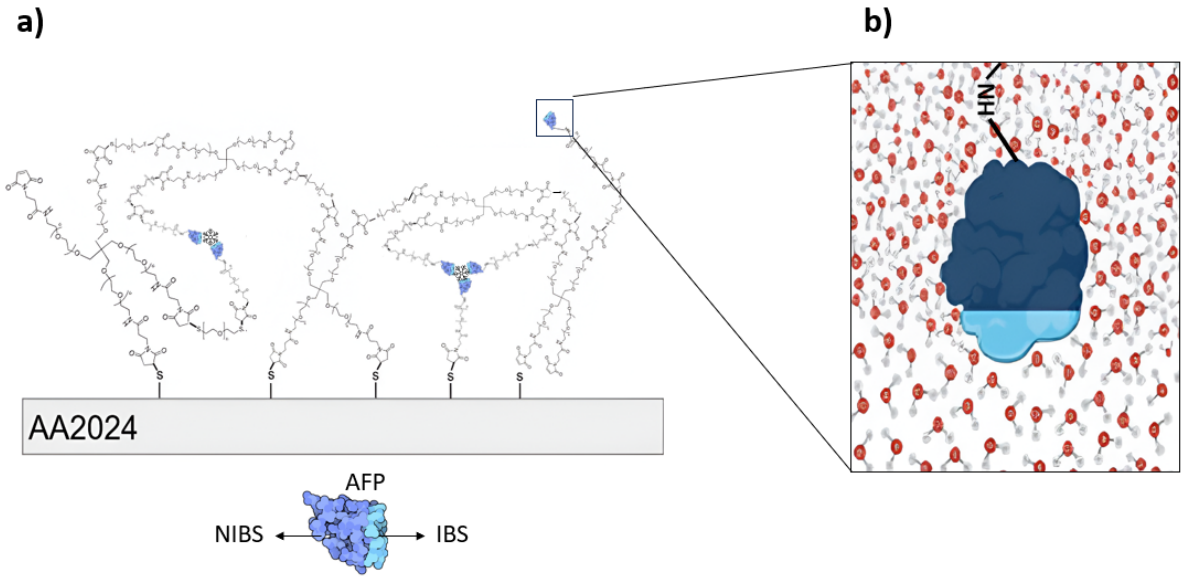

Figure 3.18: a) Mechanism of how the AFPs inhibit ice growth in hydrogel and b) water around AFP NIBS and IBS

3.2.3.2 Effect of different ice-binding proteins

Figure 3.19 a and b show the influence of the AFPs vs. the INPs in hydrogels. It is clear that INPs lead to earlier ice formation at higher temperature. This is as expected since INPs are able to position the surrounding water into an ice-like structure, which was explained before. Ice formation in the 10 wt% hydrogel-2.5mg/ml INP started at -9.7 °C while ice formation in the 10 wt% hydrogel-5mg/ml INP started at -8.98°C. Wang et al. also found that their INP hydrogels froze at an enhanced temperature around -8°C [33].

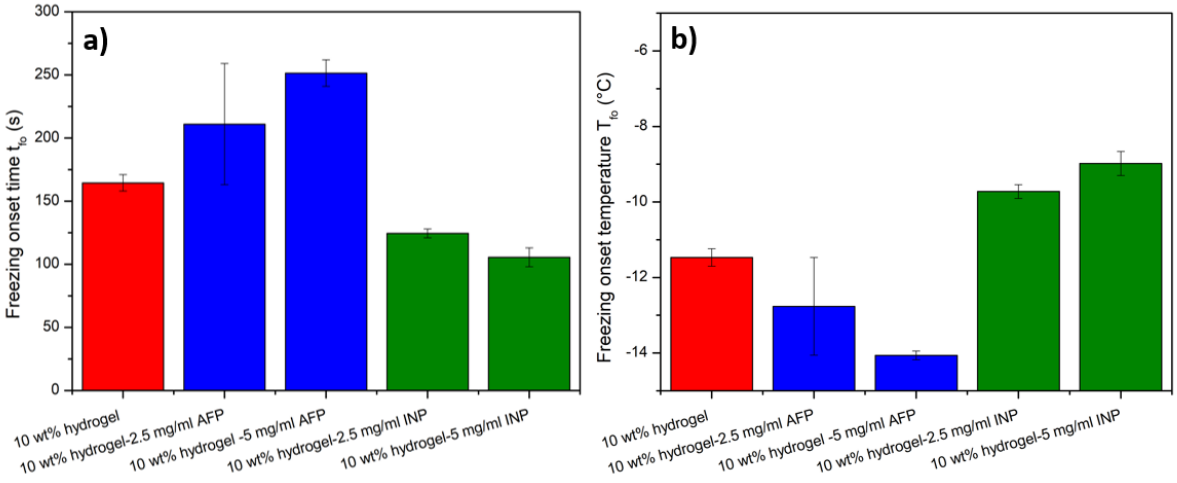

Figure 3.19: Effect of AFP concentration in hydrogels and INP concentration in hydrogels on a) t_{fo} and b) T_{fo}

3.2.4 Freezing of dehydrated hydrogels

After determining the freezing behaviour of the hydrated hydrogels, the gels are dehydrated overnight. This way, the protein environment is altered again. Now the proteins are confined within polymeric environment without the presence of water.

3.2.4.1 AFP concentration

Figure 3.20 shows the effect off different AFP concentrations within dehydrated hydrogels. From these results, we can identify two major differences with the hydrated hydrogels.

First off, the dehydrated hydrogel without any proteins freezes much later compared to the hydrated hydrogel. Generally, a hydrogel contains non-freezing, freezable bound and freezable free water. With decreasing water uptake in the hydrogel, the freezable water decreases while the non-freezing water remains constant up until a certain value. This was investigated by Ostrowska-Czubenko et al. who found a linear behaviour between the hydrogel water uptake and the freezable water content. In addition, they found that the formation of different types of water in a hydrogel goes as follows. With a very low water uptake, only non-freezing water will be present in the hydrogel. However, with increasing water content, also freezable bound water will become present. Eventually, with a sufficiently high water uptake, freezable free water becomes present in the hydrogel [52], [96]. From this information, the freezing behaviour of the dehydrated hydrogels might be explained. Most likely, the dehydrated hydrogels still contained a small amount of water which was either non-freezing or freezable bound water. Because of this, the water which is still present in the hydrogel either does not freeze or freezes much later due to the interactions between the water molecules and the polymer network. This way, the large difference in T_{fo} and t_{fo} for the hydrated vs. dehydrated hydrogels can be explained.

Secondly, with increasing AFP concentration, t_{fo} decreases while T_{fo} increases. This means that the dehydrated hydrogels freeze quicker with increasing AFP concentration. This is an opposite trend compared to the hydrated hydrogels where the freezing is delayed with increasing AFP concentration. The major difference between the hydrated and the dehydrated hydrogels is the presence of water, indicating that the water might be a critical factor to take into account. It might be possible that the water within the polymer network enabled the AFP mobility. By eliminating the water, the AFPs might be locked in place within the polymeric structure, which decreases their mobility. This might explain the differences in freezing behaviour between hydrated AFP hydrogels and dehydrated AFP hydrogels.

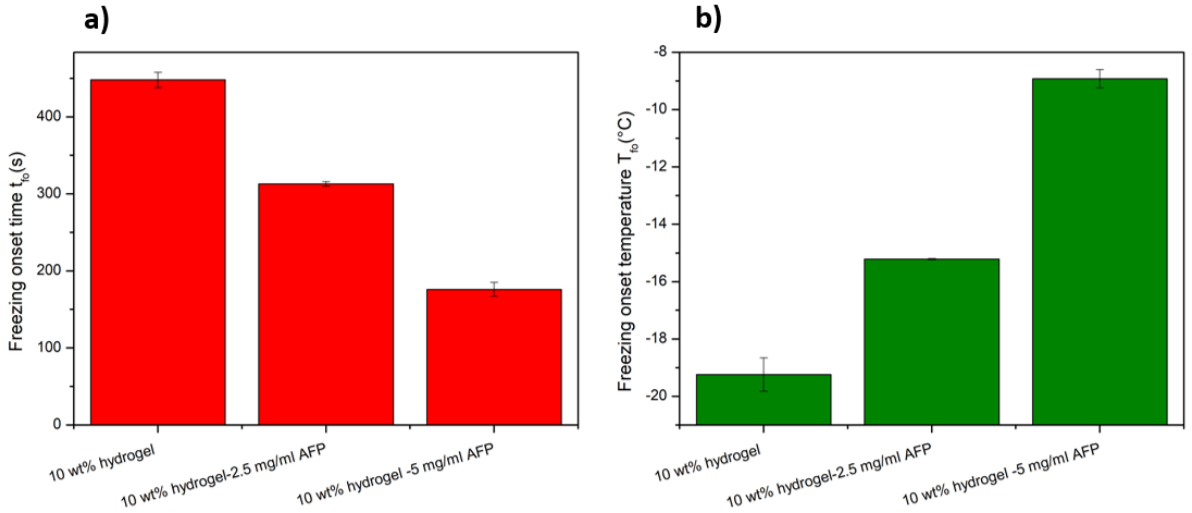

Figure 3.20: a) Effect of AFP concentration on t_{fo} in dehydrated hydrogels and b) effect of AFP concentration on T_{fo} in dehydrated hydrogels

3.2.4.2 Effect of different ice-binding proteins

The difference in freezing behaviour in the AFP and INP dehydrated hydrogels can be found in **Figure 3.21 a and b**. INP dehydrated hydrogels still maintain their ice-promoting behaviour in the dehydrated hydrogels. On the other hand, AFPs also show ice-promoting behaviour. Especially, 10wt% hydrogel-5 mg/ml AFP has an ice-promoting effect similar as the INP hydrogels. Similar as was described for the surface, the INP CRD and the AFP IBS are closely related to eachother which might explain their similar freezing behaviour.

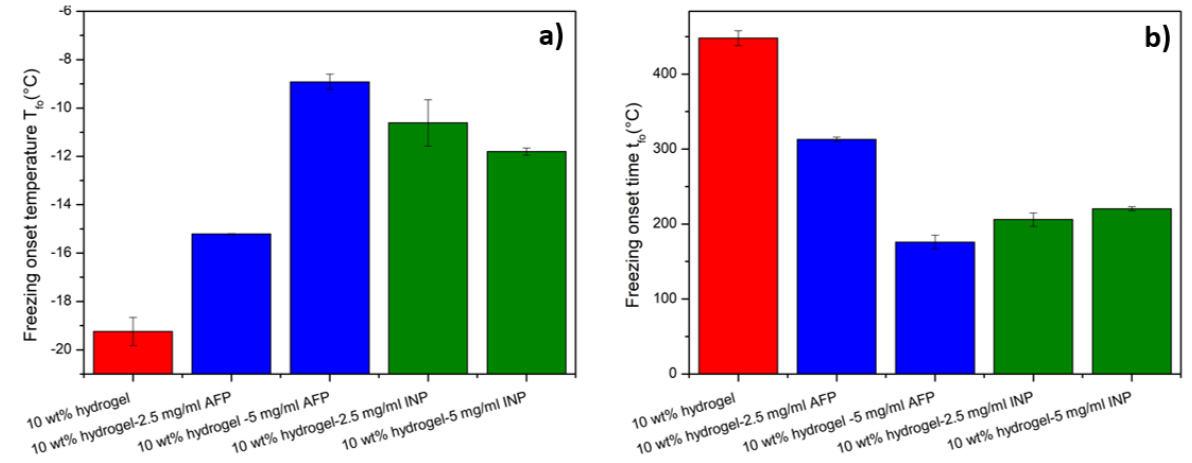

Figure 3.21: Effect of AFP concentration and INP concentration in dehydrated hydrogels on a) t_{fo} and b) T_{fo}

Chapter 4

Conclusion

In literature, AFPs are known to inhibit freezing in bulk water. This makes them an interesting candidate for the development of new anti-icing surfaces. However, up until now, there is very limited knowledge about how these proteins function in any other media, i.e. on a surface or within a coating system remains. Therefore, we set out to investigate how the environmental conditions of the AFPs affect their behavior. This is fundamental knowledge that we need to uncover before they can be used to inhibit freezing in anti-icing coatings. To investigate this, AFPs are attached directly to the surface and within a polymeric bulk environment. In a first step AFPs are directly attached to the surface. The protein concentration on the surface and the linker chain lengths are varied. Interestingly, it was found that AFPs actually act as ice-nucleating proteins when attached to the surface. This effect further increased when the protein concentration on the surface was increased. When comparing the AFP surfaces to INP surfaces, it was found that AA2024-5mg/ml AFP-PEG12 had similar ice-nucleating capabilities as the INP surfaces. In normal circumastances, AFPs will have full mobility within a liquid environment. When a small ice crystal is formed, multiple AFPs will attach to the ice with their IBS and collectively hinder further ice growth. However, by attaching the proteins to the surface, their mobility is hindered which prohibits them to work together. Furthermore, their IBS, which is normally used to attach to ice, has a structure similar to the ice crystal lattice. Because of this, the IBS can act as a template on which ice can start to grow. This is similar to the working mechanism of INPs who also structure water molecules into an ice-like formation to promote ice formation. As such, when the AFPs are attached to the surface, their IBS is presumably oriented toward the water which makes them act as INPs. This explains the freezing behaviour of the AFP surfaces.

To further investigate this theory, AFPs were attached to the surface using linkers of various chain lengths. This enhances the protein mobility on the surface. From the results it became clear that increasing the linker chain length, thus increasing the protein mobility, indeed increased the t_{fo} and decreased T_{fo}. As such, the AFP mobility is a critical factor to take into account when designing AFP surfaces.

Furthermore, during the freezing tests it was found that the type of frost that was formed on the ice-binding protein surfaces was different compared to the frost on AA2024-SH. Dendrite growth on AA2024-SH was very undirected since dendrites grew in all different directions. On the other hand, most of the AFP surfaces (AA2024-2.5mg/ml-PEG2, AA2024-2.5mg/ml-PEG12, AA2024-5.0mg/ml-PEG12) had a much more upward dendrite growth. Again, the IBS of the AFPs might

be acting as templates on which the dendrites grow in a more upward direction. INP surfaces and AA2024-2.5mg/ml-PEG24 had a much less directed dendrite growth compared to AA2024-2.5mg/ml-PEG2, AA2024-2.5mg/ml-PEG12 and AA2024-5.0mg/ml-PEG12. Since INP surfaces and AA2024-2.5mg/ml-PEG24 were more hydrophilic, there might be a competition between the directed dendrite growth and the hydrophilicity of the surface.

In a next step, the ice-binding proteins are incorporated in a hydrogel. This hydrogel should more closely mimic a polymeric coating environment which would eventually be used in industry. The freezing tests of the hydrogels showed some interesting results. With increasing AFP concentration, the t_{fo} of the hydrogel increased while the T_{fo} decreased meaning that incorporating the AFPs into the hydrogel led to a delay in ice growth. These results are the opposite of the freezing results from the surface where AFPs promoted ice-growth. As such, by changing the environment, the AFPs have a fundamentally different functioning. The hydrogel environment is able to closely mimic the AFP natural environment by immersing the AFP in a liquid. In addition, this liquid protects the AFP from any form of denaturation, which is not the case for the proteins on the surface. Due to the hydrogel synthesis approach, the AFPs also have a lot of mobility in the hydrogel, enabling them to work together in a similar way as they would within their natural environment. Again, this is different compared to the AFPs on the surface. Interestingly, when the hydrogel conditions are slightly changed, the hydrogels show a completely different freezing behaviour. When the hydrogels are dehydrated, they freeze quicker with increasing AFP concentration, which is a comparable trend as the AFP surfaces. As such, the presence of water appears to be a crucial parameters to take into account.

In conclusion, from this research it has become clear that the working mechanism of AFPs is very complex and varies depending on the environment in which they are incorporated. It was shown that they can either act as ice promotors or ice inhibitors. During this research, the AFPs were first incorporated on surfaces and subsequently in a hydrogel. The major difference between these two environments are the medium (air vs. liquid) and the protein mobility. As such, these factors should be carefully considered when designing AFP surfaces.

Chapter 5

Recommendations

This thesis has thoroughly investigated ice-binding protein in different environments. However, different aspects remain to be investigated.

First of all, from the surface data, it became clear that the ice formation on top of AFP surfaces appeared to be directed by the AFPs themselves. In can be interesting to further investigate this by carefully monitor the crystal growth on top of AFPs. In addition, their appeared to be a relationship between the directionality of the ice and the hydrophilicity of the surface. This can also be further investigated by e.g. using a less hydrophilic linker. This way, the relationship between the ice crystal directionality due to AFPs and the hydrophilicity of the surface can be further investigated.

Furthermore, the hydrogel freezing results showed promising results. Nonetheless, different factors remain to be investigated. By example, this study has only focussed on AFP type III. However, it is known that hyperactive AFPs have a much higher TH effect compared to AFP type III. Because of this, it can be interesting to investigate the effect of these AFPs into a hydrogel. In addition, hyperactive AFPs are much larger than AFP type III. As such, when the polymeric system is carefully designed, it might be possible to incorporate hyperactive AFPs without needing to attach them to the polymeric system. This way, the mobility of the hyperactive AFPs will have no restrictions which might also positively influence the freezing behaviour of the hydrogel.

Except for different types of AFPs, it could also be interesting to incorporate other solutes in the hydrogel and investigate their effect. It has been shown that low mass solutes such as sugars, salts, polyols and polycarboxylates have an effect on the TH activity. Low mass solutes are able to alter the protein solubility which influences their TH behaviour. As such, by adding these low mass solutes inside the hydrogel, the freezing point of the hydrogel might be further decreased.

The 10 wt% PEG hydrogel was a good initial environment to test the protein behaviour. However, these hydrogel are very gel-like with very high water contents making them not very durable. Since durability is a very important aspect, optimizing the hydrogel environment is a logical next step. By example, the crosslinking density of the hydrogel might be carefully increased while monitoring the AFP properties. This way, a more tightly bound polymer network can be developed while keeping the AFP properties optimal.

Appendix A

WCA results

				Mean WCA (°)	**St. dev.**
AA2024	80,84	78,64	80,86	80,11	1,04
AA2024-OH-Pir5	80,73	76,56	79,09	78,79	1,71
AA2024-OH-Pir15	73,82	69,81	68,91	70,84	2,13
AA2024-OH-NaOH/HNO3	48,3	54,84	55,52	52,87	3,25
AA2024-OH-NaOH-5s	54,65	48,05	68,8	57,17	8,66
AA2024-OH-NaOH-10s	39,87	31,41	36,53	35,94	3,48
AA2024-SH (30min)	57,56	66,56	43,11	55,74	9,66
AA2024-SH (2h)	69,17	65,3	59,51	64,66	3,97

Table A.1: WCA results of different activation treatments and immersion times in MPTS

Appendix B

Freezing tests of AFP and AFP-PEG-Maleimide water droplet

	T_{fo} (°C)
PBS droplet	-7.82
AFP droplet	-9.0
AFP-PEG-Maleimide droplet	-9.30

Table B.1: Freezing results of PBS, AFP and AFP-crosslinker water droplet to assure that modifying the protein did not alter its freezing properties

Appendix C

^{1}H-NMR results of supernatant

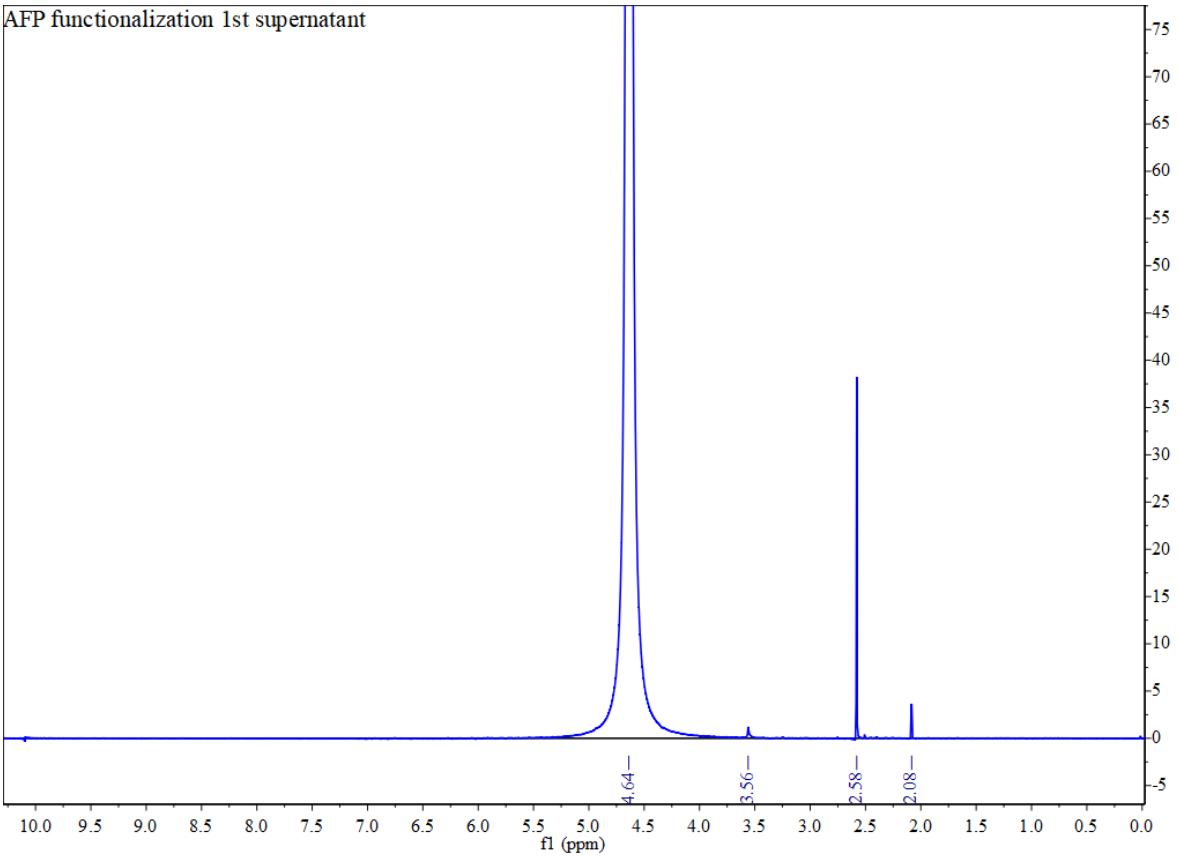

Figure C.1: Supernatant after first centrifuging step

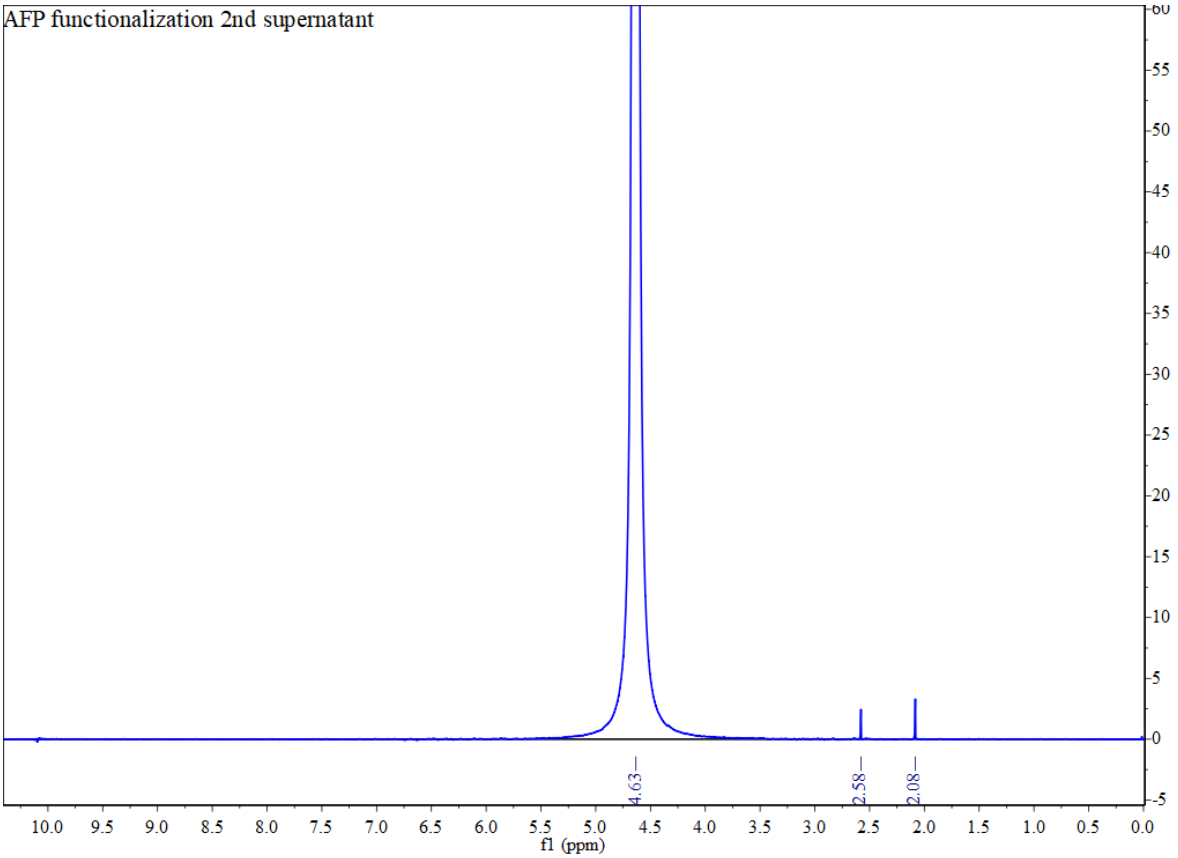

Figure C.2: Supernatant after second centrifuging step

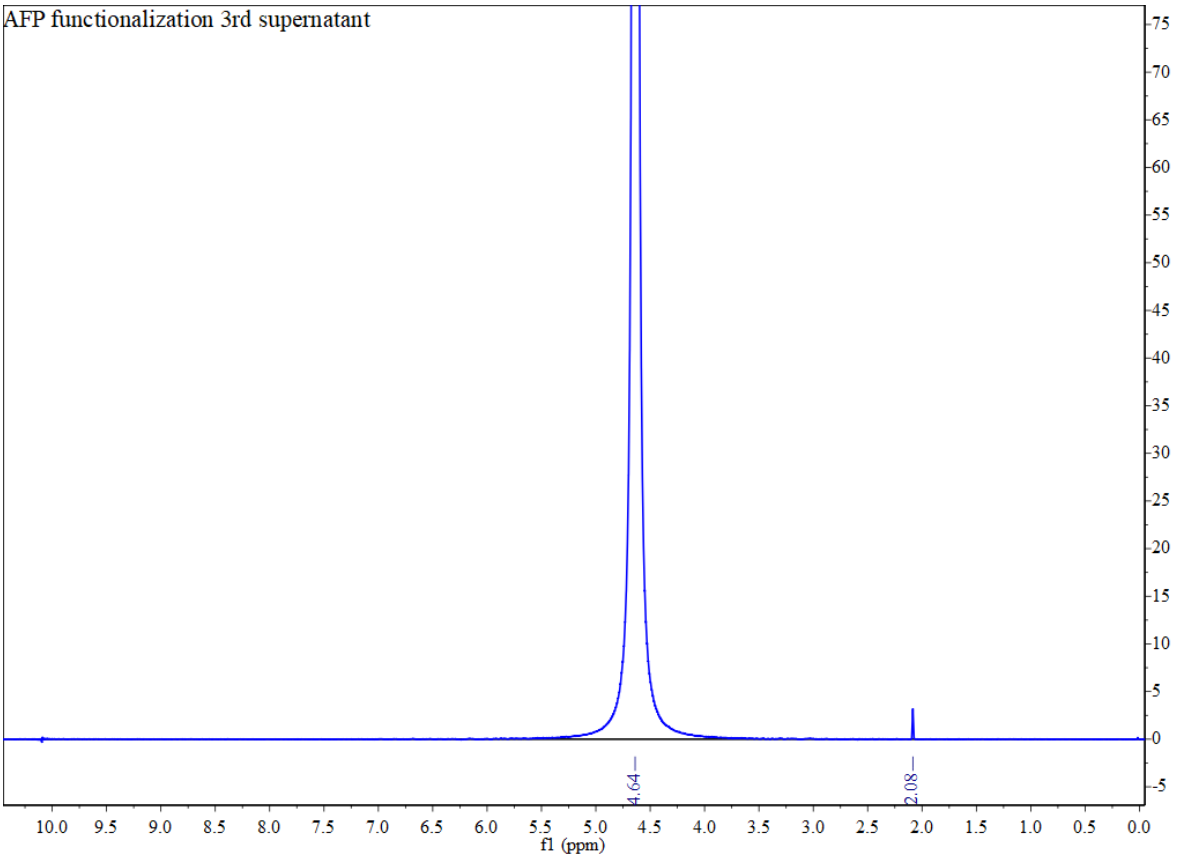

Figure C.3: Supernatant after third centrifuging step

Appendix D

^{1}H-NMR results of protein solutions

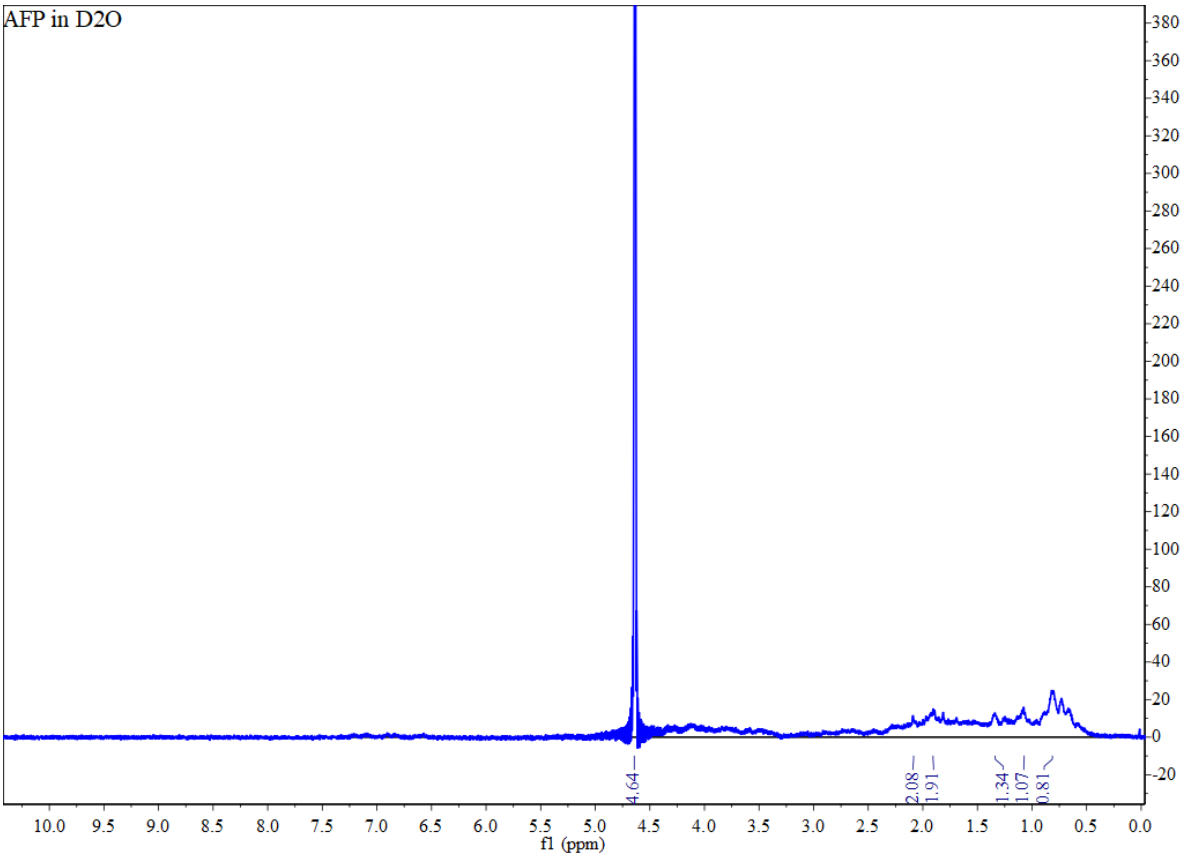

Figure D.1: AFP in D_2O

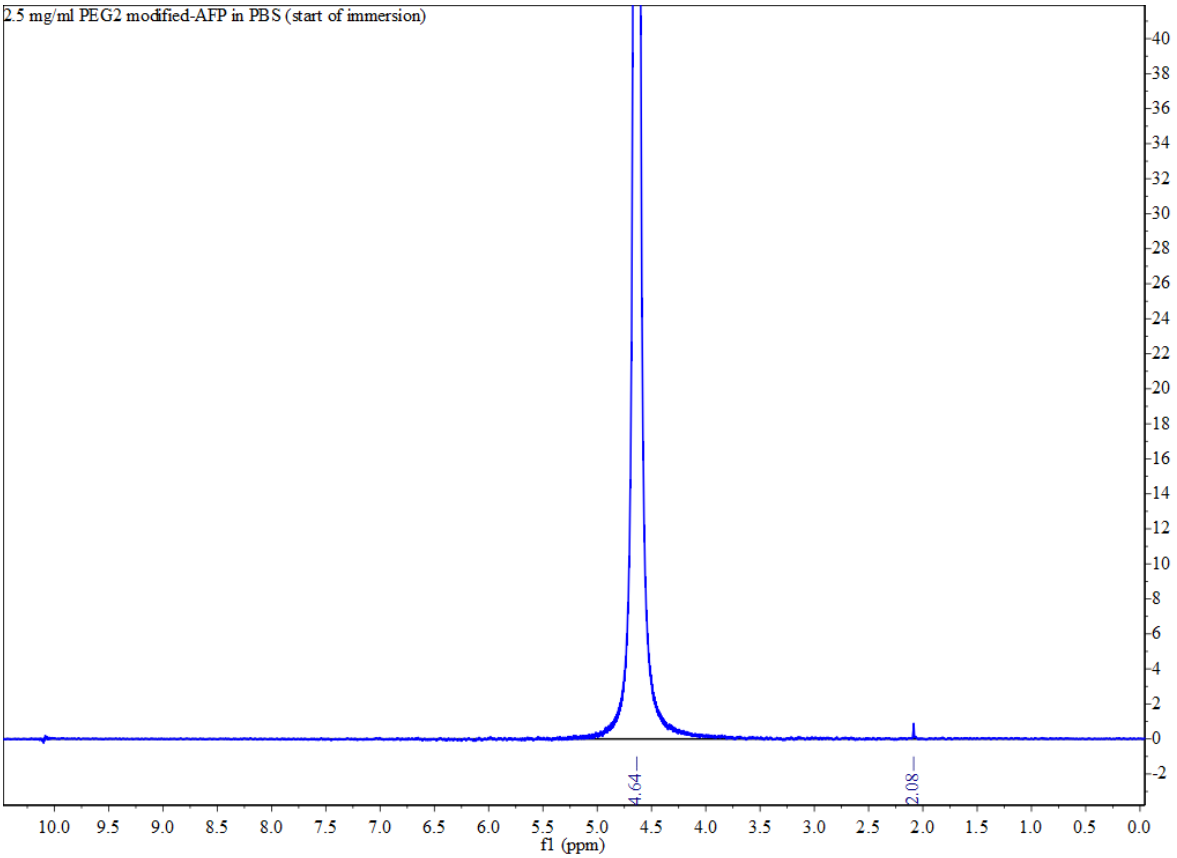

Figure D.2: AFP 2.5mg/ml-PEG2 reaction mixture at start of immersion

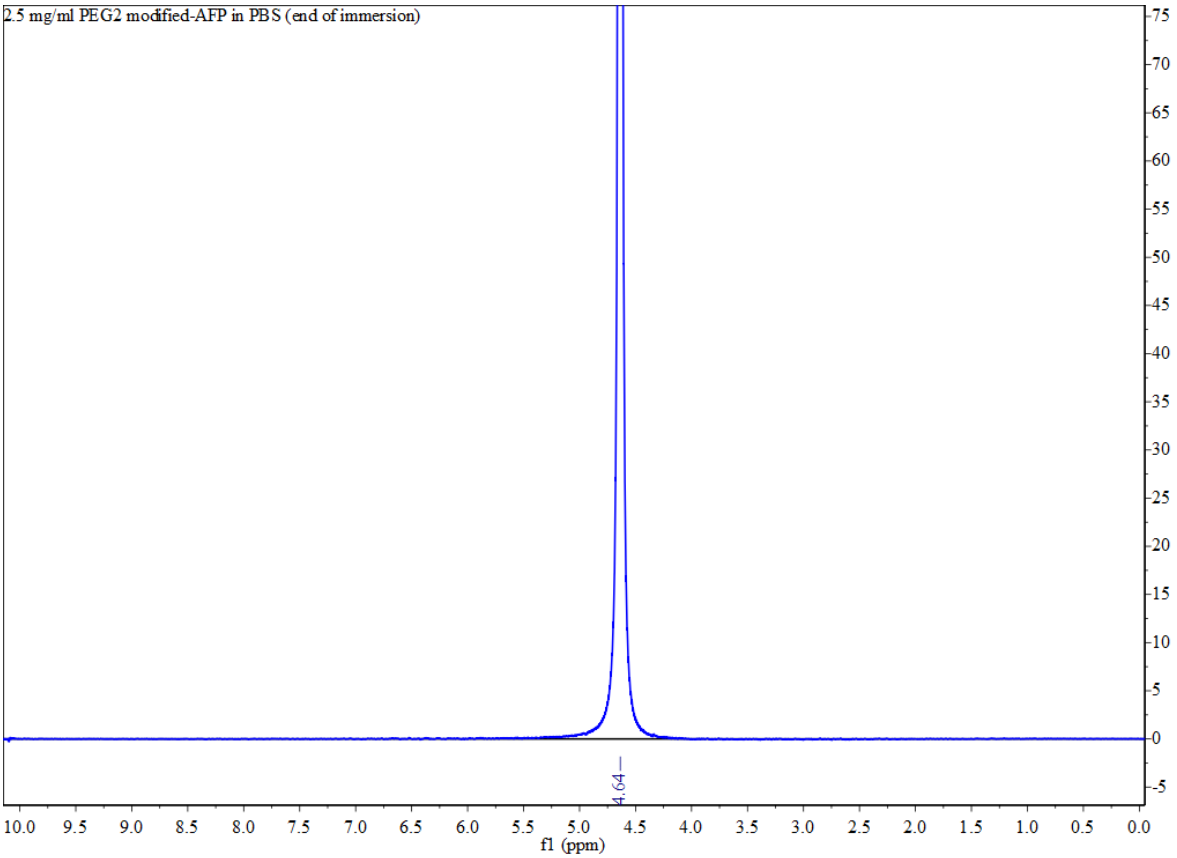

Figure D.3: AFP 2.5mg/ml-PEG2 reaction mixture at end of immersion

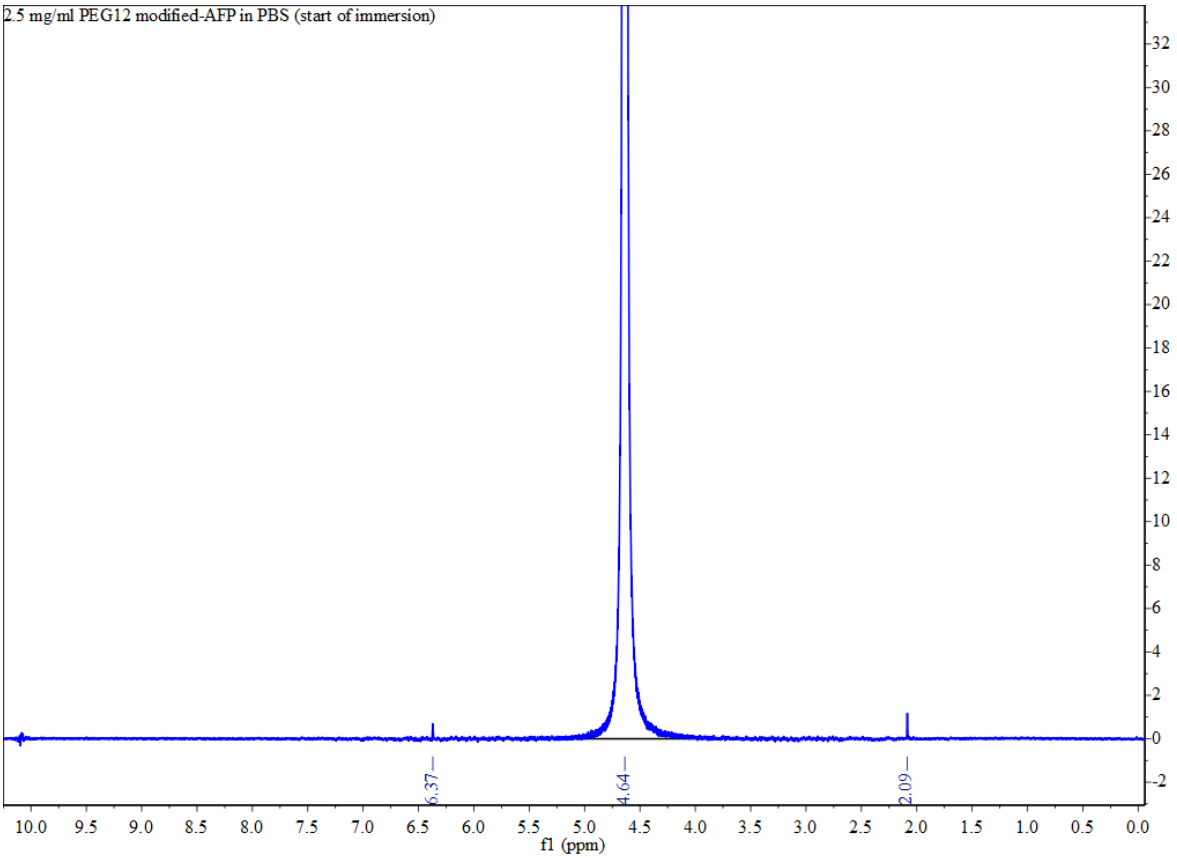

Figure D.4: AFP 2.5mg/ml-PEG12 reaction mixture at start of immersion

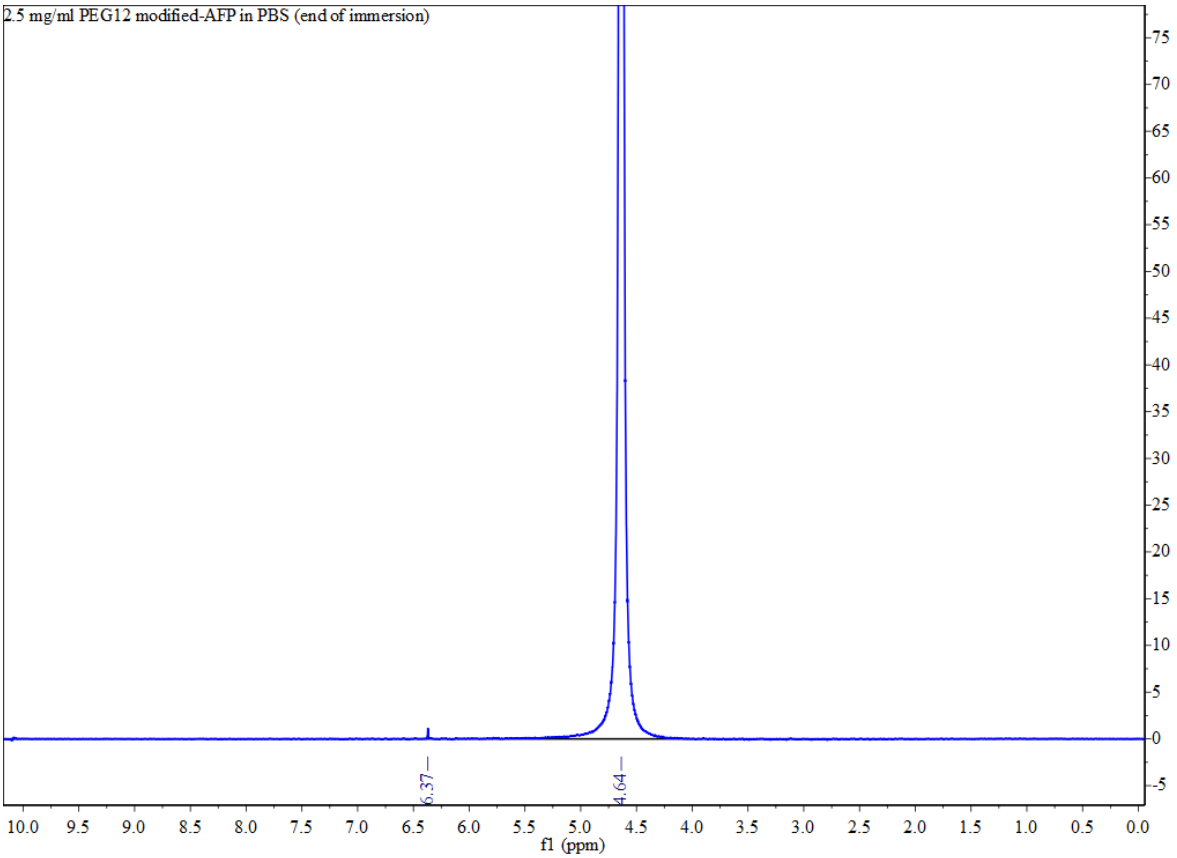

Figure D.5: AFP 2.5mg/ml-PEG12 reaction mixture at end of immersion

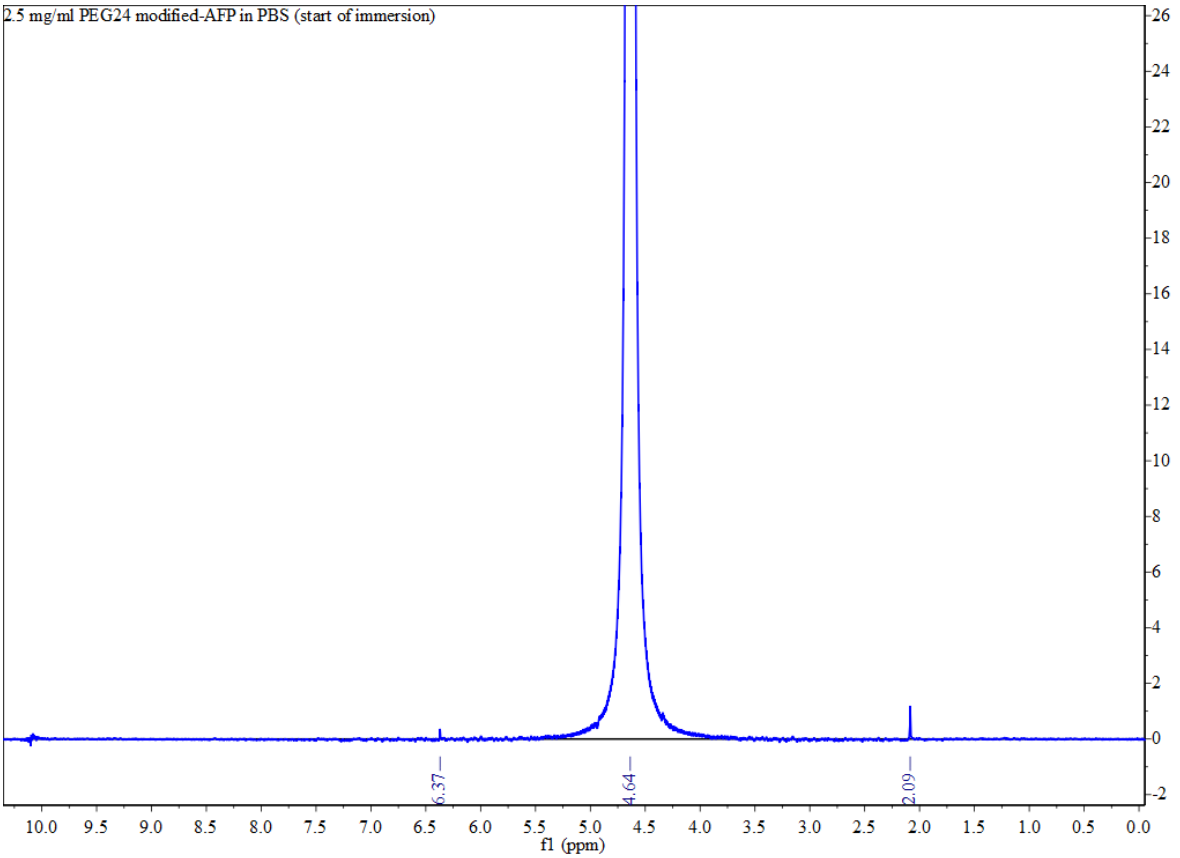

Figure D.6: AFP 2.5mg/ml-PEG24 reaction mixture at start of immersion

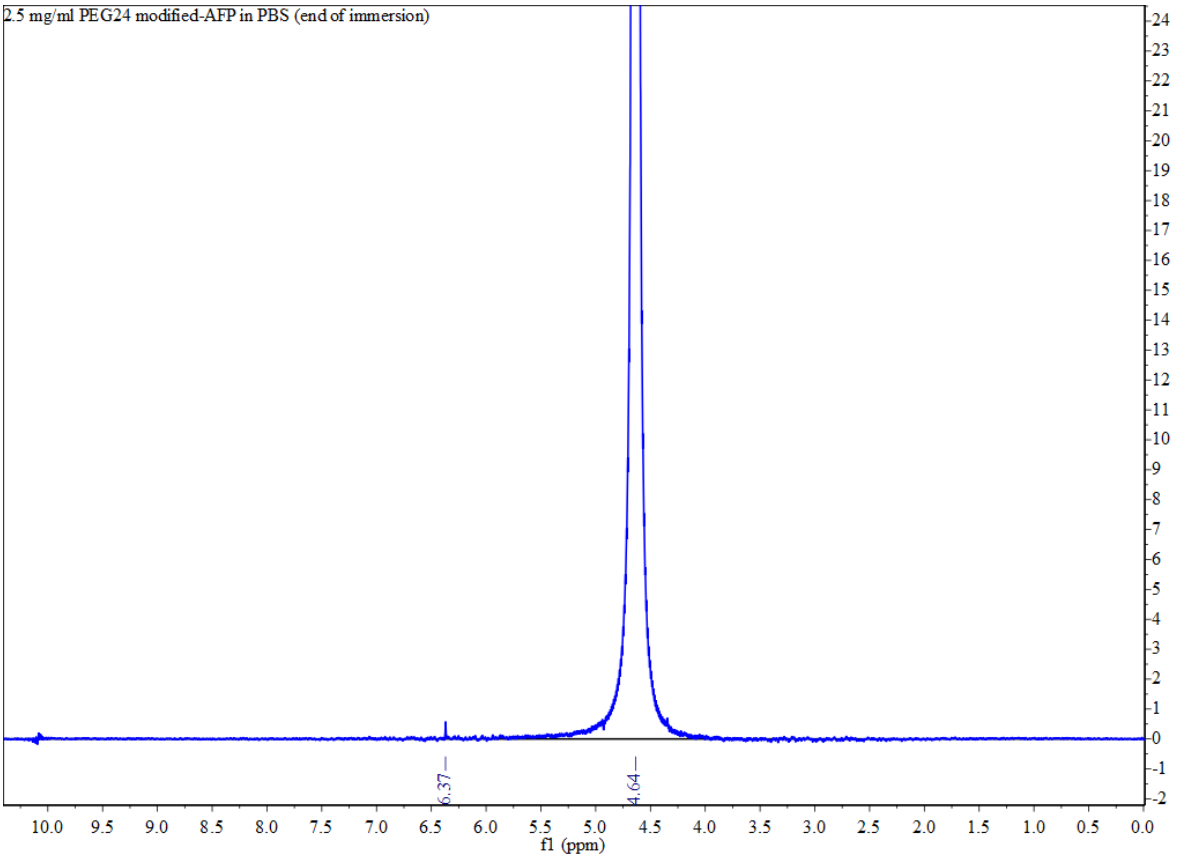

Figure D.7: AFP 2.5mg/ml-PEG24 reaction mixture at end of immersion

Appendix E

FTIR spectra of INP hydrogels

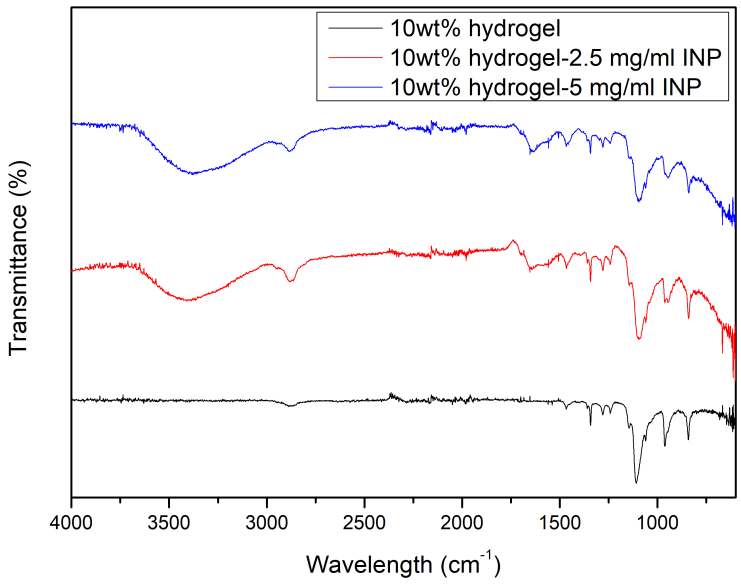

Figure E.1: Spectra of 10wt% hydrogel-2.5mg/ml INP and 10wt% hydrogel-2.5mg/ml INP

Appendix F

Freezing results of the ice-binding protein surfaces

			Mean Tfo (°C)	St. dev.
AA2024-SH	-11,71	-12,39	**-12,05**	**0,34**
AA2024-2.5mg/ml AFP-PEG12	-9,83	-11,77	**-10,80**	**0,97**
AA2024-5mg/ml AFP-PEG12	-3,00	-3,30	**-3,15**	**0,15**
AA2024-2.5mg/ml AFP-PEG2	-7,64	-9,77	**-8,71**	**1,07**
AA2024-2.5mg/ml AFP-PEG24	-16,60	-14,39	**-15,50**	**1,11**
AA2024-2.5mg/ml INP-PEG12	-8,19	-2,80	**-5,50**	**2,70**
AA2024-5mg/ml INP-PEG12	-6,00	-4,98	**-5,49**	**0,51**

Table F.1: T_{fo} of ice-binding protein surfaces

			Mean tfo (s)	St. dev.
AA2024-SH	275	290	**282,5**	**7,5**
AA2024-2.5mg/ml AFP-PEG12	225	280	**252,5**	**27,5**
AA2024-5mg/ml AFP-PEG12	172	178	**175,0**	**3,0**
AA2024-2.5mg/ml AFP-PEG2	214	219	**216,5**	**2,5**
AA2024-2.5mg/ml AFP-PEG24	334	316	**325,0**	**9,0**
AA2024-2.5mg/ml INP-PEG12	218	179	**192,5**	**25,5**
AA2024-5mg/ml INP-PEG12	210	186	**198,0**	**12,0**

Table F.2: t_{fo} of ice-binding protein surfaces

Appendix G

DSC data

AFP (mg/ml)	Area fb	Area ff	ΔH_fb (J/g)	ΔH_fb (J/g)	W_fb (%)	Mean	St.dev.	W_ff (%)	Mean	St.dev.	W_f (%)	Mean	St.dev.	W_n (%)	Mean	St.dev.
0	-0,43	-36,03	2,60	216,16	0,89			73,70			74,58			14,42		
	-0,79	-37,59	4,74	225,54	1,62			76,90			78,51			10,49		
						1,25	0,37		75,30	1,60		76,55	1,96		12,45	1,96
2,5	-0,52	-33,46	3,10	200,77	1,06			68,45			69,51			19,49		
	-0,69	-35,13	4,14	210,79	1,41			71,87			73,28			15,72		
	-0,58	-35,68	3,48	214,11	1,19	1,22	0,15	73,00	71,11	1,93	74,19	72,32	2,03	14,81	16,68	2,03
5	-0,93	-36,25	5,60	217,47	1,91			74,15			76,06			12,94		
	-0,58	-34,76	3,46	208,59	1,18			71,12			72,30			16,70		
	-1,12	-37,37	6,69	224,19	2,28	1,79	0,46	76,44	73,90	2,18	78,72	75,69	2,63	10,28	13,31	2,63
10	-1,77	-37,09	10,61	222,53	3,62			75,87			79,49			9,51		
	-1,66	-39,17	9,97	235,01	3,40			80,13			83,53			5,47		
						3,51	0,11		78,00	2,13		81,51	2,02		7,49	2,02
20	-2,41	-33,86	14,44	203,17	4,92			69,27			74,19			14,81		
	-2,61	-33,56	15,64	201,35	5,33			68,65			73,98			15,02		
						5,13	0,20		68,96	0,31		74,09	0,11		14,91	0,11

Bibliography

[1] H. Kitano, K. Ichikawa, M. Ide, M. Fukuda, and W. Mizuno, "Fourier transform infrared study on the state of water sorbed to poly(ethylene glycol) films," *Langmuir*, vol. 17, no. 6, pp. 1889–1895, 2001.

[2] H. He and Z. Guo, "Superhydrophobic materials used for anti-icing theory, application, and development," *iScience*, vol. 24, no. 11, p. 103357, 2021.

[3] X. Zhou, Y. Sun, and J. Liu, "Designing anti-icing surfaces by controlling ice formation," *Advanced Materials Interfaces*, vol. 8, no. 17, p. 2100327, 2021.

[4] B. Chen, Y. Yang, and J. Liu, "Performance optimization of aircraft deicing equipment based on genetic algorithm," *Science Progress*, vol. 103, no. 1, pp. 1–20, 2020.

[5] S. Kandagal and K. Venkatraman, *Piezo-Actuated Vibratory Deicing of a Flat Plate*, 2005.

[6] B. Tian, Z. Chunling, M. Bo, L. Kai, and Z. Chengxiang, "Vibration de-icing method with piezoelectric actuators," *Journal of Vibroengineering*, vol. 17, no. 1, pp. 61–73, 2015.

[7] Z. He, C. Wu, M. Hua, S. Wu, D. Wu, X. Zhu, J. Wang, and X. He, "Bioinspired multifunctional anti-icing hydrogel," *Matter*, vol. 2, no. 3, pp. 723–734, 2020.

[8] J. Lv, Y. Song, L. Jiang, and J. Wang, "Bio-inspired strategies for anti-icing," *ACS Nano*, vol. 8, no. 4, pp. 3152–3169, 2014.

[9] Y. Wang, Q. Zhang, P. Li, and J.-T. Huang, "A durable and sustainable superhydrophobic surface with intertwined cellulose/sio2 blends for anti-icing and self-cleaning applications," *Materials Design*, vol. 217, p. 110628, 2022.

[10] B. Liu, K. Zhang, C. Tao, Y. Zhao, X. Li, K. Zhu, and X. Yuan, "Strategies for anti-icing: low surface energy or liquid-infused?" *RSC Adv.*, vol. 6, no. 74, pp. 70 251–70 260, 2016.

[11] R. Dou, J. Chen, Y. Zhang, X. Wang, D. Cui, Y. Song, L. Jiang, and J. Wang, "Anti-icing coating with an aqueous lubricating layer," *ACS Applied Materials & Interfaces*, vol. 6, no. 10, pp. 6998–7003, 2014.

[12] J. L. O'Brien, S. F. Ahmadi, K. C. Failor, C. E. Bisbano, M. D. Mulroe, S. Nath, B. A. Vinatzer, and J. B. Boreyko, "Spatial control of condensation and desublimation using ice nucleating proteins," *Applied Physics Letters*, vol. 113, no. 15, p. 153701, 2018.

[13] M. Bar Dolev, I. Braslavsky, and P. L. Davies, "Ice-binding proteins and their function," *Annual Review of Biochemistry*, vol. 85, no. 1, pp. 515–542, 2016.

[14] A. Eskandari, T. C. Leow, M. B. A. Rahman, and S. N. Oslan, "Antifreeze proteins and their practical utilization in industry, medicine, and agriculture," *Biomolecules*, vol. 10, no. 12, 2020.

[15] H. J. Kim, J. H. Lee, Y. B. Hur, C. W. Lee, S.-H. Park, and B.-W. Koo, "Marine antifreeze proteins: Structure, function, and application to cryopreservation as a potential cryoprotectant," *Marine Drugs*, vol. 15, no. 2, 2017.

[16] A. H. Naing and C. K. Kim, "A brief review of applications of antifreeze proteins in cryopreservation and metabolic genetic engineering," *3 Biotech*, vol. 9, no. 9, p. 329, 2019.

[17] H. Xiang, X. Yang, L. Ke, and Y. Hu, "The properties, biotechnologies, and applications of antifreeze proteins," *International Journal of Biological Macromolecules*, vol. 153, pp. 661–675, 2020.

[18] A. Białkowska, E. Majewska, A. Olczak, and A. Twarda-Clapa, "Ice binding proteins: Diverse biological roles and applications in different types of industry," *Biomolecules*, vol. 10, no. 2, 2020.

[19] J. A. Raymond and A. L. DeVries, "Adsorption inhibition as a mechanism of freezing resistance in polar fishes." *Proceedings of the National Academy of Sciences*, vol. 74, no. 6, pp. 2589–2593, 1977.

[20] M. Urbańczyk, J. Góra, R. Latajka, and N. Sewald, "Antifreeze glycopeptides: from structure and activity studies to current approaches in chemical synthesis," *Amino Acids*, vol. 49, no. 2, pp. 209–222, 2017.

[21] Y. Celik, R. Drori, N. Pertaya-Braun, A. Altan, T. Barton, M. Bar-Dolev, A. Groisman, P. L. Davies, and I. Braslavsky, "Microfluidic experiments reveal that antifreeze proteins bound to ice crystals suffice to prevent their growth," *Proceedings of the National Academy of Sciences*, vol. 110, no. 4, pp. 1309–1314, 2013.

[22] E. Kristiansen and K. E. Zachariassen, "The mechanism by which fish antifreeze proteins cause thermal hysteresis," *Cryobiology*, vol. 51, no. 3, pp. 262–280, 2005.

[23] I. Voets, "From ice-binding proteins to bio-inspired antifreeze materials," *Soft Matter*, vol. 13, no. 28, p. 4808–4823., 2017.

[24] E. Kristiansen, *Thermal Hysteresis*. Cham: Springer International Publishing, 2020, pp. 131–158.

[25] P. Westh, H. Ramløv, P. Wilson, and A. DeVries, "Vapour pressure of aqueous antifreeze glycopeptide solutions," *Cryo-Letters*, vol. 18, no. 5, pp. 277–282, 1997.

[26] E. Kristiansen and K. Zachariassen, "The mechanism by which fish antifreeze proteins cause thermal hysteresis," *Cryobiology*, vol. 51, no. 3, pp. 262–280, 2006.

[27] M. Lukas, R. Schwidetzky, R. Eufemio, M. Bonn, and K. Meister, "Toward understanding bacterial ice nucleation," *The Journal of Physical Chemistry B*, vol. 126, 2022.

[28] D. Kim and A. E. Herr, "Protein immobilization techniques for microfluidic assays," *Biomicrofluidics*, vol. 7, no. 4, p. 041501, 2013. [Online]. Available: https://doi.org/10.1063/1.4816934

[29] Y. Jeong, S. Jeong, Y. K. Nam, and S. M. Kang, "Development of freeze-resistant aluminum surfaces by tannic acid coating and subsequent immobilization of antifreeze proteins," *Bulletin of the Korean Chemical Society*, vol. 39, no. 4, pp. 559–562, 2018.

[30] K. Liu, C. Wang, J. Ma, G. Shi, X. Yao, H. Fang, Y. Song, and J. Wang, "Janus effect of antifreeze proteins on ice nucleation," *Proceedings of the National Academy of Sciences*, vol. 113, no. 51, p. 14739–14744, 2016.

[31] J. A. Shadish and C. A. DeForest, "Site-selective protein modification: From functionalized proteins to functional biomaterials," *Matter*, vol. 2, no. 1, pp. 50–77, 2020.

[32] Y. Gwak, J.-I. Park, M. Kim, H. Kim, M. Kwon, S. Oh, Y.-P. Kim, and E. Jin, "Creating anti-icing surfaces via the direct immobilization of antifreeze proteins on aluminum," *Scientific Reports*, vol. 5, no. 12019, 2015.

[33] Z. Wang and P. Cole, "Methods and applications of expressed protein ligation," *Methods in molecular biology*, vol. 2133, pp. 1–13.

[34] A. Esser-Kahn, V. Trang, and M. Francis, "Incorporation of antifreeze proteins into polymer coatings using site-selective bioconjugation," *Journal of the American Chemical Society*, vol. 132, no. 38, pp. 13 264–13 269, 2010.

[35] C. Rosen and M. Francis, "argeting the n terminus for site-selective protein modification," *Nat Chem Biol*, vol. 13, pp. 697–705, 2017.

[36] G. T. Hermanson, "Chapter 2 - functional targets for bioconjugation," in *Bioconjugate Techniques (Third Edition)*, third edition ed., G. T. Hermanson, Ed. Boston: Academic Press, 2013, pp. 127–228.

[37] T. Charpentier, A. Neville, P. Millner, R. Hewson, and A. Morina, "An investigation of freezing of supercooled water on anti-freeze protein modified surfaces," *Journal of Bionic Engineering*, vol. 10, no. 2, p. 139–147, 2013.

[38] L. E. Wilkins, M. Hasan, A. E. R. Fayter, C. Biggs, M. Walker, and M. I. Gibson, "Site-specific conjugation of antifreeze proteins onto polymer-stabilized nanoparticles," *Polym. Chem.*, vol. 10, no. 23, pp. 2986–2990, 2019.

[39] Q. Wei and R. Haag, "Universal polymer coatings and their representative biomedical applications," *Mater. Horiz.*, vol. 2, pp. 567–577, 2015.

[40] C. MacDonald, R. Morrow, A. Weiss, and M. Bilek, "Covalent attachment of functional protein to polymer surfaces: A novel one-step dry process," *Journal of the Royal Society, Interface / the Royal Society*, vol. 5, pp. 663–9, 07 2008.

[41] G. T. Hermanson, "Chapter 13 - silane coupling agents," in *Bioconjugate Techniques (Third Edition)*, third edition ed., G. T. Hermanson, Ed. Boston: Academic Press, 2013, pp. 535–548. [Online]. Available: https://www.sciencedirect.com/science/article/pii/B9780123822390000133

[42] M. Sypabekova, A. Hagemann, D. Rho, and S. Kim, "Review: 3-aminopropyltriethoxysilane (aptes) deposition methods on oxide surfaces in solution and vapor phases for biosensing applications," *Biosensors*, vol. 13, p. 36, 12 2022.

[43] Y. Kobashigawa, Y. Nishimiya, K. Miura, S. Ohgiya, A. Miura, and S. Tsuda, "A part of ice nucleation protein exhibits the ice-binding ability," *FEBS Letters*, vol. 579, no. 6, pp. 1493–1497, 2005.

[44] Y. Zhuo, J. Chen, S. Xiao, T. Li, F. Wang, J. He, and Z. Zhang, "Gels as emerging anti-icing materials: a mini review," *Mater. Horiz.*, vol. 8, no. 12, pp. 3266–3280, 2021.

[45] S. Hartmann, M. Ling, L. S. Dreyer, A. Zipori, K. Finster, S. Grawe, L. Z. Jensen, S. Borck, N. Reicher, T. Drace, D. Niedermeier, N. C. Jones, S. V. Hoffmann, H. Wex, Y. Rudich, T. Boesen, and T. Šantl-Temkiv, "Structure and protein-protein interactions of ice nucleation proteins drive their activity," *Frontiers in Microbiology*, vol. 13, 2022.

[46] S. P. Zustiak, Y. Wei, and J. B. Leach, "Protein–hydrogel interactions in tissue engineering: Mechanisms and applications," *Tissue Engineering Part B: Reviews*, vol. 19, no. 2, pp. 160–171, 2013.

[47] L. Abune and Y. Wang, "Affinity hydrogels for protein delivery," *Trends in Pharmacological Sciences*, vol. 42, no. 4, pp. 300–312, 2021.

[48] P. M. Kharkar, M. S. Rehmann, K. M. Skeens, E. Maverakis, and A. M. Kloxin, "Thiol–ene click hydrogels for therapeutic delivery," *ACS Biomater Sci Eng.*, vol. 2, no. 2, pp. 165–179, 2016.

[49] X. Fan, W. Zhou, Y. Chen, L. Yan, Y. Fang, and H. Liu, "An antifreezing/antiheating hydrogel containing catechol derivative urushiol for strong wet adhesion to various substrates," *ACS Applied Materials & Interfaces*, vol. 12, no. 28, pp. 32 031–32 040, 2020.

[50] T. Li, P. F. Ibáñez-Ibáñez, V. Håkonsen, J. Wu, K. Xu, Y. Zhuo, S. Luo, J. He, and Z. Zhang, "Self-deicing electrolyte hydrogel surfaces with pa-level ice adhesion and durable antifreezing/antifrost performance," *ACS Applied Materials & Interfaces*, vol. 12, no. 31, pp. 35 572–35 578, 2020.

[51] K. Piechocki, M. Kozanecki, and J. Saramak, "Water structure and hydration of polymer network in pmeo2ma hydrogels," *Polymer*, vol. 210, p. 122974, 2020.

[52] V. Gun'ko, I. Savina, and M. S.V., "Properties of water bound in hydrogels," *Gels*, vol. 3, no. 4, p. 37, 2017.

[53] B. Huang, S. Jiang, Y. Diao, X. Liu, W. Liu, J. Chen, and H. Yang, "Hydrogels as durable anti-icing coatings inhibit and delay ice nucleation," *Molecules*, vol. 25, no. 15, 2020.

[54] K. Inamori, M. Kyo, K. Matsukawa, Y. Inoue, T. Sonoda, K. Tatematsu, K. Tanizawa, T. Mori, and Y. Katayama, "Optimal surface chemistry for peptide immobilization in on-chip phosphorylation analysis," *Analytical Chemistry*, vol. 80, no. 3, pp. 643–650, 2008.

[55] D. Nazarov, E. Zemtsova, A. Solokhin, R. Valiev, and V. Smirnov, "Modification of the surface topography and composition of ultrafine and coarse grained titanium by chemical etching," *Nanomaterials*, vol. 7, no. 1, p. 15, Jan 2017. [Online]. Available: http://dx.doi.org/10.3390/nano7010015

[56] I. Boukerche, S. Djerad, L. Benmansour, L. Tifouti, and K. Saleh, "Degradability of aluminum in acidic and alkaline solutions," *Corrosion Science*, vol. 78, pp. 343–352, 2014. [Online]. Available: https://www.sciencedirect.com/science/article/pii/S0010938X13004496

[57] P. Ahmadi, H. Eivaz Mohammadloo, and R. Behgam, "Effect of practical parameters on the structure and corrosion behavior of vanadium/zirconium conversion coating on aa 2024 aluminum alloy," *Journal of Coatings Technology and Research*, vol. 16, 06 2019.

[58] Y. Hu, B. Yuan, F. Cheng, and X. Hu, "Naoh etching and resin pre-coating treatments for stronger adhesive bonding between cfrp and aluminium alloy," *Composites Part B: Engineering*, vol. 178, p. 107478, 2019.

[59] Y. Huang, D. Sarkar, and X. Grant Chen, "Superhydrophobic aluminum alloy surfaces prepared by chemical etching process and their corrosion resistance properties," *Applied Surface Science*, vol. 356, pp. 1012–1024, 2015. [Online]. Available: https://www.sciencedirect.com/science/article/pii/S0169433215019790

[60] L. Muñoz, F. Pineda, C. Martínez, M. Sancy, M. Urzua, M. Flores, M. V. Encinas, and M. A. Páez, "Improving the interaction between aluminum surfaces and polymer coatings," *Surface and Coatings Technology*, vol. 358, pp. 435–442, 2019. [Online]. Available: https://www.sciencedirect.com/science/article/pii/S0257897218312611

[61] M. Olgiati, P. J. Denissen, and S. J. Garcia, "When all intermetallics dealloy in aa2024-t3: Quantifying early stage intermetallic corrosion kinetics under immersion," *Corrosion Science*, vol. 192, p. 109836, 2021.

[62] A. E. Hughes, A. M. Glenn, N. Wilson, A. Moffatt, A. J. Morton, and R. G. Buchheit, "A consistent description of intermetallic particle composition: An analysis of ten batches of aa2024-t3," *Surface and Interface Analysis*, vol. 45, no. 10, pp. 1558–1563, 2013.

[63] P. Kwolek, M. Wojnicki, and E. Csapó, "Mechanism of corrosion inhibition of intermetallic al2cu in acidic solution," *Applied Surface Science*, vol. 551, p. 149436, 2021.

[64] E. Merino, A. Durán, and Y. Castro, "The role of silane sol-gel coatings on the corrosion protection of magnesium alloys," in *Current Trends in Magnesium (Mg) Research*, S. S. Sunkari, Ed. Rijeka: IntechOpen, 2022, ch. 4. [Online]. Available: https://doi.org/10.5772/intechopen.102085

[65] M. Mihelčič, A. Surca, A. Kreta, and M. Gaberšček, "Spectroscopical and electrochemical characterisation of a (3-mercaptopropyl)trimethoxysilane - based protective coating on aluminium alloy 2024," *Croatica Chemica Acta*, vol. 90, 01 2017.

[66] D. Tsiourvas, A. Tsetsekou, M. Arkas, S. Diplas, and E. Mastrogianni, "Covalent attachment of a bioactive hyperbranched polymeric layer to titanium surface for the biomimetic growth of calcium phosphates," *J Mater Sci Mater Med*, vol. 22, no. 1, pp. 85–96, 2011.

[67] T. Sieber, J. Ducke, A. Rietig, T. Langner, and J. Acker, "Recovery of li(ni0.33mn0.33co0.33)o2 from lithium-ion battery cathodes: Aspects of degradation," *Nanomaterials*, vol. 9, p. 246, 02 2019.

[68] M. Taghavikish, S. Subianto, N. Dutta, and N. Roy Choudhury, "Novel thiol-ene hybrid coating for metal protection," *Coatings*, vol. 6, no. 2, p. 17, Apr 2016.

[69] T. Oh, "Comparison between sioc thin film by plasma enhance chemical vapor deposition and sio2 thin film by fourier transform infrared spectroscopy," *Journal of The Korean Physical Society - J KOREAN PHYS SOC*, vol. 56, 04 2010.

[70] F. Kundie, C. Azhari, and Z. Ahmad, "Effect of nano- and micro-alumina fillers on some properties of poly(methyl methacrylate) denture base composites," *Journal of the Serbian Chemical Society*, vol. 83, pp. 56–56, 01 2017.

[71] L. M. Miller, M. W. Bourassa, and R. J. Smith, "Ftir spectroscopic imaging of protein aggregation in living cells," *Biochimica et Biophysica Acta (BBA) - Biomembranes*, vol. 1828, no. 10, pp. 2339–2346, 2013, fTIR in membrane proteins and peptide studies.

[72] M. Lozano, P. Rodriguez-Ulibarri, J. Echeverría, M. Beruete, M. Sorolla Ayza, and M. Beriain, "Mid-infrared spectroscopy (mir) for simultaneous determination of fat and protein content in meat of several animal species," *Food Analytical Methods*, vol. 10, pp. 3462–3469, 2017.

[73] S. Tsuda, A. Yamauchi, N. M.-M. U. Khan, T. Arai, S. Mahatabuddin, A. Miura, and H. Kondo, "Fish-derived antifreeze proteins and antifreeze glycoprotein exhibit a different ice-binding property with increasing concentration," *Biomolecules*, vol. 10, no. 3, p. 423, Mar 2020. [Online]. Available: http://dx.doi.org/10.3390/biom10030423

[74] C. Garnham, R. Campbell, and D. P.L., "Anchored clathrate waters bind antifreeze proteins to ice," *Proc Natl Acad Sci U S A.*, vol. 108, no. 18, pp. 7363–7367, 2011.

[75] A. Hudait, N. Odendahl, Y. Qiu, F. Paesani, and V. Molinero, "Ice-nucleating and antifreeze proteins recognize ice through a diversity of anchored clathrate and ice-like motifs," *Journal of the American Chemical Society*, vol. 140, no. 14, pp. 4905–4912, 2018.

[76] J. H. Pu, J. Sun, Q. Sheng, W. Wang, and H. S. Wang, "Dependences of formation and transition of the surface condensation mode on wettability and temperature difference," *Langmuir*, vol. 36, no. 1, pp. 456–464, 2020.

[77] J. Sun and H. S. Wang, "On the early and developed stages of surface condensation: Competition mechanism between interfacial and condensate bulk thermal resistances," *Scientific Reports*, vol. 6, p. 35003, 10 2016.

[78] M. Rahimi, P. Fojan, L. Gurevich, and A. Afshari, "Effects of aluminium surface morphology and chemical modification on wettability," *Applied Surface Science*, vol. 296, pp. 124–132, 2014.

[79] X. Lu, C. Zheng, and H. Zhang, "Improvement of surface hydrophilicity and biological sample-compatibility of molecularly imprinted polymer microspheres by facile surface modification with -cyclodextrin," *European Polymer Journal*, vol. 115, pp. 12–21, 2019.

[80] G. Rodrigues and R. Silva, "Numerical analysis of the minimization of frost formation in flat plate with different coatings," 11 2018.

[81] C. Huang, Y. Zhao, and T. Gu, "Ice dendrite growth atop a frozen drop under natural convection conditions," *Crystals*, vol. 12, no. 3, 2022.

[82] H. Nada and F. Y., "Antifreeze proteins: computer simulation studies on the mechanism of ice growth inhibition," *Polymer journal*, vol. 44, pp. 690–698, 2012.

[83] J. Liu, C. Zhu, K. Liu, Y. Jiang, Y. Song, J. Francisco, Z. Cheng, and J. Wang, "Distinct ice patterns on solid surfaces with various wettabilities," *Proceedings of the National Academy of Sciences*, vol. 114, p. 201712829, 10 2017.

[84] H. Gandee, Y. Zhou, J. Lee, J. Chomali, H. Xu, and S. Adera, "Unique ice dendrite morphology on state-of-the-art oil-impregnated surfaces," *Proceedings of the National Academy of Sciences*, vol. 120, 12 2022.

[85] S. Kamyar, M. Ahmad, S. D. Jazayeri, S. Sedaghat, P. Shabanzadeh, H. k. Jahangirian, M. Mahdavi Shahri, and Y. Abdollahi, "Synthesis and characterization of polyethylene glycol mediated silver nanoparticles by the green method," *International journal of molecular sciences*, vol. 13, pp. 6639–50, 12 2012.

[86] R. Naohara, S. Namai, J. Kamiyama, and T. Ikeda-Fukazawa, "Structure and diffusive properties of water in polymer hydrogels," *The Journal of Physical Chemistry B*, vol. 126, no. 40, pp. 7992–7998, 2022.

[87] B. Cursaru, P. Stanescu, and M. Teodorescu, "The states of water in hydrogels synthesized from diepoxy-terminated poly(ethylene glycol)s and aliphatic polyamines," *U.P.B. Sci. Bull., Series B*, vol. 72, pp. 99–114, 12 2010.

[88] A. Thorat and R. Suryanarayanan, "Characterization of phosphate buffered saline (pbs) in frozen state and after freeze-drying," *Pharmaceutical Research*, vol. 36, 05 2019.

[89] A. C. Fogarty and D. Laage, "Water dynamics in protein hydration shells: The molecular origins of the dynamical perturbation," *The Journal of Physical Chemistry B*, vol. 118, no. 28, pp. 7715–7729, 2014.

[90] N. Yamamoto, M. Nakanishi, R. Rajan, and H. Nakagawa, "Protein hydration and its freezing phenomena: Toward the application for cell freezing and frozen food storage," *Biophysics and Physicobiology*, vol. 18, 11 2021.

[91] S. Abasi, R. Davis, D. A. Podstawczyk, and A. Guiseppi-Elie, "Distribution of water states within poly(hema-co-hpma)-based hydrogels," *Polymer*, vol. 185, p. 121978, 2019.

[92] E. I. Howard, M. P. Blakeley, M. Haertlein, I. P. Haertlein, A. Mitschler, S. J. Fisher, A. C. Siah, A. G. Salvay, A. Popov, C. M. Dieckmann, T. Petrova, and A. Podjarny, "Neutron structure of type-iii antifreeze protein allows the reconstruction of afp–ice interface," *Journal of Molecular Recognition*, vol. 24, no. 4, pp. 724–732, 2011.

[93] Z. F. Brotzakis, I. K. Voets, H. J. Bakker, and P. G. Bolhuis, "Water structure and dynamics in the hydration layer of a type iii anti-freeze protein," *Phys. Chem. Chem. Phys.*, vol. 20, pp. 6996–7006, 2018.

[94] M. C. Branco, D. J. Pochan, N. J. Wagner, and J. P. Schneider, "The effect of protein structure on their controlled release from an injectable peptide hydrogel," *Biomaterials*, vol. 31, no. 36, pp. 9527–9534, 2010.

[95] J. Ladd, Z. Zhang, S. Chen, J. C. Hower, and S. Jiang, "Zwitterionic polymers exhibiting high resistance to nonspecific protein adsorption from human serum and plasma," *Biomacromolecules*, vol. 9, no. 5, pp. 1357–1361, 2008.

[96] J. Ostrowska-Czubenko, M. Pieróg, and M. Gierszewska-Drużyńska, "State of water in noncrosslinked and crosslinked hydrogel chitosan membranes–dsc studies," *Progress on Chemistry and Application of Chitin and its Derivatives*, no. 16, pp. 147–156, 2011.